BioMed Research International

Research and Application of Minimally Invasive Precision Surgery

Lead Guest Editor: YingQi Zhang
Guest Editors: Tao Yu, Shenghui Liao, and Shi-Min Chang

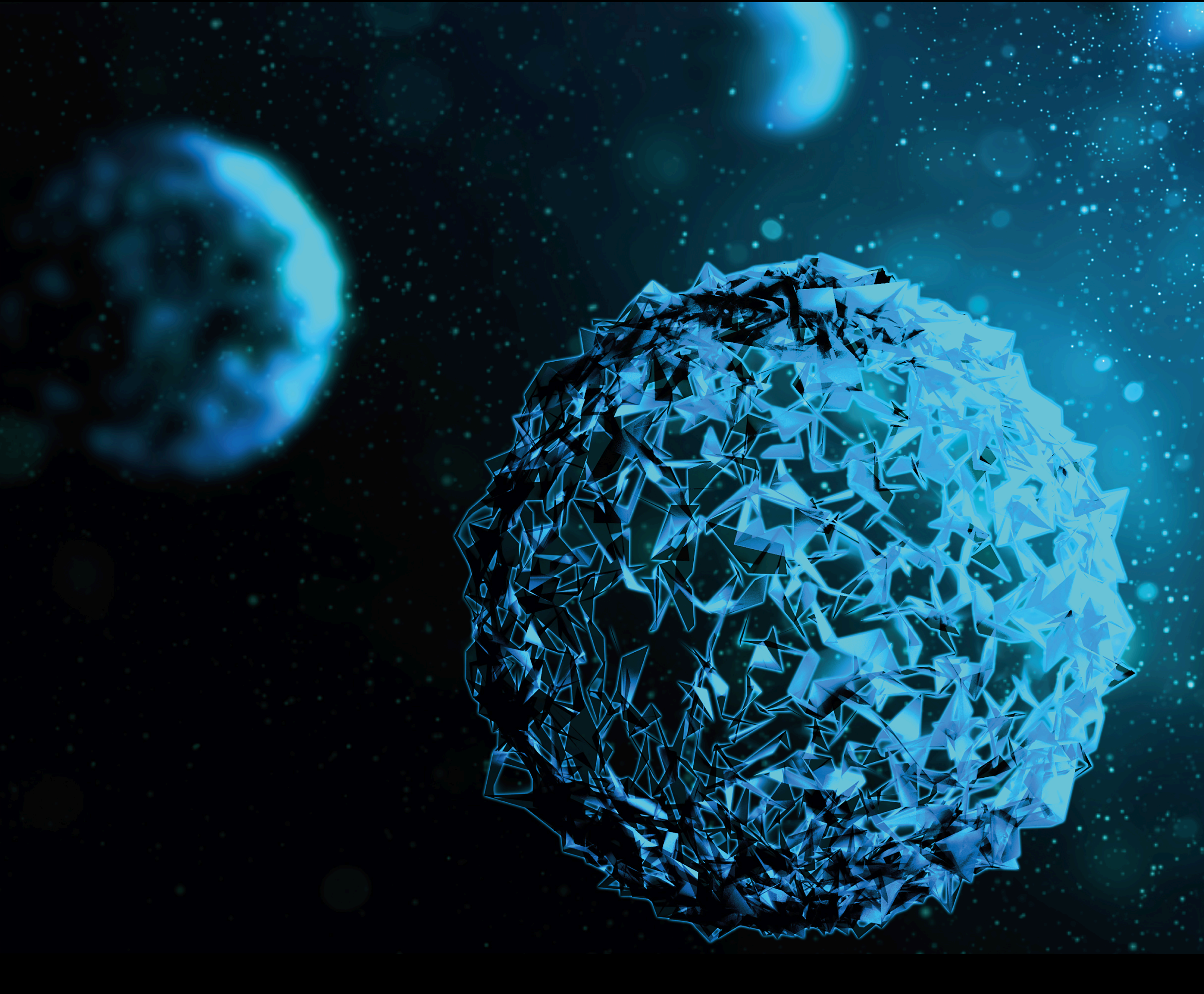

Research and Application of Minimally Invasive Precision Surgery

BioMed Research International

Research and Application of Minimally Invasive Precision Surgery

Lead Guest Editor: YingQi Zhang
Guest Editors: Tao Yu, Shenghui Liao, and Shi-Min Chang

Copyright © 2022 Hindawi Limited. All rights reserved.

This is a special issue published in "BioMed Research International." All articles are open access articles distributed under the Creative Commons Attribution License, which permits unrestricted use, distribution, and reproduction in any medium, provided the original work is properly cited.

Section Editors

Penny A. Asbell, USA
David Bernardo, Spain
Gerald Brandacher, USA
Kim Bridle, Australia
Laura Chronopoulou, Italy
Gerald A. Colvin, USA
Aaron S. Dumont, USA
Pierfrancesco Franco, Italy
Raj P. Kandpal, USA
Fabrizio Montecucco, Italy
Mangesh S. Pednekar, India
Letterio S. Politi, USA
Jinsong Ren, China
William B. Rodgers, USA
Harry W. Schroeder, USA
Andrea Scribante, Italy
Germán Vicente-Rodriguez, Spain
Momiao Xiong, USA
Hui Zhang, China

Academic Editors

Surgery

Ming Chen, Taiwan
Andrea Ferri, Italy
Georg Gradl, Germany
Christian R. Habermann, Germany
Ho-Seong Han, Republic of Korea
Shiro Imagama, Japan
Hiroki Ito, Japan
Jussuf Thomas Kaifi, USA
Kan Kajimoto, Japan
Kazutaka Kamiya, Japan
Hirotoshi Kobayashi, Japan
Achim Langenbucher, Germany
Myong Cheol Lim, Republic of Korea
Kosei Maemura, Japan
Takahisa Matsuda, Japan
Ken Ohnita, Japan
Giuseppe Piccinni, Italy
Claudia Maria Radu, Italy
Zbigniew Rybak, Poland
József Szalma, Hungary
Mariarita Tarallo, Italy

Orthopedics

Y. Ahn, Republic of Korea
Fabiano Bini, Italy
Barbara Buffoli, Italy
Feng Cai, China
Frederic Cailotto, France
Antonio Capone, Italy
Chul Hyun Cho, Republic of Korea
Marcello De Fine, Italy
Xing Du, China
Thaqif El Khassawna, Germany
Giuseppe Filardo, Italy
Mattia Fortina, Italy
You-Shui Gao, China
Alberto Grassi, Italy
Zbigniew Gugala, USA
Ying-Hui Hua, China
Joby John, United Kingdom
Jean-François Kaux, Belgium
Deepak Kumar Khajuria, USA
Amal Khoury, Israel
Naomi Kobayashi, Japan
Panagiotis Korovessis, Greece
Arvind G. Kulkarni, India
Zhu Kun-Peng, China
Yong Seuk Lee, Republic of Korea
Kai-Uwe Lewandrowski, Brazil
Chenshuang Li, USA
Jianfeng Li, China
Sheldon Lin, USA
Matthew R. McCann, Canada
Hiroaki Minehara, Japan
Jose A. Parraca, Portugal
Dmitry Popkov, Russia
Thomas S. Roukis, USA
Ajoy Prasad Shetty, India
Hae-Ryong Song, Republic of Korea
Kentaro Uchida, Japan

Radovan Zdero, Canada
Chunfeng Zhao, USA

Contents

Hindawi
BioMed Research International
Volume 2022, Article ID 2227679, 9 pages
https://doi.org/10.1155/2022/2227679

Research Article

Percutaneous Bilateral Endoscopic Lumbar Interbody Fusion: Technical Note and Preliminary Results

Huan Chen,[1,2] Huan Zhang,[3] Erping Yang,[2] Qinjie Ling ,[1] and Erxing He [1]

[1]*Spine Surgery, The First Affiliated Hospital of Guangzhou Medical University, Guangzhou, China*
[2]*Department of Orthopedics, Huanggang Central Hospital of Yangtze University, Hubei, China*
[3]*Huanggang Central Hospital of Yangtze University, Hubei, China*

Correspondence should be addressed to Qinjie Ling; kmjw1982@163.com

Qinjie Ling and Erxing He contributed equally to this work.

Received 22 April 2021; Accepted 23 February 2022; Published 11 April 2022

Academic Editor: Ying-Qi Zhang

Copyright © 2022 Huan Chen et al. This is an open access article distributed under the Creative Commons Attribution License, which permits unrestricted use, distribution, and reproduction in any medium, provided the original work is properly cited.

Objective. The purpose of this study was to investigate the feasibility and clinical efficacy of the percutaneous bilateral endoscopy technique (microendoscopic trans-Kambin's triangle lumbar interbody fusion + percutaneous endoscopic transforaminal decompression of the lumbar spinal canal, ME-TKT-LIF+ PETD) in the treatment of lumbar degenerative diseases. *Methods*. From May 2016 to September 2018, 29 patients (16 males and 13 females) who suffered from neurologic symptoms due to degenerative lumbar spine disease and underwent percutaneous bilateral endoscopy technique were enrolled. A microendoscope was used for fusion, and a percutaneous endoscope was used for spinal canal decompression. These patients' perioperative and clinical outcome-related parameters were collected and analyzed. *Results*. The mean intraoperative blood loss was 72.8 ± 40.6 ml, the operation time was 87.1 ± 10.1 min, the postoperative ambulatory time was 1.69 ± 1.0 days, the hospital stay was 2.6 ± 1.3 days, and the follow-up period was 22.34 ± 4.2 months. The visual analog scale (VAS) and the Oswestry disability index (ODI) were significantly improved at the early postoperative and last follow-up, respectively. According to the modified MacNab criteria, 11 (11/29) cases were rated as excellent, 15 (15/29) as good, and 3 (3/29) as fair, and the excellent and good rate was 89.7%. Twenty-eight (28/29) cases demonstrated solid fusion, and the fusion rate was 96.6%. *Conclusion*. The percutaneous bilateral endoscopy technique is safe and feasible in the treatment of lumbar degenerative diseases, with the advantage that more normal anatomical structures are preserved. It is an optional method of lumbar interbody fusion.

1. Introduction

In 1997, Foley first carried out microendoscopic discectomy (MED) to treat lumbar degenerative diseases. Paravertebral muscles were bluntly dilated by cannulas, and the operation was performed under microendoscopy [1]. The idea of minimally invasive surgery and endoscopic technology has indeed been introduced into spinal surgery. In 2006, Ruetten et al. developed percutaneous endoscopic lumbar discectomy (PELD) [2]. PELD causes little damage to the normal anatomical structure, and its clinical efficacy has been widely verified [3].

Based on the surgical techniques described above, various lumbar interbody fusion procedures, such as microendoscopic transforaminal lumbar interbody fusion (ME-TLIF), percutaneous endoscopic transforaminal lumbar interbody fusion (PE-TLIF), biportal endoscopic transforaminal lumbar interbody fusion (BE-TLIF), and endoscopic lumbar interbody fusion (Endo-LIF), have recently been performed [4–8]. Overall, endoscopic approaches to these procedures can be divided into two types: posterolateral and trans-Kambin's triangle approaches. The posterolateral approach was similar to traditional minimally invasive surgery transforaminal lumbar interbody fusion (MIS-TLIF), with the articular processes and a part of the vertebral lamina still needing to be excised [9, 10]. Although the trans-Kambin's triangle approach was less invasive than the posterolateral approach, it had limited decompression of the central spinal canal and the traversing nerve root [11]. To preserve normal anatomical structures such as the lamina and articular processes and allow the nerve tissues in the spinal canal to be directly decompressed, we performed the percutaneous bilateral endoscope technique. This technique included microendoscopic trans-Kambin's triangle lumbar interbody fusion (ME-TKT-LIF) and percutaneous endoscopic transforaminal decompression of the lumbar spinal canal (PETD). A microendoscope was used for fusion, and a percutaneous endoscope was used for spinal canal decompression. The purpose of this retrospective study was to investigate the feasibility and clinical efficacy of the percutaneous bilateral endoscopy technique (ME-TKT-LIF+ PETD) in the treatment of lumbar degenerative diseases.

2. Material and Methods

2.1. Patient Data. This retrospective study included 29 patients who all presented with neuropathic intermittent claudication and radicular leg pain (May 2016 to September 2018). The inclusion criteria were as follows: (1) lumbar degenerative/isthmic spondylolisthesis grade 1 or 2; (2) lumbar disc herniation with segmental instability; and (3) lumbar foraminal stenosis with segmental instability. Patients were excluded as follows: (1) lumbar spondylolisthesis grade 3 or above; (2) severe lumbar canal stenosis; (3) L5-S1 segment lesion with a high iliac crest; and (4) tumors, infections, and fractures involving lumbar vertebrae.

A total of 16 males and 13 females were recruited in this study, with an average age of 59.4 ± 9.1 years (range 42 to 74). Seventeen patients were diagnosed with lumbar spondylolisthesis, 9 with lumbar disc herniation with segmental instability, and 3 with lumbar foraminal stenosis with segmental instability. All patients had single-segment lesions: L3-L4 in 3 patients, L4-L5 in 22 patients, and L5-S1 in 4 patients (Table 1). Preoperative symptoms in all patients were unilateral radicular radiation pain with or without intermittent claudication.

2.2. Surgical Technique. The procedures of all our patients were performed under general anesthesia and took the prone position on the operating table when C-arm fluoroscopy was feasible. Somatosensory-evoked potentials, motor-evoked potentials, and electromyography were used to monitor the involved nerve roots. Cushions were placed on the chest and hip joints, leaving the abdomen hanging. According to the standard anteroposterior position, the direction and angle line of the intervertebral foramen approach on both sides of the lesion segment were determined under C-arm fluoroscopy and marked on the skin (Figure 1). The surgical site of the patient was routinely sterilized and covered with sterile and waterproof towels (taking the L4/5 segment as an example).

Percutaneous endoscopic transforaminal decompression of the lumbar spinal canal (PETD) (Figure 1): On the symptomatic side of the patient, a primary guide rod with a diameter of approximately 4 mm and a blunt tip was inserted at a distance of approximately 10 to 14 cm from the midline of the vertebral column, with the direction pointing to the superior articular process. After the tip of the primary guide rod touched the superior articular process, C-arm fluoroscopy was performed to confirm contact. The guide rod was slid to the ventral side and advanced 1-2 cm to the intervertebral disc through the intervertebral foramen, which was again confirmed by C-arm fluoroscopy. The surgical incision on the skin was extended to a length of 7 mm. The soft tissue was gradually expanded through a series of retractors. A part of the superior articular process was excised by the trepan under the cannula with a hook at the end, which can prevent the nerve root and epidural sac from being damaged. The location reached by the terminal of the trepan was confirmed by fluoroscopy, if necessary. The trepan and the cannula were replaced by the 6.9-mm beveled working channel (Figure 2), and then, the endoscope was placed. On the basis of the patient's preoperative symptoms, physical signs, and imaging results, the degenerated nucleus pulposus tissue was removed, and the spinal canal was decompressed accurately under continuous irrigation with normal saline (Figure 3).

Microendoscopic trans-Kambin's triangle lumbar interbody fusion (ME-TKT-LIF) (Figure 1): On the opposite side, as in the abovementioned surgical method, a 4 mm primary guide rod directed to the superior articular process was inserted at a distance of approximately 6 to 8 cm from the midline, and the blunt tip of the guide rod reached the surface of the superior articular process under the control of C-arm fluoroscopy (Figure 2). After that, the tip of the guide rod was slid to the ventral side and then entered the center of the intervertebral space through the intervertebral foramen at an angle of approximately 40-50 degrees; its depth and final position were adjusted through C-arm fluoroscopy. Through the skin incision extended to 2.5 cm, soft tissue progressive dilatation was performed. Except for the primary guide rod, the dilatation cannula and working channel were not inserted into Kambin's triangle but instead just placed on the outer surface of the superior articular process. Then, the dilatation cannula was removed, and only the primary guide rod and working channel were retained. After the microscopic endoscope system was fixed on the working channel with a diameter of 22 mm, the primary guide rod was removed under full visibility, and the exiting nerve root was protected by a special nerve retractor (Figure 2). "Special nerve retractor" has been approved by the ethics committee of author's hospital before clinical application. Under the endoscope, the special nerve retractor was used to dilate the exiting nerve root to the ventral side moderately, which enlarged the Kambin's triangle, and played a barrier role to protect the exiting nerve root. The superior articular process was then partially excised, and the Kambin's triangle was further enlarged (Figure 4). In some patients with foraminal stenosis, we performed foraminoplasty under microendoscopic visualization. We used reamers, curettes, and forceps for endplate preparation, and most of the annulus fibrosus and nucleus materials in the intervertebral space were removed to reach the cranial and caudal endplates. The raspatories were used to determine the size of the cage. Under the fine visualization of the endoscope, the mixed bone chips of autogenous bone and allograft bone were implanted into

Table 1: Demographic characteristics of patients.

Characteristics	Values
Mean age(years)	59.4 ± 9.1
Sex (M/F)	16/13
Diagnosis	
Lumbar spondylolisthesis	17
Lumbar disc herniation with segmental instability	9
Lumbar foraminal stenosis with segmental instability	3
Level of fusion	
L3-L4	3
L4-L5	22
L5-S1	4

Note: mean values are presented as mean ± standard deviation; M = Male, F=Female.

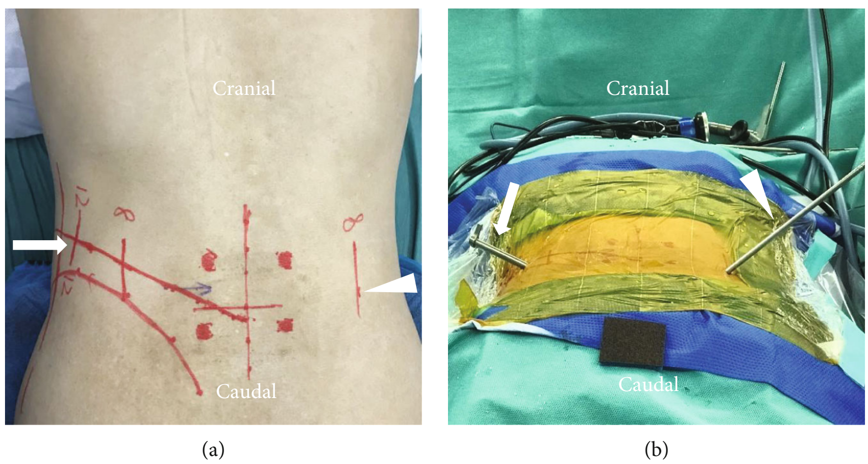

Figure 1: Mark line on skin, the incisions of PETD and ME-TKT-LIF are, respectively, represented by the arrow and triangle (a). The working channel of the percutaneous endoscope (arrow), the primary guide rod (triangle) (b).

the intervertebral space, and then, the cage with the optimal size corresponding to the height of the intervertebral space was gently hammered into the intervertebral space (Figure 3). The size of the cage was equivalent to that used in conventional open surgery, and finally, the integrity check of the exiting nerve root was performed. Nerve structures in the spinal canal need not be exposed.

Percutaneous pedicle screws and connecting rods were implanted without placing drainage tubes, and then, the incision was sutured intradermally (Figures 5–7).

2.3. Clinical Assessment. The following parameters were recorded: operation time; blood loss; postoperative ambulatory time; hospitalization time; follow-up time and complications; and VAS and ODI scores for lumbar and lower extremity pain preoperatively, 1 month postoperatively, and 1 year postoperatively. The satisfaction of clinical outcomes at the last follow-up was assessed using modified MacNab criteria and was divided into four grades: excellent, good, fair, and poor. Flexion-extension lateral radiography and computed tomography were used to evaluate intervertebral fusion [12]. The clinical efficacy was assessed by an independent physician who was blinded to all patients.

2.4. Statistical Analysis. VAS and ODI scores before and after operation were compared by a paired-sample Wilcoxon signed rank test. In this study, SPSS version 17.0 (SPSS, Chicago, IL, USA) was used for statistical analysis, and $P < 0.05$ was set as the level of significance.

3. Results

This study included 29 patients (16 males and 13 females) with lumbar degenerative diseases, with a mean age of 59.4 ± 9.1 years (range 42-74 years), operation time of 87.1 ± 10.1 min (range 65-110 min), intraoperative blood loss of 72.8 ± 40.6 ml (range 35 ml-250 ml), postoperative ambulatory time of 1.69 ± 1.0 days (range 1-5 days), hospitalization time of 2.6 ± 1.3 days (range 1-7 days), and follow-up period of 22.34 ± 4.2 months (range 12-24 months). The VAS for preoperative leg pain was 7.5 ± 0.7, the VAS for preoperative back pain was 4.4 ± 1.3, the VAS for leg pain 1 month postoperation was 1.3 ± 0.8, the VAS for back pain 1 month postoperation was 1.7 ± 0.9, the VAS for leg pain 12 months postoperation was 0.9 ± 0.7, the VAS for back pain 12 months postoperation was 0.5 ± 0.6, the preoperative ODI (%) was 61.0 ± 4.6, the ODI (%) 1 month postoperation was 19.5 ±

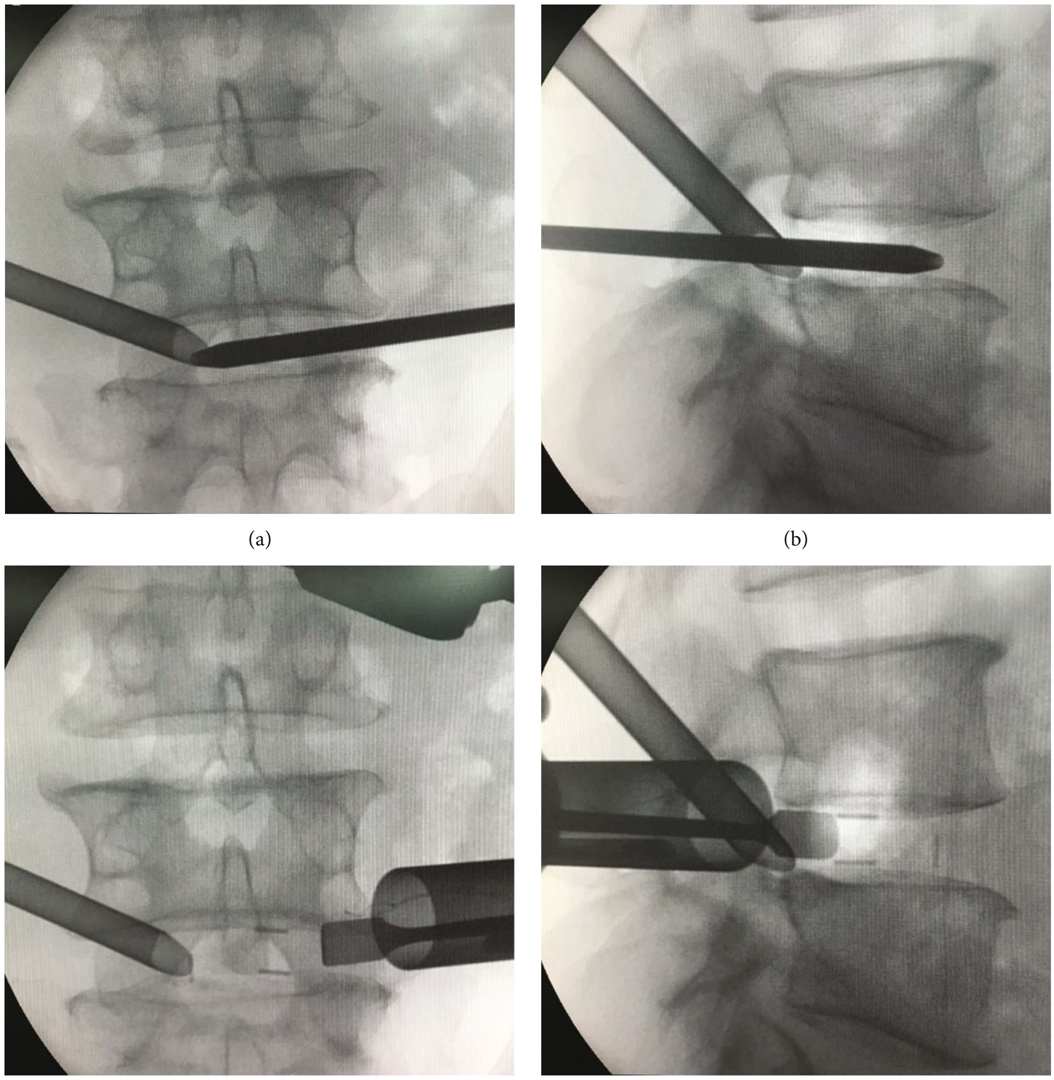

Figure 2: Intraoperative fluoroscopy. Working channel of PETD and primary guide rod of ME-TKT-LIF (a, b). Two working channel, exiting nerve root retractor, and cage (c, d).

4.0, and the ODI (%) 12 months postoperation was 17.6 ± 2.4. The VAS and ODI scores before and after the operation were significantly different ($P \leq 0.001$). At the last follow-up, 28 (28/29) cases demonstrated solid fusion through computed tomography and flexion-extension lateral radiography, and the fusion rate was 96.6%. According to the modified MacNab criteria, 11 (11/29) cases were rated as excellent, 15 (15/29) as good, and 3 (3/29) as fair, and the excellent and good rate was 89.7% (Table 2).

4. Discussion

For lumbar degenerative diseases requiring interbody fusion, various procedures such as MIS-TLIF, ME-TLTF, PE-TLIF, BE-TLIF, and End-LIF have been developed at present [4–8]. These techniques are superior to traditional open surgery in trauma, bleeding volume, and postoperative rehabilitation [13]. As described in the literature, surgical approaches can be divided into posterolateral approaches and trans-Kambin's triangle approaches. The advantage of the posterolateral approach is that the central spinal canal and the traversing nerve roots can be effectively decompressed but require excessive resection of normal anatomical structures, such as the articular process joint, laminae, ligamentum flavum, and epidural fat. After these normal tissues are excised, obvious epidural scars will form postoperatively [14, 15]. In contrast to the posterolateral approach, the trans-Kambin's triangle approach required only the resection of approximately 1/4 of the superior articular process while preserving most of the normal anatomy. However, this approach can only decompress the exiting nerve root, with limited decompression for the traversing root and spinal canal [16, 17]. The efficacy of PELD for spinal canal decompression has been demonstrated [10]. The bilateral

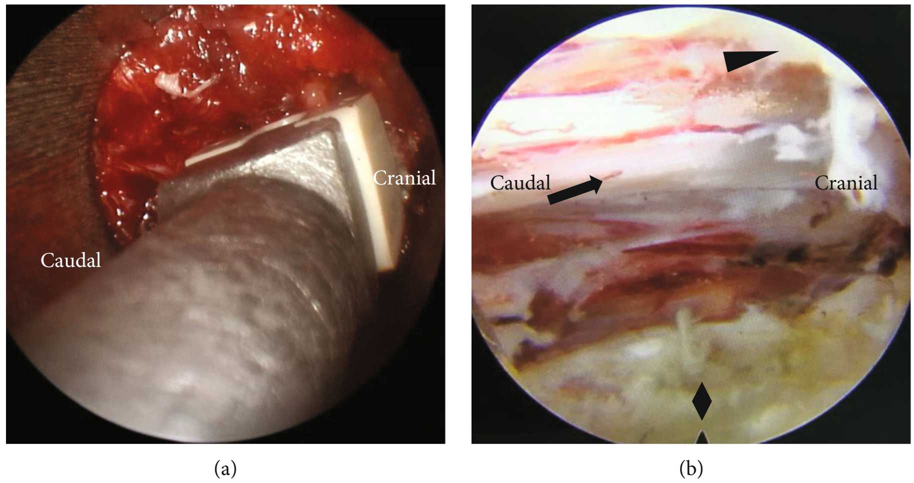

FIGURE 3: Intraoperative images of ME-TKT-LIF, cage was implanted under microscopic endoscope (a). Intraoperative images of PETD, ligamentum flavum (triangle), traversing nerve root (arrow), intervertebral disc (rhombus) (b).

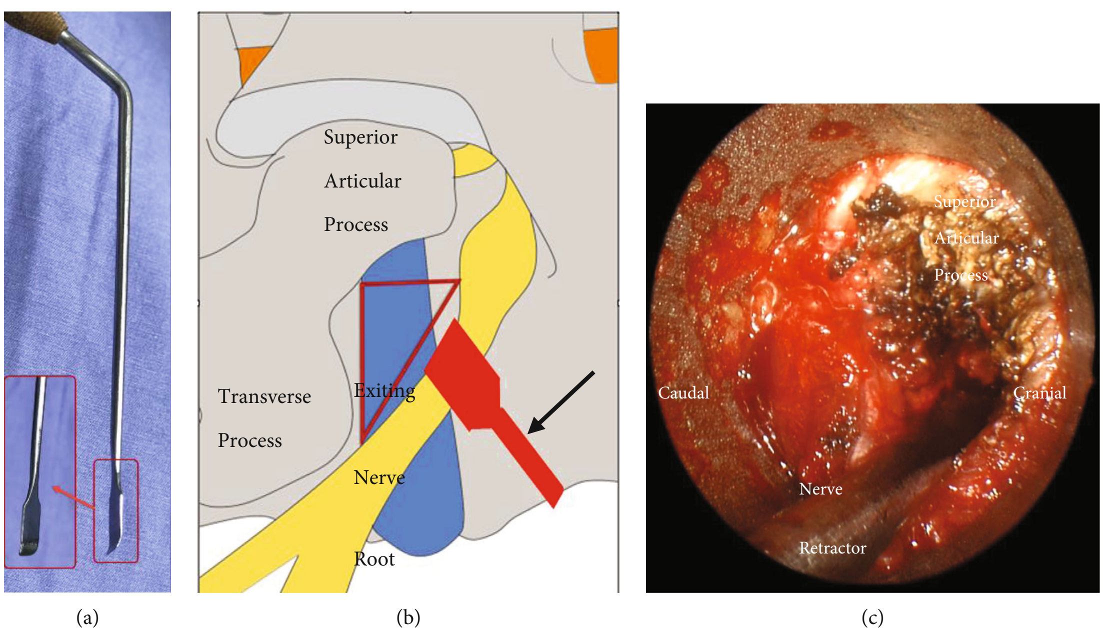

FIGURE 4: Special nerve retractor (a). Anatomy graph that showed the special nerve retractor dilating the exiting nerve root to enlarge the Kambin's Triangle. Red triangle line was the Kambin's triangle. The black arrow pointed to the special nerve retractor (b). Surgical vision of working place under the ME-TKT-LIF system. The superior articular process was partially resected under endoscope (c).

endoscope technology introduced in this paper combines trans-Kambin's triangle approach and PELD to complement each other's shortcomings.

ME-TKT-LIF was developed on the basis of MED. ME-TKT-LIF is an air-based endoscopic lumbar fusion procedure, and the operating instruments are similar to those of traditional open surgery. However, the surgery was performed under the channel and endoscope, and the learning curve was steep. The primary guide rod of ME-TKT-LIF is passed through Kambin's triangle into the intervertebral space at an angle of approximately 45°, similar to the YESS technique [18]. The working channel is placed at the external orifice of the intervertebral foramen, with the superior articular process as the fulcrum. The dural sac and the traversing nerve root are not exposed, and the exiting nerve root is protected by the nerve root retractor under visualization. The height and width of the lumbar Kambin's triangle are 12-18 mm and 10-12 mm, respectively [19]. According to the description of Andrew [20], Kambin's triangle is a Mitsubishi cone with a small outer part and a large inner part, so only approximately 1/4 of the superior articular process needs to be removed to complete the implantation of the cage. ME-TKT-LIF uses a large 22-mm channel with extensive and reasonable removal of the annulus fibrosus and the cartilage endplate under full endoscopy. The unrestricted choice of cage size and type, along with adequate interbody

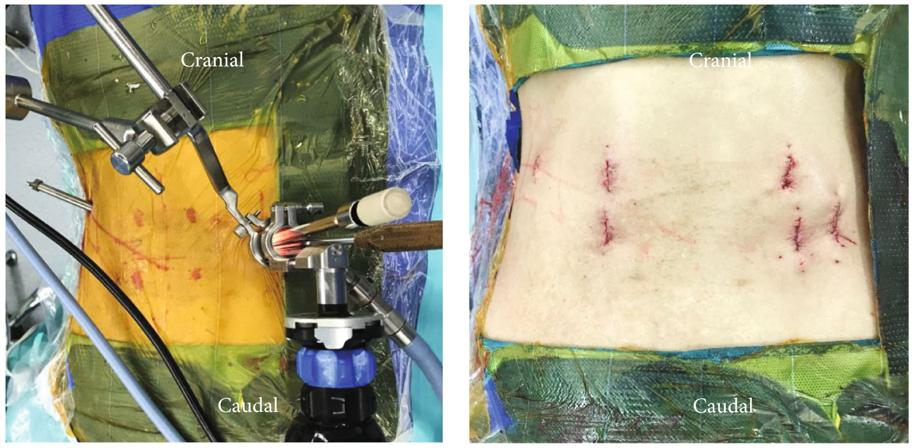

(a) (b)

Figure 5: Panoramic photograph of the percutaneous bilateral endoscope technology (a). The photo shows the stitched incision (b).

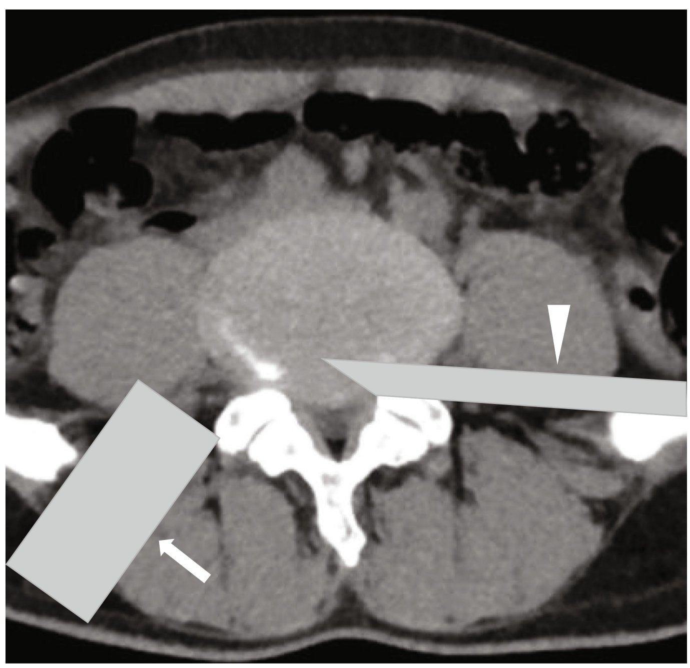

Figure 6: Pattern diagram of the location of the two working channels during the operation, PETD working channel (triangle) on the symptomatic side, ME-TKT-LIF working channel (arrow) on the opposite side.

bone grafting, is prerequisite for improved fusion rates. The articular process, ligamentum flavum, posterior longitudinal ligament, and epidural fat were not removed, thus reducing the possibility of epidural scar formation and shortening the operation time. The complications of PE-TLIF have been reported in the literature to be 20% to 35%, mainly including endplate collapse, fusion failure, and pedicle screw or rod fracture [21]. Only expandable cages or small cages can be used in PE-TLIF due to the working channel diameter of 10–12 mm.

The ME-TKT-LIF procedure is an indirect decompression process for the central spinal canal. Obviously, in patients with symptoms of radioneuralgia, indirect decompression alone is not feasible. However, the most obvious advantage of PETD is the direct and accurate decompression of the spinal canal while preserving normal anatomical structures such as the articular process joint, ligamentum flavum, and epidural fat. The establishment of the working channel of ME-TKT-LIF and PETD is performed simultaneously on different side, which can reduce the numbers of fluoroscopic examination and shorten the operation time. In this technique, the establishment of the working channels of ME-TKT-LIF and PETD all depends on the integrity of the superior articular process. PETD and ME-TKT-LIF both need to use the primary guide rod first. The primary guide rod, approximately 4 mm in diameter and blunt in tip, is inserted with its direction pointing to the superior articular process. After the tip of the guide rod reach the superior

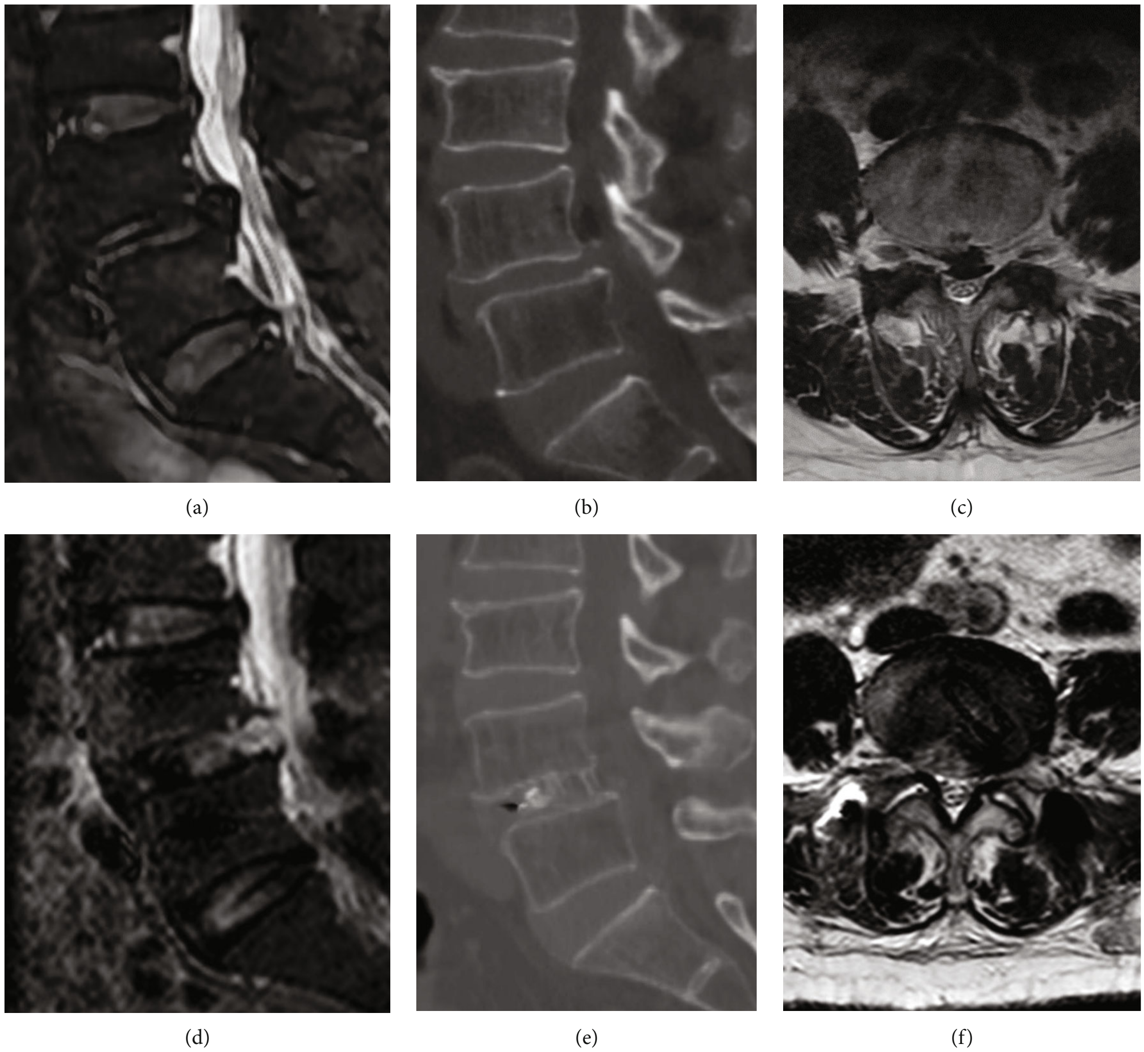

Figure 7: Case examples with pre- and postoperative magnetic resonance imaging (MRI) scans and computed tomography (CT) scans. A 73-year-old female patient was diagnosed as lumbar spondylolisthesis before operation. Preoperative sagittal MRI scan (a), preoperative sagittal CT scan (b), preoperative transverse MRI scan (c), postoperative sagittal MRI scan (d), postoperative sagittal CT scan (e), and postoperative transverse MRI scan (f).

articular process, the guide rod is slid to the ventral side and into the intervertebral disc through the intervertebral foramen. If the two processes performed on the same side, after the PETD is finished, the superior articular process is incomplete. In ME-TKT-LIF, the primary guide rod cannot utilize this anatomy; it is hard to establish a working channel and the risk of nerve root increase. The operation was performed under general anesthesia, and the peripheral nerves involved were monitored using somatosensory-evoked potentials, motor-evoked potentials, and electromyography, which improved patient comfort and ensured safety. The primary guide with a diameter of 4 mm and a bullet-shaped tip also help to avoid injury to the exiting nerve roots.

The mean operative time in this study was 87.1 ± 10.1 min. During the operation, it is not necessary to resect the articular process joint, and the simultaneous placement of the working channel on both sides can help to shorten the operation time. The mean intraoperative bleeding volume was 72.8 ± 40.6 ml. The mean postoperative ambulation time was 1.69 ± 1.0 days, and the mean hospital stay was 2.6 ± 1.3 days. Similar to other minimally invasive endoscopic lumbar fusion techniques, this technique outperforms MIS-TLIF in terms of bleeding volume, postoperative ambulation time, and hospital stay. The mean time to ambulation and discharge after MIS-TLIF is up to 3.2 days and 9.3 days, respectively [22]. For MIS-TLIF, most surgeons used a retractor in combination with a microscope [23], while we used a series of expanding cannulae and a working channel. ME-TKT-LIF is an endoscopic TLIF, not a microscope-assisted TLIF. The retractor is more traumatic to the muscle than to the channel [24]. ME-TKT-LIF utilizes the natural structure of the intervertebral foramen, and the angle and direction of its working channel can be easily adjusted without removing the zygapophyseal joint, thus completing the endplate preparation well. However, MIS-TLIF requires the resection of more normal anatomical structures to complete the decompression of the target area. In the present study,

Table 2: characteristics of clinical outcome.

Characteristics	Values
Follow-up period	22.34 ± 4.2
Blood loss	72.8 ± 40.6 ml
Operation time	87.1 ± 10.1 min
Postoperative ambulatory time	1.69 ± 1.0 days
Hospitalization time	2.6 ± 1.3 days
VAS for leg pain	
Preoperative	7.5 ± 0.7
1 month postoperative	1.3 ± 0.8 ($P \leq 0.001$)
12 months postoperative	0.9 ± 0.7 (P ≤ 0.001)
VAS for back pain	
Preoperative	4.4 ± 1.3
1 month postoperative	1.7 ± 0.9 (P ≤ 0.001)
12 months postoperative	0.5 ± 0.6 ($P \leq 0.001$)
ODI (%)	
Preoperative	61.0 ± 4.6
1 month postoperative	23.1 ± 6.6 ($P \leq 0.001$)
12 months postoperative	20.1 ± 5.1 (P ≤ 0.001)
MacNab	
Excellent	11(11/29)
Good	15(15/29)
Fair	3(3/29)
Poor	0
Excellent and good rate	89.7%

Note: mean values are presented as mean ± standard deviation; $P \leq 0.001$ versus preoperative data.

the postoperative VAS score (back pain and leg pain) and ODI both improved significantly compared to presurgery scores. Preoperatively, the patient presented with intermittent claudication and radicular pain in the lower extremities, and the mean VAS score for leg pain was higher than the mean VAS score for back pain. The decompression of the dural sac and nerve root by PETD ensures satisfactory short-term postoperative efficacy. This study showed that the fusion rate and efficacy satisfaction of this technique reached 96.6% and 89.7%, respectively. The use of a large 22-mm channel can both adequately and effectively resect the diseased intervertebral disc and implant an intervertebral cage of the same size as that for open surgery to ensure osseous fusion. Previous studies have shown that lumbar intervertebral fusion employs a stand-alone endoscopic TLIF procedure with a complication rate of up to 36% [25]. Therefore, fusion should be accompanied by percutaneous pedicle screws or others internal fixation. ME-TKT-LIF and percutaneous pedicle screws provide the assurance of satisfactory rates of long-term therapeutic results.

In one case, the symptoms of lower extremity pain were not resolved significantly after surgery, and MRI examination revealed partial residue in the spinal canal. After conservative treatment, the VAS score at 1 month was 2. Intraoperative incomplete decompression was considered. At the last follow-up, computed tomography of one patient showed no obvious trabecular bone bridge in the intervertebral space, and the patient had no symptoms. Measures to continue follow-up observations were given.

This research and this technology have deficiencies. First, the sample size of this study was small, there was an absence of a control group, and the mean follow-up period was not long enough, which may not be sufficient to prove the effectiveness of this procedure. Second, surgeons need to be proficient in both endoscopic techniques, and the learning curve is steep. Third, ME-TKT-LIF and PETD are mechanical combinations in this technology, and a better model needs to be developed.

5. Conclusion

Under appropriate patient selection and surgical indications, the percutaneous bilateral endoscopy technique is effective and feasible for the treatment of lumbar degenerative diseases, with the advantage that more normal anatomical structures are preserved. It is an optional method of lumbar interbody fusion.

Data Availability

The data used to support the findings of this study are available from the corresponding author upon request.

Conflicts of Interest

The authors declare that they have no conflicts of interest.

References

[1] M. M. Smith and K. T. Foley, "Microendoscopic discectomy," *Neurosurgery*, vol. 3, pp. 301–307, 1997.

[2] S. Ruetten, M. Komp, H. Merk, and G. Godolias, "Use of newly developed instruments and endoscopes: full-endoscopic resection of lumbar disc herniations via the interlaminar and lateral transforaminal approach," *Journal of Neurosurgery: Spine*, vol. 6, no. 6, pp. 521–530, 2007.

[3] J. Mlaka, R. Rapcan, M. Burianek et al., "Endoscopic discectomy as an effective treatment of a herniated intervertebral disc," *Bratislavske lekarske listy*, vol. 121, no. 3, pp. 199–205, 2020.

[4] Y. Ahn, M. S. Youn, and D. H. Heo, "Endoscopic transforaminal lumbar interbody fusion: a comprehensive review," *Expert Review of Medical Devices*, vol. 16, no. 5, pp. 373–380, 2019.

[5] E. He, J. Guo, Q. Ling, Z. X. Yin, Y. Wang, and M. Li, "Application of a narrow-surface cage in full endoscopic minimally invasive transforaminal lumbar interbody fusion," *International Journal of Surgery*, vol. 42, pp. 83–89, 2017.

[6] J. Hwa Eum, D. Hwa Heo, S. K. Son, and C. K. Park, "Percutaneous biportal endoscopic decompression for lumbar spinal stenosis: a technical note and preliminary clinical results," *Journal of neurosurgery: Spine*, vol. 24, no. 4, pp. 602–607, 2016.

[7] W. Wu, S. Yang, W. Diao et al., "Analysis of clinical efficacy of endo-LIF in the treatment of single-segment lumbar degenerative diseases," *Journal of Clinical Neuroscience*, vol. 71, pp. 51–57, 2020.

[8] M. S. Youn, J. K. Shin, T. S. Goh, and J. S. Lee, "Full endoscopic lumbar interbody fusion (FELIF): technical note," *European Spine Journal*, vol. 27, no. 8, pp. 1949–1955, 2018.

[9] J. P. G. Kolcun, G. D. Brusko, G. W. Basil, R. Epstein, and M. Y. Wang, "Endoscopic transforaminal lumbar interbody fusion without general anesthesia: operative and clinical outcomes in 100 consecutive patients with a minimum 1-year follow-up," *Neurosurgical Focus*, vol. 46, no. 4, pp. E14–E14, 2019.

[10] J. Wu, H. Liu, S. Ao et al., "Percutaneous endoscopic lumbar interbody fusion: technical note and preliminary clinical experience with 2-year follow-up," *BioMed Research International*, vol. 2018, Article ID 5806037, 8 pages, 2018.

[11] D. H. Heo, D. C. Lee, H. S. Kim, C. K. Park, and H. Chung, "Clinical results and complications of endoscopic lumbar interbody fusion for lumbar degenerative disease: a meta-analysis," *World Neurosurgery*, vol. 145, pp. 396–404, 2021.

[12] R. R. Shah, S. Mohammed, A. Saifuddin, and B. A. Taylor, "Comparison of plain radiographs with CT scan to evaluate interbody fusion following the use of titanium interbody cages and transpedicular instrumentation," *European Spine Journal*, vol. 12, no. 4, pp. 378–385, 2003.

[13] Z. Ba, F. Pan, Z. Liu et al., "Percutaneous endoscopical transforaminal approach versus PLF to treat the single-level adjacent segment disease after PLF/PLIF: 1 -2 years follow-up," *International Journal of Surgery*, vol. 42, pp. 22–26, 2017.

[14] M. Annertz, B. Jönsson, B. Strömqvist, and S. Holtås, "No relationship between epidural fibrosis and sciatica in the lumbar postdiscectomy syndrome. A study with contrast-enhanced magnetic resonance imaging in symptomatic and asymptomatic patients," *Spine*, vol. 20, pp. 449–453, 1995.

[15] S. Ruetten, O. Meyer, and G. Godolias, "Epiduroscopic diagnosis and treatment of epidural adhesions in chronic back pain syndrome of patients with previous surgical treatment: first results of 31 interventions," *Zeitschrift fur Orthopadie und ihre Grenzgebiete*, vol. 140, no. 2, pp. 171–175, 2002.

[16] P. H. Wu, H. S. Kim, Y. J. Lee et al., "Uniportal full endoscopic posterolateral transforaminal lumbar interbody fusion with endoscopic disc drilling preparation technique for symptomatic foraminal stenosis secondary to severe collapsed disc space: a clinical and computer tomographic study with technical note," *Brain Sciences*, vol. 10, no. 6, p. 373, 2020.

[17] D. H. Heo, Y. H. Hong, D. C. Lee, H. J. Chung, and C. K. Park, "Technique of biportal endoscopic transforaminal lumbar interbody fusion," *Neurospine*, vol. 17, Suppl 1, pp. S129–S137, 2020.

[18] A. T. Yeung, "Minimally invasive disc surgery with the yeung endoscopic spine system (YESS)," *Surgical Technology International*, vol. 8, pp. 267–277, 1999.

[19] R. Hoshide, E. Feldman, and W. Taylor, "Cadaveric analysis of the Kambin's triangle," *Cureus*, vol. 8, article e475, 2016.

[20] A. A. Fanous, L. M. Tumialán, and M. Y. Wang, "Kambin's triangle: definition and new classification schema," *Journal of Neurosurgery: Spine*, vol. 32, 2020.

[21] S. Lee, H. Y. Erken, and J. Bae, "Percutaneous transforaminal endoscopic lumbar interbody fusion: clinical and radiological results of mean 46-month follow-up," *BioMed Research International*, vol. 2017, Article ID 3731983, 9 pages, 2017.

[22] F. Shunwu, Z. Xing, Z. Fengdong, and F. Xiangqian, "Minimally invasive transforaminal lumbar interbody fusion for the treatment of degenerative lumbar diseases," *Spine*, vol. 35, no. 17, pp. 1615–1620, 2010.

[23] R. E. Isaacs, V. K. Podichetty, P. Santiago et al., "Minimally invasive microendoscopy-assisted transforaminal lumbar interbody fusion with instrumentation," *Journal of Neurosurgery: Spine*, vol. 3, no. 2, pp. 98–105, 2005.

[24] Y. Kou, J. Chang, X. Guan, Q. Chang, and H. Feng, "The endoscopic lumbar interbody fusion and minimally invasive transforaminal lumbar interbody fusion for the treatment of lumbar degenerative diseases: a systematic review and meta-analysis," *World Neurosurgery*, vol. 152, pp. e352–e368, 2021.

[25] F. Jacquot and D. Gastambide, "Percutaneous endoscopic transforaminal lumbar interbody fusion: is it worth it?," *International Orthopaedics*, vol. 37, no. 8, pp. 1507–1510, 2013.

Hindawi
BioMed Research International
Volume 2022, Article ID 5564604, 13 pages
https://doi.org/10.1155/2022/5564604

Research Article

Clinical Application Study of Minimally Invasive Double-Reverse Traction in Complex Tibial Plateau Fractures

Faqi Cao,[1] Hang Xue,[1] Chenchen Yan,[1] Ze Lin,[1] Bobin Mi,[1] Adriana C. Panayi,[2] Tian Xia,[1] Wu Zhou,[1] Hui Li,[1] and Guohui Liu[1]

[1]*Department of Orthopedics, Union Hospital, Tongji Medical College, Huazhong University of Science and Technology, 1277 Jiefang Avenue, Wuhan, 430022 Hubei, China*
[2]*The Division of Plastic Surgery, Brigham and Women's Hospital, Harvard Medical School, Boston, MA, USA*

Correspondence should be addressed to Wu Zhou; 2016xh0120@hust.edu.cn, Hui Li; 513706563@qq.com, and Guohui Liu; liuguohui@hust.edu.cn

Received 6 January 2021; Revised 21 August 2021; Accepted 6 December 2021; Published 22 January 2022

Academic Editor: Harry Schroeder

Copyright © 2022 Faqi Cao et al. This is an open access article distributed under the Creative Commons Attribution License, which permits unrestricted use, distribution, and reproduction in any medium, provided the original work is properly cited.

The aim of this study was to evaluate the clinical application of double-reverse traction for minimally invasive reduction of complex tibial plateau fractures. A retrospective analysis was performed to identify all patients admitted to the Department of Orthopedics, Union Hospital, Tongji Medical College, Huazhong University of Science and Technology, from March 2017 to December 2019 with Schatzker type VI tibial plateau fractures. 12 patients were identified (7 men and 5 women) with an average age of 46.15 ± 13 (39-58) years old. All patients were treated with double-reverse traction and closed reduction. After the fracture was reduced, the bone plate was fixed by percutaneous minimally invasive implantation. Outcomes assessed in this study include operation time and intraoperative blood loss. Imaging was performed during the postoperative follow-up, and functional recovery was evaluated at the final follow-up according to the Hospital for Special Surgery (HSS) score and the International Knee Joint Literature Committee (IKDC) functional score. Patients were followed up for 12.54 ± 1.5 (8-15) months. The average operation time was 63.63 ± 21 (35-120) minutes, and the average intraoperative blood loss was 105.45 ± 21 (60-200) mL. The Rasmussen imaging score was either excellent or good in all cases. The knee joint HSS score was 86.15 ± 6 (79-90) points, and the IKDC score was 80.01 ± 11 (75-90) points. No complications, such as wound infection, incision disunion, loosening of internal fixation, and internal fixation failure, occurred. In the treatment of Schatzker VI type complex tibial plateau fracture, the dual-reverse traction minimally invasive technique has the advantages of safety and effectiveness, less soft tissue injury, and allowing early joint movement, which is worthy of clinical promotion.

1. Introduction

Tibial plateau fractures are common intra-articular fractures in the adult population, accounting for 1.66% of total body fractures. The Schatzker classification is currently one of the most widely implemented clinical fracture classifications [1]. Schatzker II-VI fractures account for 85.85% of tibial plateau fractures, with Schatzker type VI fractures, which are caused by high-energy injuries, often causing severe peripheral soft tissue damage, joint collapse, and tibial condylar separation. Successful treatment of such fractures is a notable challenge in the field of orthopedic trauma [2].

The current conventional treatment of tibial plateau fractures consists of conservative management, internal fixation, external fixation, and joint replacement. Moreover, as for Schatzker type VI tibial plateau fractures, the current mainstream approach mainly involves double-incision and double-plate therapy accompanied by arthroscopic treatment. However, when patients receive such conventional treatments, they may suffer iatrogenic trauma, which aggravates soft tissue damage and increases the incidence of complications such as postoperative infection [3]. The prognostic complications mentioned above all cause great difficulties for clinicians and need to be fixed urgently. Therefore, minimally invasive reduction and fixation offers great potential for the treatment of such fractures. The double-reverse traction repositor (DRTR), developed by Professor Yingze Zhang, has shown significant advantages in the treatment of complex tibial plateau fractures. This surgical method, noted to be simple and quick, allows for minimally invasive reduction and fixation with few postoperative complications. In the current study, we assess the outcomes of 12 patients with complex type VI tibial plateau fractures who were treated with the DRTR. The purpose of this study is to assess the efficacy of the DRTR surgical technique as a minimally invasive treatment of type VI tibial plateau fractures and to demonstrate the safety and efficacy of this technique by roughly comparing it with those associated with common-sense open internal fixation [4].

2. Materials and Methods

2.1. Patient Information. We retrospectively analyzed 12 patients (7 men and 5 women) with Schatzker type VI tibial plateau fractures who had been admitted to the Department of Orthopedics, Union Hospital, Tongji Medical College, Huazhong University of Science and Technology, from March 2017 to December 2019. The average age of the patients was 46.15 ± 13 (39-58) years old. Cause of injury included motor vehicle accidents (6 patients), electric vehicle falls (4 patients), and crush injuries (2 patients). All patients underwent relevant assessment during admission to exclude surgical contraindications. The average time from injury to operation was 8.52 ± 3 days. The classification of the damage of the soft tissue adopted AO-IC, IC-1(3 patients), IC-2(8 patients), and IC-3(1 patient), (Table 1).

2.2. Inclusion and Exclusion Criteria. We included all patients: (1) between 18-65 years, (2) with Schatzker VI tibial plateau fractures, (3) with injuries due to high-energy velocity and torsion, (4) with normal lower limb function prior to injury, (5) who had a closure time from injury to surgery of less than 3 weeks patients, (6) with no other peri-knee fractures, and (7) who agreed to receive minimally invasive treatment with double-reverse traction.

Patients excluded were those (1) with open, knee degeneration, pathological fractures, or severe knee joint degeneration; (2) with a history of peripheral nerve, vascular injury, and compartment syndrome; and (3) with poor general condition or with severe systemic diseases.

This study has been approved by the Medical Ethics Committee of the Union Hospital, and informed consent was obtained from all included patients.

2.3. Method of Operation. All surgeries were performed by the chief physician. Surgery was initiated after satisfactory general anesthesia. The patient was placed in the supine position. φ2.5 mm Kirschner wires were placed on the femoral condyle and the distal tibia. Two traction bows were placed on the Kirschner wire and connected with the double reverse traction repositor. Bone traction must be performed along the long axis of the tibia and extended until the calf muscles are tightened. Reduction of the fracture block was observed under C-arm digital subtracting X-ray system. The force line of the knee joint was adjusted with the double-reverse traction device restoring the length and force line of the front and lateral tibia under C-arm digital subtracting X-ray system. The gap on the outer platform was retracted. The articular surface of the distal femur was used as a guide to restore the articular surface of the tibial plateau during the reduction process. If the articular surface was collapsed, a 2.5 mm guide pin was inserted under fluoroscopy from the inner and lower part of the tibial tubercle about 5 cm below and 1 cm behind the tibial spine. If the medial fracture line involved the positioning point, it could be lowered appropriately. The guide needle was pushed forward to 1 to 2 cm below the collapsed bone mass and, based on the guide pin, a ring drill or a hollow gradient drill to gradually open to about 1.5 cm. Using the self-developed collapsed bone block top rod system to insert into the bone tunnel, adjust the angle and gently tap the end of the top rod under fluoroscopy to gradually lift the collapsed fracture block up and restore the flatness of the articular surface. A bicortical iliac strip of appropriate size is removed from the autogenous iliac bone to support the bone graft through the bone tunnel. After bone grafting, a minimally invasive incision is created and the lateral plate is inserted. A drill is placed horizontally at the proximal end for temporary fixation, a locking screw is placed at the distal end, and the medial plate is inserted. The squeezed bolts are inserted into the positioning holes on the outer plate depth, which is required to determine the length prior to insertion, and the width of the joint surface is reset. Performer adjusts the position of the inner plate on the opposite side to ensure that the bolts pass through the inner plate nail holes. The bolts are tightened, and the tail broken. Finally, screw in the remaining screws of the medial and lateral plates in turn removes the traction frame, grinds the articular surface over the flexion position, and strikes the heel in the extension position to further flatten the articular surface. Routine postoperative arthroscopic exploration showed that the articular surface fractures were reduced well with the step smaller than 2 mm (probing hook diameter). Typical case is shown in Figures 1, 2, and 3.

Patients received routine anticoagulation and detumescence treatment 24 hours after surgery. The quadriceps muscle function was passively exercised on the first day after surgery. The drainage tube was removed on the second day after surgery. After the sixth week, patients were able to start ambulating without weight-bearing. 12 weeks after surgery, depending on the healing condition of the fracture, patients were gradually able to walk with weight.

2.4. Follow-Up and Observation Indicators. The patients were followed up for 1, 3, and 6 months after surgery, and imaging was performed. Final follow-up imaging was scored according to the Rasmussen evaluation standard. The functional recovery of the affected knee joint was evaluated using the New York Special Surgery Hospital (HSS) score and the International Knee Documentation

Table 1: Basic information of included patient.

Group	Number of cases	Gender	Cause of injury	Age	Time before operation	Classification of soft tissue
	Cases	Male/ female	Vehicle accidents/fall injury/crush injuries	Years	Days	IC1/IC2/IC3
DRTR	12	7/5	6/4/2	46.15 ± 13	8.52 ± 3	3/8/1

The data included is of patients who were available at 12 months.

Committee (IKDC) functional score. Postoperative complications were monitored, and intraoperative data such as operation time and intraoperative blood loss were collected.

2.5. Statistical Methods. Data entry and statistical analysis were performed using SPSS13.0 (SPSS Corporation, USA) statistical software. The Kolmogorov-Smirnov test was used to verify whether distribution conforms to normal distribution. The age of patients, time from injury to operation, follow-up time, operation time, and HSS and IKDC scores are expressed as $\bar{x} \pm s$. The α value of the inspection level was set to 0.05.

3. Results and Discussion

All patients underwent successful surgical treatment, and there was no attrition to surgical follow-up. The follow-up time was 8-15 months, with an average of 12 months. One patient had obvious skin contusion before operation and epidermal necrosis after operation which improved with dressing change. All other patients showed no complications such as wound infection and nonunion after operation. Postoperative X-ray imaging in the double-reverse traction group showed satisfactory fracture reduction and proper position of the bone plate and screws. The average operation time was 63.63 ± 21 (35-120) min, and the average intraoperative blood loss was 105.45 ± 21 (60-200) mL. At the final follow-up, all patients scored excellent or good on the Rasmussen imaging score. The average knee HSS score was 86.15 ± 6 (79-90) points, and the average IKDC score was 80.01 ± 11 (75-90) points. Lower limb length difference was 1.12 ± 0.58 (0-2.21) cm.

Tibial plateau fractures are intra-articular fractures with high incidence. Schatzker VI fracture is the most severe type of tibial plateau fracture. It is mostly caused by high-energy impact injuries such as vehicle accidents and falls from heights. Schatzker type VI fractures usually manifest as comminuted fractures which involve the entire tibial condyle and articular surface [5]. They are often accompanied by damage to the cruciate ligament and meniscus, causing serious changes in the normal anatomical relationship of the tibial condyle [6]. Following a Schatzker type VI fracture, the soft tissue around the knee joint has relatively poor blood supply, which can result in wound infection and skin necrosis and even hinder bone union. Current treatment for Schatzker type VI fractures is limited to incision reduction, rigid internal fixation, and early functional exercise. However, the traditional open reduction and internal fixation surgery requires long incisions, large soft tissue damage, long operation time, and large dissection range, and, hence, the incidence of postoperative complications is also higher [7]. The literature supports that maintaining the overall force line of the lower limbs is more important than anatomical reduction of the articular surface. Recovery of the knee joint stability is an important factor affecting the long-term efficacy of tibial plateau fracture treatment [8]. Rehabilitation does not entirely depend on the anatomy of the articular surface. Satisfactory results can be obtained with repositioning if the overall force line of the lower limbs recovers well, even if part of the articular surface is uneven. Koval et al. showed that there was no significant correlation between the reduction of the articular surface as shown through imaging and clinical efficacy.

With the development of biomechanics and their clinical application, it has become evident that fracture treatment should not only aim to restore anatomical position but also protect the soft tissue. Treatment of fractures does not only restore the anatomical position but also allows protection of the soft tissues [9]. This is particularly important in fractures like Schatzker VI tibial plateau, in which the soft tissue around the knee joint is seriously injured, the skin tension is high, and tension blisters easily form, and clinical treatment is more challenging. If the traditional internal and external steel plate is used for fixation, the surgical incision is long, and trauma to the tissue is extensive [10]. A clinical case pointed out that DRTR has achieved good results in the treatment of complex tibial plateau fractures [11]. In addition, studies have also pointed out that DRTR has the advantages of soft tissue damage when dealing with high-energy impact injuries of the knee joint [12]. Concurrently, blood supply to the anterior tibia is poor, and complications such as skin necrosis can easily occur after surgery. The use of minimally invasive technology in the field of orthopedics is receiving more and more attention. The goal of this technology is to minimize soft tissue damage, preserve the blood supply of the fracture as much as possible, and reduce iatrogenic injury. With extensive experience in clinical practice, Professor Yingze Zhang creatively put forward the theory of “homeopathic reduction” of fractures, whereby he recommends conforming to the mechanical axis of the limbs and the soft tissue movement trajectory and resetting the fracture ends through traction. In the surgical treatment of tibial plateau fractures, restoring the lower limb force line and height of the collapsed articular surface while maintaining the stability of the plateau fracture after reduction is the focus of treatment. The double-

(a)

(b)

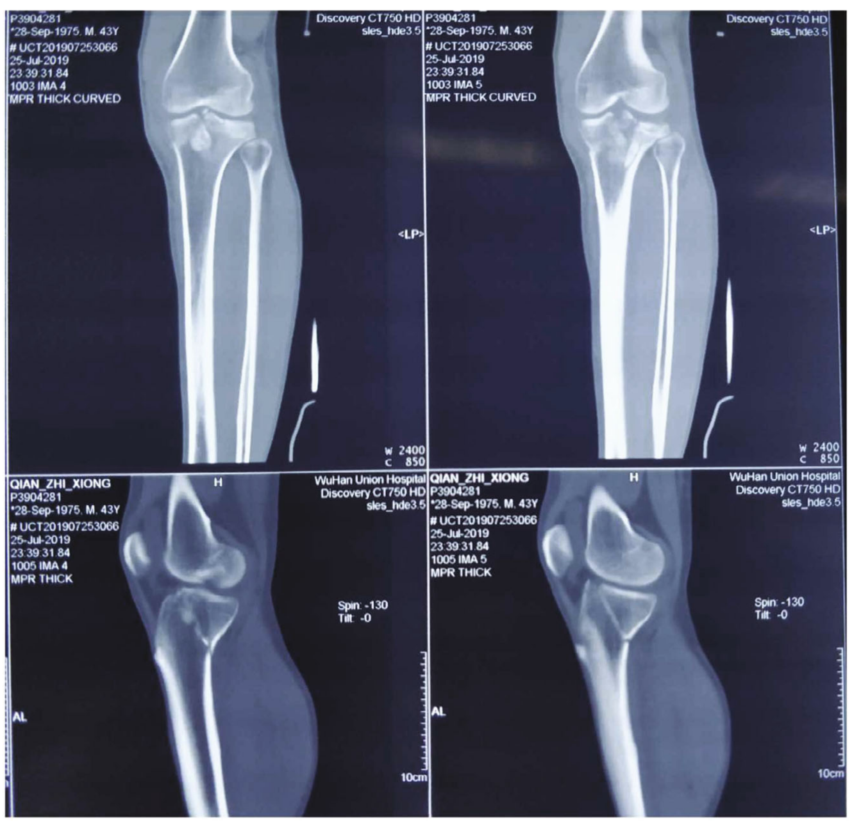

(c)

Figure 1: Continued.

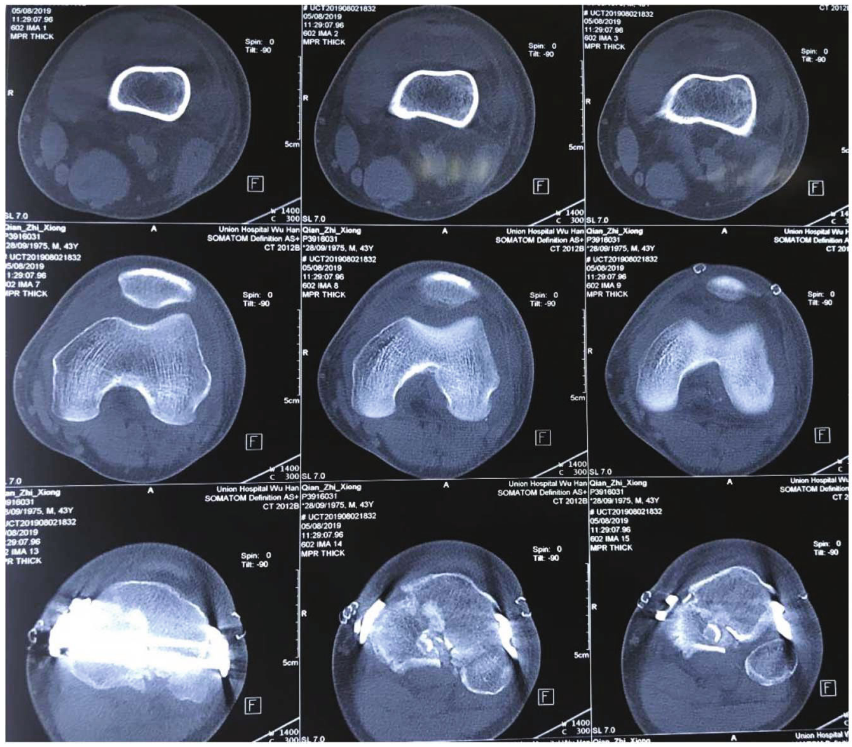

(d)

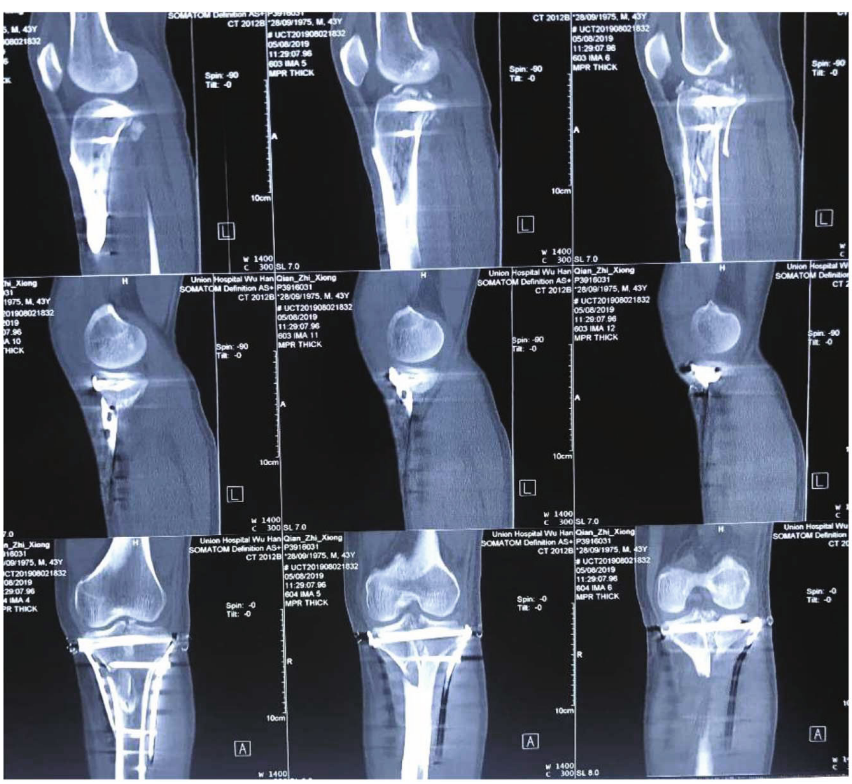

(e)

(f)

Figure 1: Continued.

(g) (h) (i) (j)

Figure 1: Continued.

(k)

(l)

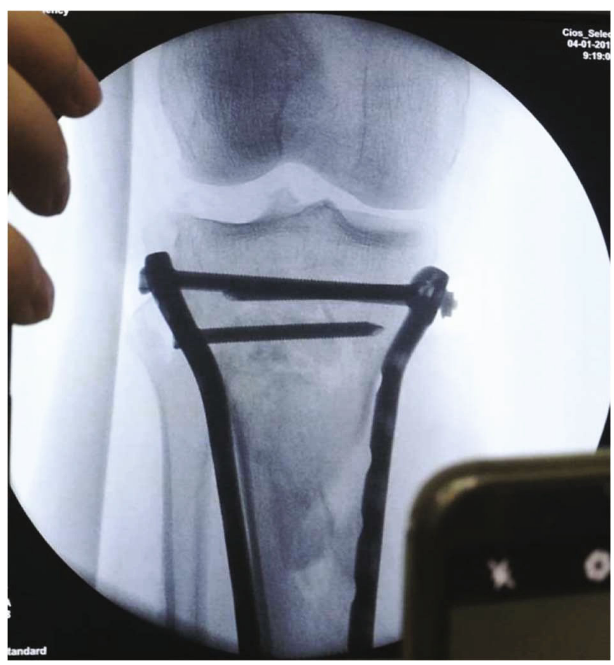

(m)

Figure 1: A 43-year-old male with Schatzker type VI tibial plateau fracture with spur sign. (a, b) X-rays of tibial plateau fracture presurgery. (c–e) Preoperative CT imaging results of the tibial plateau fracture. (f) X-rays of tibial plateau obtained after operation. (g, h) Intraoperative and 3 days postoperative incisions of the entire injured limb.(i) Application of double-reverse traction repositor (DRTR) during operation. (j–m) Intraoperative fluoroscopic X-ray images of the fracture sites before and after the application of the traction device.

reverse traction device developed by Professor Yingze Zhang uses the self-traction of the ligaments around the knee joint and the joint capsule to achieve the reduction and maintenance effect. At the same time, it provides effective traction and can maintain the reduction of the fractured end. This is particularly useful in fractures that require continuous traction and reduction [13].

In this study, the different positions of the double-reverse traction distal device were adjusted to restore the force line of patient's lower limbs, correct the knee joint varus, and effectively maintain the fractured end [14]. Furthermore, the joint was not opened during the operation, avoiding iatrogenic injury of the knee ligament and joint capsule, which is beneficial for the stability and functional

(a)

(b)

(c)

(d)

Figure 2: Continued.

(e) (f) (g)

(h) (i)

Figure 2: Follow-up results of the 43-year-old male mentioned in Figure 1 were obtained at 6 and 13 months after operation. (a, b) X-rays of tibial plateau obtained 6 months after operation. (c, d) X-rays of tibial plateau obtained 13 months after operation. (e, f) Photographs of the knee joint in extended and flexed positions 6 months after operation. (g–i) Photographs of the knee joint in extended, flexed, and feather-weightbearing positions 12 months after operation.

recovery of the knee joint. In patients with obvious articular surface collapse that cannot be recovered, the medial tibial bone tunnel is established ,and the self-made collapsed bone block top rod system is inserted into the bone tunnel. The end of the top rod is gently tapped under fluoroscopy to adjust the angle in order to achieve a gradual lift of the collapsed fracture block, thereby restoring the flatness of the articular surface. An appropriate bicortical iliac strip must be removed from the autogenous iliac bone to support the bone graft in the bone tunnel. In line with the principles of tibial plateau fracture surgery, this procedure firmly fixes the fracture and allows early nonweight-bearing knee exercises and improved limb movements [15]. The minimally invasive treatment concept enabled by the "Zhang Traction Frame" should be a goal pursued both by doctors and patients as, in comparison to the commonly used traction beds in clinical practice, it has great advantages. In addition, it is helpful for large-scale promotion and application in hospitals at all levels across the country. A disadvantage of our study is the fact that it is retrospective, the number of cases is small, and the patients included in the study had no serious other compound injuries that may have caused delays in surgical treatment. In addition, the follow-up time is not very long, and further follow-up of the long-term treatment effect of the operation is needed to evaluate the incidence of osteoarthritis and other data. In a future cohort study, we aim to observe and follow up more cases [16].

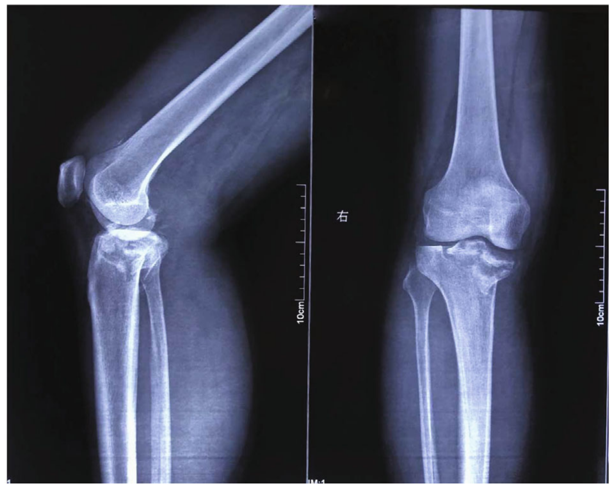

(a)

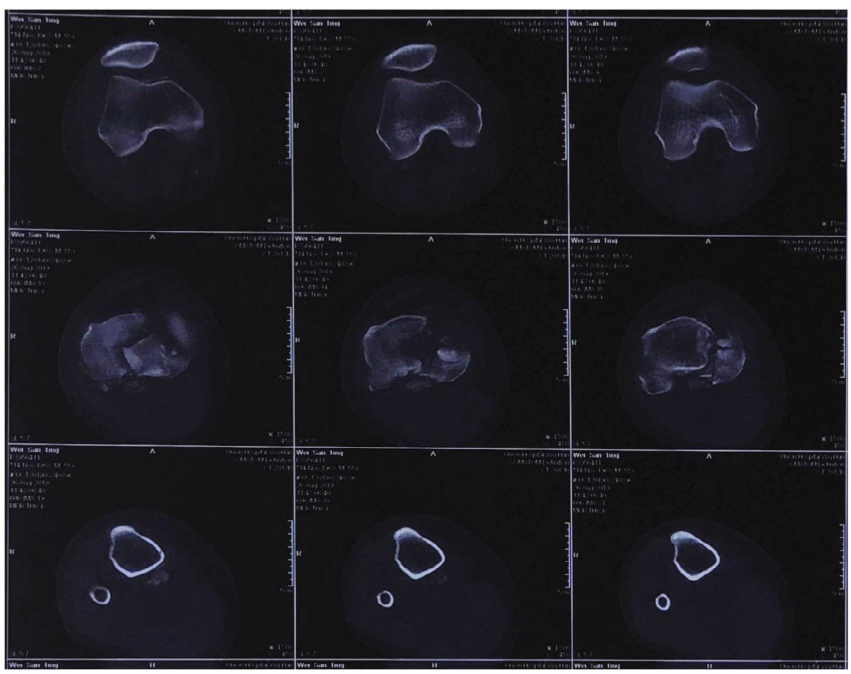

(b)

Figure 3: Continued.

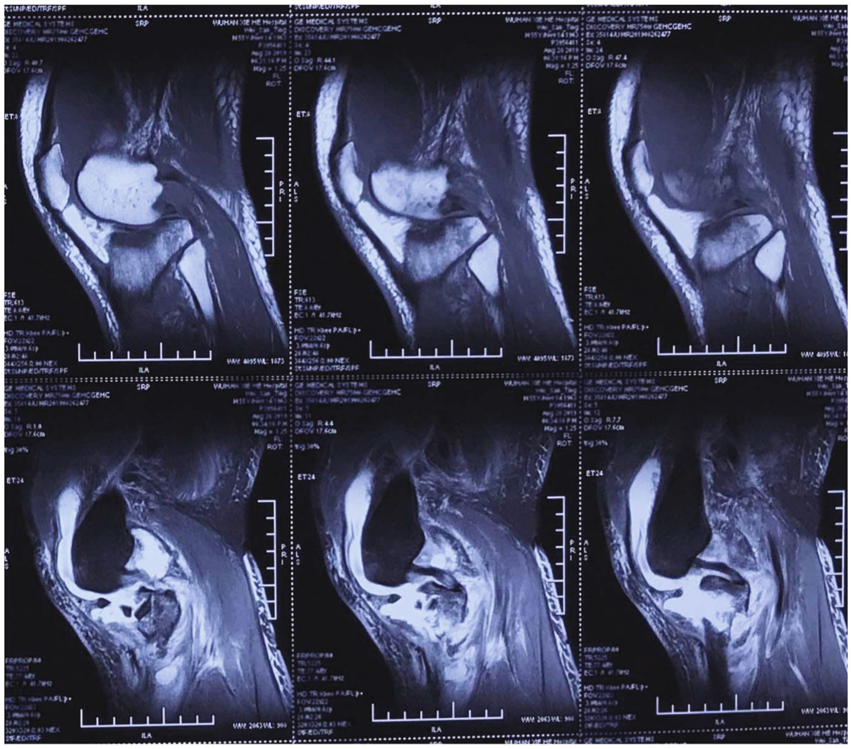

(c)

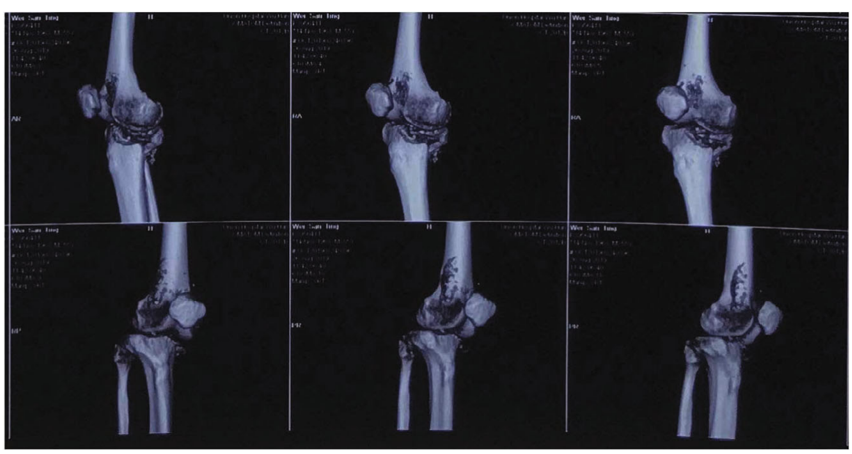

(d)

Figure 3: Continued.

(e) (f)

Figure 3: A 55-year-old male as a typical case of articular surface collapse. (a) X-rays of tibial plateau obtained before operation. (b) CT of tibial plateau obtained before operation. (c) MRI of the knee joint before operation. (d) CT of tibial plateau in 3D before operation. (e) X-rays of tibial plateau obtained right after operation. (f) Postoperative appearance of the affected limb.

In summary, for the treatment of Schatzker type VI tibial plateau fractures caused by high-energy impact injuries, double-reverse traction and minimally invasive closed reduction and internal fixation can achieve satisfactory results in a short period of time. Compared with traditional surgical methods, this technique has obvious advantages and is worthy of increased clinical application.

4. Conclusions

In patients with Schatzker VI complex tibial plateau fractures, minimally invasive double-reverse traction is a treatment method with short operation time, minimal bleeding, quick postoperative recovery, low infection rate, and satisfactory clinical efficacy.

Data Availability

The data used to support the findings of this study are available from the corresponding author upon request.

Conflicts of Interest

The authors declare that there is no conflict of interest regarding the publication of this paper.

Authors' Contributions

Guohui Liu, Hui Li, and Wu Zhou designed the study. Guohui Liu conducted the surgical procedure. Adriana C. Panayi and Bobin Mi collected the data of the study. Faqi Cao, Hang Xue, and Chenchen Yan drafted the manuscript. Hui Li and Guohui Liu revised the manuscript before submission. All authors read and approved the final manuscript. Faqi Cao, Hang Xue, and Chenchen Yan contributed equally to this work.

Acknowledgments

This study was supported by the research project of 2019 Free Innovation Pre-research Fund, Platform Scientific Research Fund, from Union Hospital, Tongji Medical College, Huazhong University of Science and Technology (no. 900002725).

References

[1] C. L. Barnes, J. W. Mesko, S. M. Teeny, and S. C. York, "Treatment of medial compartment arthritis of the knee: a survey of the American Association of Hip and Knee Surgeons," *The Journal of Arthroplasty*, vol. 21, no. 7, pp. 950–956, 2006.

[2] L. Wang, Y. Zhang, Z. Song, H. Chang, Y. Tian, and F. Zhang, "A novel method of using elastic bionic fixation device for distal tibiofibular syndesmosis injury," *International Orthopaedics*, vol. 42, no. 9, pp. 2219–2229, 2018.

[3] P. Yuwen, H. Lv, W. Chen et al., "Age-, gender- and Arbeitsgemeinschaft für Osteosynthesefragen type-specific clinical characters of adult tibial plateau fractures in eighty-three hospitals in China," *International Orthopaedics*, vol. 42, no. 3, pp. 667–672, 2018.

[4] W. Zhao and Y. Zhang, "Comparison and predictive factors analysis for efficacy and safety of Kirschner wire, anatomical plate fixation and cannulated screw in treating patients with open calcaneal fractures," *Medicine*, vol. 98, no. 43, article e17498, 2019.

[5] H. Lv, W. Chen, T. Zhang et al., "Traumatic fractures in China from 2012 to 2014: a national survey of 512,187 individuals," *Osteoporosis International*, vol. 31, no. 11, pp. 2167–2178, 2020.

[6] J. Li and Y. Zhang, "History of orthopaedics in China: a brief review," *International Orthopaedics*, vol. 42, no. 3, pp. 713–717, 2018.

[7] H. Chang, Z. Zheng, D. Shao, Y. Yu, Z. Hou, and Y. Zhang, "Incidence and radiological predictors of concomitant meniscal and cruciate ligament injuries in operative tibial plateau fractures: a prospective diagnostic study," *Scientific Reports*, vol. 8, no. 1, article 13317, 2018.

[8] J. Li, Y. Zhu, B. Liu, T. Dong, W. Chen, and Y. Zhang, "Incidence and risk factors for surgical site infection following open reduction and internal fixation of adult tibial plateau fractures," *International Orthopaedics*, vol. 42, no. 6, pp. 1397–1403, 2018.

[9] Y. Zhu, S. Liu, X. Zhang, W. Chen, and Y. Zhang, "Incidence and risks for surgical site infection after adult tibial plateau fractures treated by ORIF: a prospective multicentre study," *International Wound Journal*, vol. 14, no. 6, pp. 982–988, 2017.

[10] S. Li, Y. Yin, R. Zhang, W. Chen, and Y. Zhang, "Minimally invasive treatment for fractures of lower extremity amputees using a rapid reductor," *International Orthopaedics*, vol. 43, no. 6, pp. 1473–1478, 2019.

[11] D. Q. Li, D. Y. Song, J. D. Ni, M. L. Ding, and J. Huang, "A case report of Schatzker type VI tibial plateau fracture treated with double reverse traction closed reduction combined with minimally invasive percutaneous plate osteosynthesis technique: a case report," *Medicine*, vol. 96, no. 45, article e8394, 2017.

[12] R. Zhang, Y. Yin, S. Li, L. Jin, Z. Hou, and Y. Zhang, "Traction table versus double reverse traction repositor in the treatment of femoral shaft fractures," *Scientific Reports*, vol. 8, no. 1, article 5952, 2018.

[13] W. Chen, H. Lv, S. Liu et al., "National incidence of traumatic fractures in China: a retrospective survey of 512 187 individuals," *The Lancet Global Health*, vol. 5, no. 8, pp. e807–e817, 2017.

[14] Y. Yin, R. Zhang, S. Li, J. Guo, Z. Hou, and Y. Zhang, "Negative-pressure therapy versus conventional therapy on split-thickness skin graft: a systematic review and meta-analysis," *International Journal of Surgery*, vol. 50, pp. 43–48, 2018.

[15] W. Chen, W. C. Lee, H. Y. Chan, P. C. Chang, N. N. Lo, and S. J. Yeo, "Drain use in total knee arthroplasty is neither associated with a greater transfusion rate nor a longer hospital stay," *International Orthopaedics*, vol. 40, no. 12, pp. 2505–2509, 2016.

[16] W. Chen and Y. Zhang, "Prominent and fruitful development of orthopaedic research in China," *International Orthopaedics*, vol. 42, no. 3, pp. 455–459, 2018.

Hindawi
BioMed Research International
Volume 2021, Article ID 2698642, 9 pages
https://doi.org/10.1155/2021/2698642

Research Article

Classification and Treatment Strategies of Concomitant Fibular Column Injuries in Tibial Plateau Fractures

Xiang Yao,[1] **Bin Lv**,[1] **MinJie Hu**,[1] **Jishan Yuan**,[1] **Xiaochen Fan**,[1] **Kaihua Zhou**,[2] **JiLei Tang**,[3] **and Lei Wang**[1]

[1]*Department of Orthopaedics, The Affiliated People's Hospital of Jiangsu University, Zhenjiang, Jiangsu Province 212000, China*
[2]*Department of Orthopaedics, Qingpu Branch of Zhongshan Hospital, Fudan University, Shanghai 201700, China*
[3]*Department of Orthopaedics, Affiliated Qidong Hospital of Nantong University, Nantong 226200, China*

Correspondence should be addressed to Kaihua Zhou; 519706255@qq.com, JiLei Tang; 554849240@qq.com, and Lei Wang; wanglei0505779@126.com

Received 22 May 2021; Accepted 10 August 2021; Published 7 September 2021

Academic Editor: Andrea Scribante

Copyright © 2021 Xiang Yao et al. This is an open access article distributed under the Creative Commons Attribution License, which permits unrestricted use, distribution, and reproduction in any medium, provided the original work is properly cited.

Background. About 1/3 of tibial plateau fractures are associated with proximal fibula fractures, but most proximal fibula fractures are often ignored. The aim of this study was to precisely explain the classification and treatment strategies of six injury types of the fibular column associated with tibial plateau fractures. *Methods*. Patients with ipsilateral proximal fibula and tibial plateau fractures treated in our hospital were retrospectively reviewed from Aug 2007 to Mar 2020. Two experienced surgeons and two radiologists divided fibular column injury into 6 injury types according to the AO classification and four-column nine-segment classification. The treatment scheme (surgically treated or conservatively treated) was also recorded. *Results*. In total, 355 proximal fibula fractures were included. Type 2 fibular head fracture was the most common type of injury in 122, and the segregate of superior tibiofibular syndesmosis was the rarest type in 3. In avulsion injury proximal of fibular pattern, the proportion of patients who need surgical intervention is the highest. *Conclusions*. Six injury types in the four-column nine-segment classification covered all types of bony and soft tissue injuries of the fibular column and concisely explained the injury mechanism. The classification is helpful for the precise judgement and decision-making of the concomitant fibular column injuries in tibial plateau fractures.

1. Introduction

The proximal fibula is close to the posterolateral tibial plateau and is closely connected by the superior tibiofibular syndesmosis. The proximal fibula provides functional stability to the posterolateral structures of the knee and plays a crucial role in the anatomy and clinical function of the knee. The PLC is composed of the fibular collateral ligament (FCL), biceps femoris tendon (BFT), popliteus tendon, and the arcuate complex which consists of the popliteofibular ligament, the arcuate ligament, and the variably present fabellofibular ligament [1]. Proximal fibula fracture represents an injury to the posterior lateral corner (PLC) of the knee, a primary stabilizer of varus stress, external tibial rotation, and posterior tibial translation (3). The repairing of the proximal fibula injury can reconstruct the stability of the posterolateral structures of the knee.

About 1/3 of tibial plateau fractures are combined with proximal fibula fractures, and bone fragment morphology greatly affects the choice of surgical approach and fixation strategy of the tibial plateau fracture. More than 40 kinds of tibial plateau fractures have not been paid enough attention to the often-concomitant proximal fibula fractures. The widely used Schatzker classification 1974 and AO classification 2007 did not mention the fibular fracture [2, 3]. Luo's three-column concept and Schatzker 2018 supplementary classification marked the anterior point of the fibular head as a landmark point merely [4, 5]. A comprehensive and practical classification of proximal fibula fractures associated with tibial plateau fracture is strongly needed.

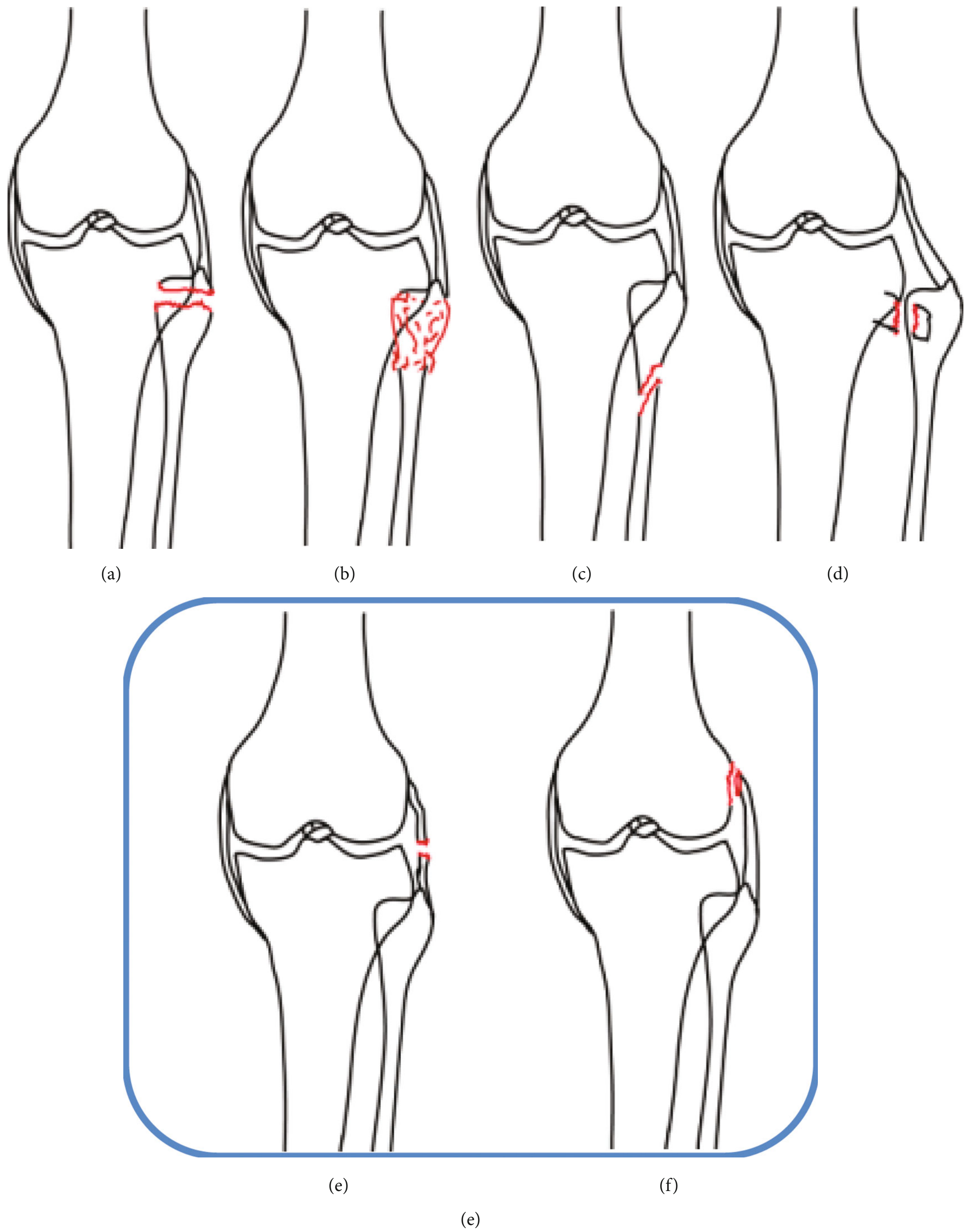

Figure 1: The six morphologies of fibular column injury in the four-column nine-segment classification: (a) type 1: avulsion fracture of fibular apex ("arcuate sign"); (b) type 2: fibular head fracture; (c) type 3: proximal diaphyseal fracture; (d) type 4: proximal tibiofibular joint dislocation; (e) expanding type 1 (EX1): LCL tear; (f) expanding type 2 (EX2): avulsion fracture of lateral femoral condyle.

Focus on the local, Bozkurt et al. first described the classification of proximal fibula combined with TPF in 2005 (type 1, involved avulsion fractures; type 2, fibula head fractures and/or fracture associated with proximal tibiofibular joint; type 3, fibular neck or head and neck fractures; and type 4, fibula proximal diaphysis fractures) [6]. In 2018, we proposed a comprehensive "four-column and nine-segment" classification that described the injury types of the proximal tibia and fibula. We first named the bony and soft tissue structure of proximal fibula as "fibular column" and defined the six new-style injury types [7]. In the AO classification 2018 edition, the proximal fibula fracture was coded independently as 4F1A/4F1B (qualifications: extra-articular or intra-articular) and divided into the simple fracture and multifragmentary fracture [8]. In 2019, Zheng et al. divided this special fracture into five patterns according to

Table 1: Demographic characteristics of patients and fractures.

	Characteristics	
Patients ($n = 352$)	Sex ratio (male/female)	192/160 (1 : 0.83)
	Age (±SD, years)	53.9 ± 13.0
	Age (±SD, years; male/female)	52.6 ± 12.8/56.1 ± 12.8
Knees ($n = 355$)	Left only	207 (58.8%)
	Right only	142 (40.3%)
	Bilateral	3 (0.9%)
	Left/right	210/145 (1 : 0.69)
AO/OTA classification	41.A	31 (8.7%)
	41.B	127 (35.7%)
	41.C	197 (55.4%)
Columns involved ($n = 355$)	1 column	—
	2 columns	85 (23.9%)
	3 columns	149 (41.8%)
	4 columns	121 (33.8%)
TPII ($n = 355$)	Total	7.9 ± 2.6
	Columns	3.1 ± 0.8
	Segments	4.8 ± 2.0
	Male/female	7.9 ± 2.7/8.0 ± 2.6
	Left/right	7.6 ± 2.5/8.0 ± 2.7
	Mild comminuted (2-5)	84 (23.6%)
	Moderate comminuted (6-9)	174 (48.8%)
	Severe comminuted (10-13)	97 (27.1%)

Table 2: Morphology of fractures according to the four-column nine-segment classification.

Column		Segment	
Medial	146	a	109
		b	103
Intermedial	291	c	77
		d	196
		e	177
		f	182
Lateral	313	g	271
		h	246
Fibular	355	i	355

Table 3: The morphology of fibular column injury in the four-column nine-segment classification and related treatment.

	Injury type		Surgically treated	Conservatively treated
Fibular column	Type 1	122	38	84
	Type 2	193	15	178
	Type 3	37	3	34
	Type 4	3	2	1
	Total	355	58	297
	EX1	—		
	EX2	21/1170	6	15

EX1: extending type 1; EX2: extending type 2; "—": data not available.

fracture line and degree of comminution (avulsion fractures, fibular head cleavage fractures, fibular head depressed fractures, comminuted fractures, and fibular neck or shaft fractures). More precisely, Cohen et al. classified the avulsion of fibular head into three subtypes (fibular styloid, fibular head which involves the arcuate complex, and fibular head which involves the metaphyseal) in 2018 [9].

However, there is no literature summarizing the injury mechanism and treatment strategies for this special fracture according to certain classifications to date. The four-column nine-segment classification (Yao classification) seems to be more comprehensive and clear in the current classifications. The aim of this study was to explain the precise treatment strategy of concomitant fibular column injuries in TPFs depending on the four-column nine-segment classification.

2. Methods

After approval was obtained from the authors' institution's human subject review board, medical records, including digital radiologic data of all the patients treated for tibial plateau fracture from Aug 2007 to March 2020, were reviewed. On

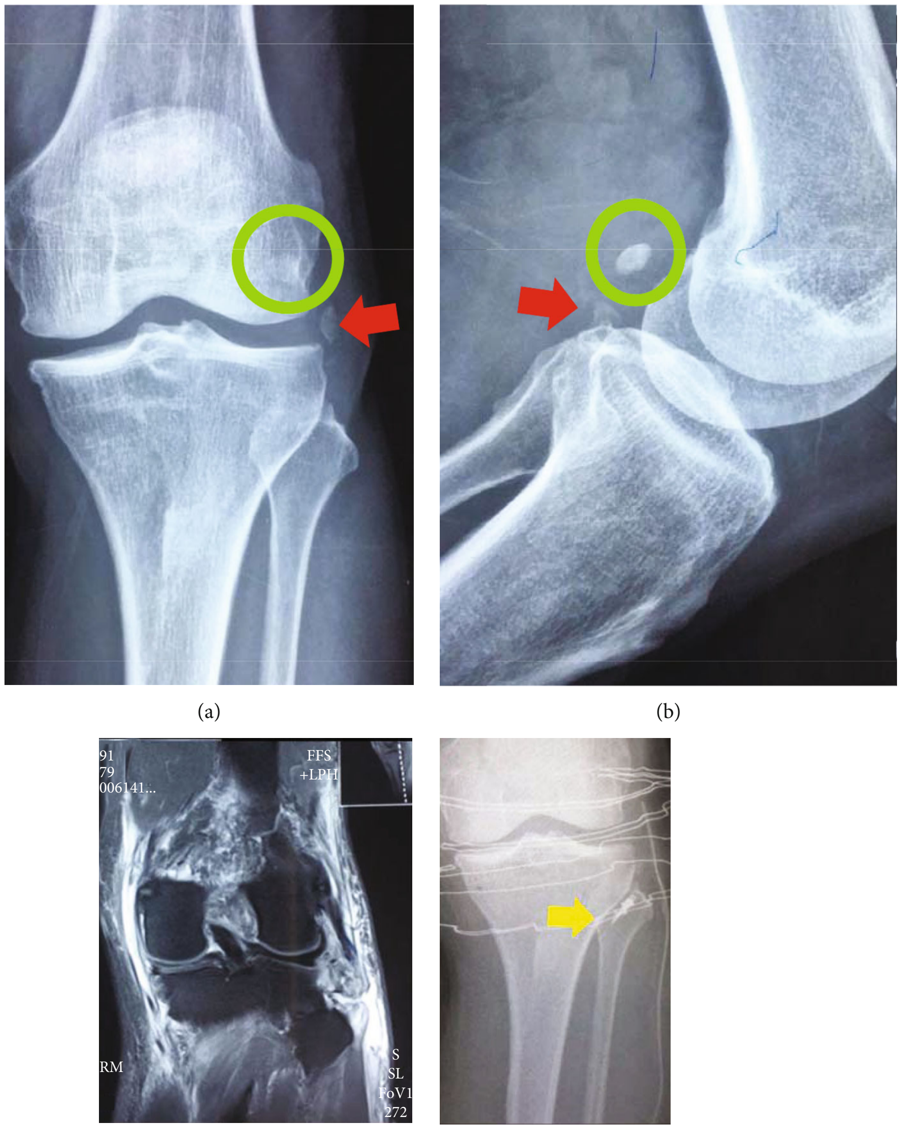

Figure 2: A type 1 fibular column injury case: (a, b) the preoperative X-ray; (c) the MRI shows avulsion of lateral collateral ligament; (d) the avulsion fracture of fibular apex was fixed by suture anchor. Green cycle: sesamoid; red arrow: avulsion fracture of fibular apex; yellow arrow: metal anchor.

admission to the hospital, anteroposterior (AP) and lateral X-ray and 3D computerized tomography (CT) images of the patients were obtained. Four observers, including 2 orthopedic trauma surgeons and 2 radiologists, reviewed the X-ray and computed tomography (CT) and on clinical picture archiving and communication system workstations. The fracture type was determined through consensus by the 4 observers. None of the observers had a conflict of interest regarding the patients. The exclusion criteria were age under 18 years, previous deformity, pathological fracture, inadequate imaging documentation, metabolic bone disease, or a history of knee surgery.

All the tibial plateau fractures were classified according to the AO and "four-column and nine-segment" classification. The tibial plateau injury index (TPII) and treatment scheme (surgically treated or conservatively treated) were also recorded. The six injury types of the fibular column (segment i) were the following: type 1: avulsion fracture of the fibular apex ("arcuate sign"), type 2: fibular head fracture, type 3: proximal diaphyseal fracture, and type 4: proximal tibiofibular joint dislocation. The two expanding types were the following: EX1: LCL tear and EX2: avulsion fracture of the lateral femoral condyle (Figure 1).

2.1. Statistics. Statistical analysis was carried out using IBM SPSS Statistics 19 (SPSS Inc, Chicago, USA). Qualitative data are shown as n (percentage), and quantitative data are expressed as the mean $\pm$ SD. A two-sided t-test was used to determine the significance of differences between the gender and sides. $P < 0.05$ was considered statistically significant.

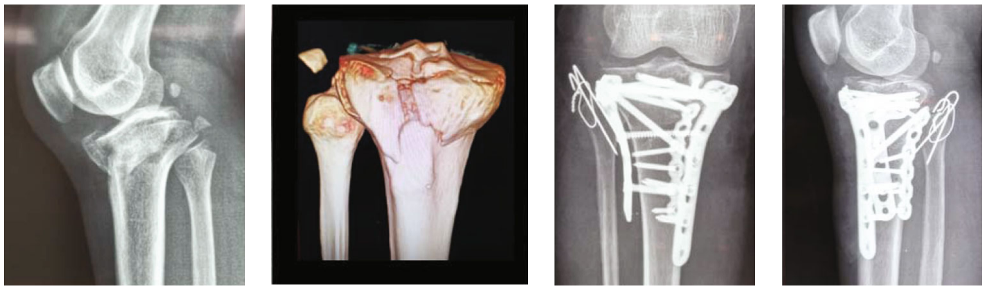

(a) (b) (c) (d)

Figure 3: A type 1 case fixed with Kirschner wire by tension band technique: (a) preoperative lateral X-ray; (b) preoperative CT; (c, d) preoperative X-ray.

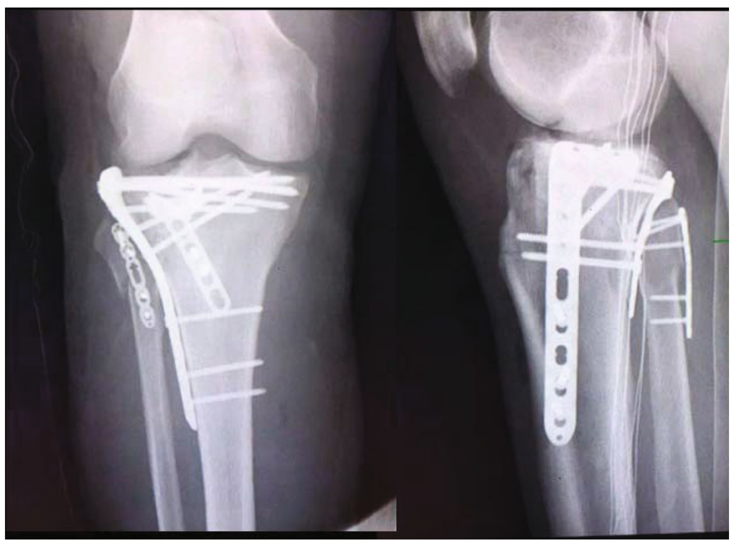

Figure 4: A type 2 case fixed by a mini locking plate: (a, b) preoperative X-ray.

3. Results

3.1. Results. Totally, 1160 patients with 1170 knees suffering TPFs were retrospectively analyzed. Thereinto, 352 patients with 355 knees (355/1170, 30.3%) combined tibial plateau fractures with proximal fibular injury (types 1 to 4) were enrolled in this study. Of these 352 patients, 192 were men and 160 were women with 1 male patient and 2 female patients involved with bilateral tibial plateau fractures. The average age was 53.9 ± 13.0 years (male/female 52.6 ± 12.8/56.1 ± 12.8 years) (Table 1). The cause of injury included electric bicycle and motorcycle accident, car accident, fall from a height, and sports injury.

According to the AO/OTA classification, there were 31 patients with type A (8.7%), 127 patients with type B (35.7%), and 197 patients with type C (55.4%). According to the Yao classification, there were 85 patients with 2 columns (23.9%), 149 patients with 3 columns (41.8%), and 121 patients with 4 columns (33.8%). TPII is 7.9 ± 2.6 (Table 1). Intermedial column and lateral column injury was the most, and the medial column was the least (Table 2).

Of the four injury types to the proximal fibula, type 2 fibular head fracture (193/355, 54.4%) was the most common. Type 1 fibular apex (122/355, 34.4%) was the second, and the third was the 37 (10.4%) cases of the type 3 fracture; only 3 (0.8%) cases of type 4 were found. EX1 was omitted for invisibility in CT, EX2 has 21 cases, and the proportion was 1.8% (21/1170).

In type 1, 38 patients needed surgery and 84 patients were conservative. In type 2, 18 patients needed surgery and 175 patients were conservative. In type 3, 3 patients needed surgery and 34 patients were conservative. In type 4, 2 patients needed surgery and 1 patient was conservative. In type EX2, 6 patients needed surgery and 15 patients were conservative (Table 3).

4. Discussion

In this study, we analyzed the incidence and treatment strategies of the largest sample size of concomitant fibular column injuries in TPFs. The current study demonstrated that 30.3% (355/1170) of tibial plateau fractures were associated with proximal fibula fractures, which was in accordance with previous studies [10]. The prevalence of proximal fibular fractures associated with tibial plateau fracture was 22.2%-38.3% [6, 11, 12].

Among the four injury types, the type 2 fibular head compression fracture (193/355, 54.4%) was the most common, the type 1 avulsion fracture of the fibular head (122/355, 34.4%) was the second, and type 3 the proximal

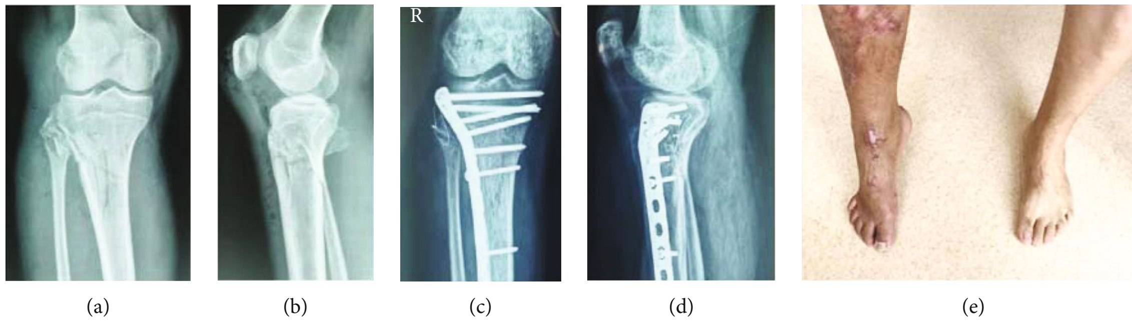

Figure 5: A tibial plateau fracture case with type 2 fibular column injury fixed with a steel wire. The patient showed iatrogenic peroneal nerve injury with foot drop and paresthesia postoperatively: (a, b) preoperative X-ray; (c, d) postoperative X-ray; (e) the symptom of right foot drop.

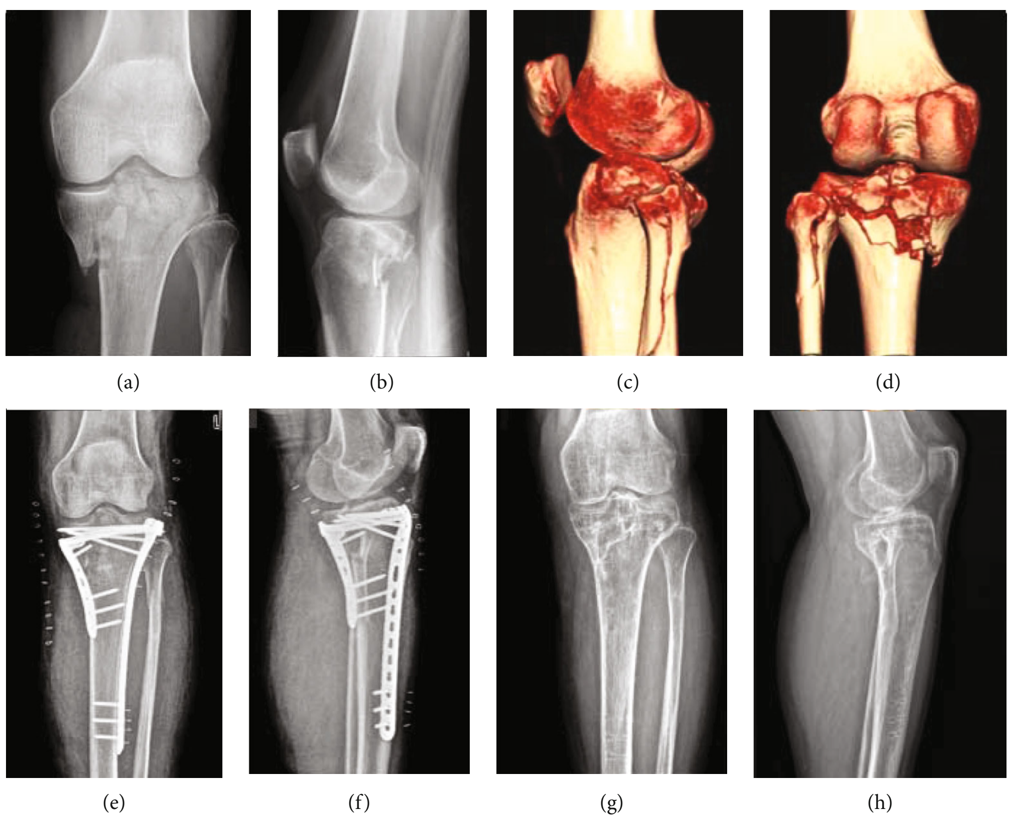

Figure 6: A tibial plateau fracture case with type 3 fibular column injury: (a, b) preoperative X-ray; (c, d) preoperative CT; (e, f) postoperative X-ray; (g, h) X-rays after removal of implant.

diaphyseal fracture was the least. Only three cases were found in the proximal tibiofibular joint dislocation, which was a severe traumatic marker for neurovascular injury and compartment syndrome [3].

In terms of injury type, in the Yao classification, type 1 means the avulsion of fibular apex or head (arcuate fracture or arcuate sign) just consistent with type 1 injury in Bozkurt classification and Zheng classification. In Yao classification, type 2 compressed fibular head fracture contained Bozkurt classification type 2 + 3 and Zheng classification type 2 + 3 + 4, regardless of the morphology of the fracture (cleavage, depressed, or comminuted). In the Yao classification, type 3 equaled to type 4 in Bozkurt classification and type 5 in Zheng classification.

In addition to the above three common injury types, Yao classification defined three neostyle injury types: type 4, EX1, and EX2. Uncommon type 4 (3/355, 0.85%) was a severe traumatic marker for neurovascular injury and compartment syndrome [6]. EX1 was imponderable in this study, and 21 cases (21/1170, 1.8%) of EX2 of the fibular column were found. It is the first time that LCL tear (EX1) and avulsion of the lateral femoral condyle (EX2) are considered fibular column injury type in any classification for the proximal calf.

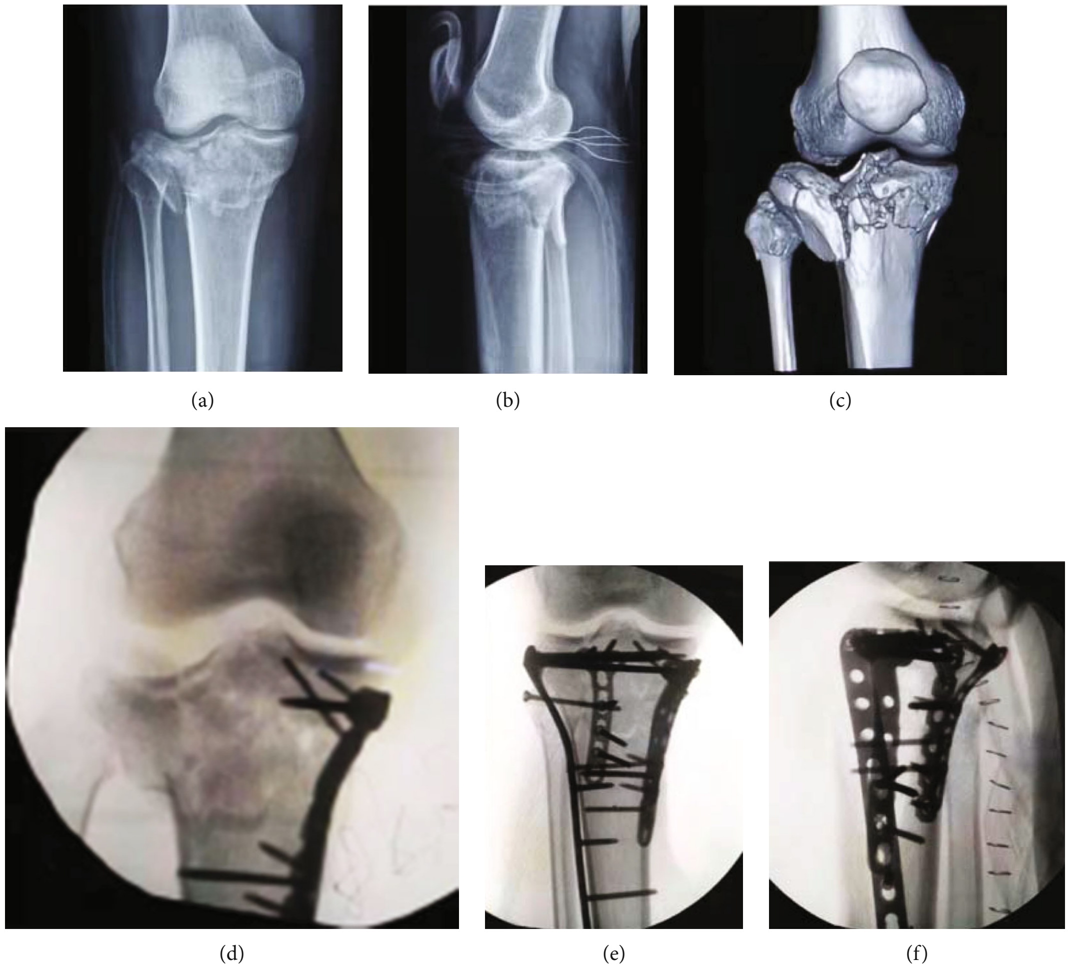

Figure 7: A tibial plateau fracture case combined with a superior tibiofibular dislocation (type 4 injury in four-column nine-segment classification) was fixed by plates and a positioning screw: (a) preoperative A-P view X-ray; (b) preoperative lateral-view X-ray; (c) preoperative three-dimensional CT imaging; (d) intraoperative A-P view X-ray showed the obvious dislocation of the superior tibiofibular joint; (e) intraoperative A-P view X-ray after the placement of the positioning screw; (f) intraoperative lateral-view X-ray.

Based on the Yao classification, type 1 avulsion of fibular apex (head) fracture is more common in tension injury and is usually caused by varus/hyperextension force. Fixation of avulsion of the fibula head is important for the restoration of stability of the posterolateral corner. The smaller and undisplaced avulsions are more likely to be treated conservatively, while the bigger and displaced fragment required fixation/repair or reconstruction. In the cohort, 38 of 122 cases underwent surgical treatment. The recommended fixation scheme included lag screw ± washer, suture tunnel, and suture anchor technique [13–15]. Figure 2 shows a type 1 case fixed by the suture anchor technique.

Kirschner wire and tension band technique or locking plates only are not recommended for spontaneous loosening and lack of effective compression (Figure 3).

The type 2 fibular head compression fracture is highly related to the mechanism of valgus or compression injury of the knee. The impacted fracture site is relatively stable, and most of this injury just required conservative treatment. If it is obviously unstable, it can also be fixed with a screw and plate (Figure 4).

There is the possibility of iatrogenic injury of the common peroneal nerve in the operation of the peroneal head and neck. Less than 10% (15/193) of type 2 cases received surgical treatment. Figure 5 shows 1 TPF patient with fibular type 2 that underwent a fix using steel wire. Unfortunately, the patient developed iatrogenic foot drop and sensory disturbance of common peroneal injury after the operation.

The incidence of type 3 injury is low (37/355) which is difficult to expound by a certain injury mechanism. The elastic intramedullary pin scheme which does not need to expose the nerve could be an option worth considering. Figure 6 shows a TPF case with type 3 fibular column injury.

Only three (3/355, 0.85%) cases with type 4 proximal tibiofibular joint dislocation were found in this cohort. The proximal tibiofibular joint dislocation was first described by Ogden in 1974 [16]. It is difficult to be identified on X-ray, and 3D-CT can effectively identify the separated proximal fibula. A hook test could be used to judge the stability during operation similar to the inferior tibiofibular syndesmosis. For fresh dislocation, screw, suture button, and tight rope could be used to restore the proximal tibiofibular joint [17–19]. Temporary screw fixation could be utilized but

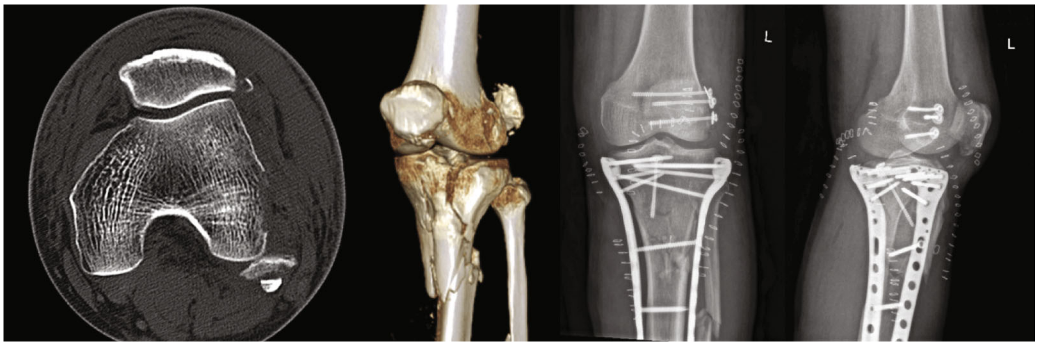

Figure 8: A case of extending type 2 (EX2) avulsion of lateral femoral condyle fixed by lag screws: (a) preoperative axial view CT imaging; (b) preoperative three-dimensional CT imaging; (c, d) postoperative A-P view X-ray.

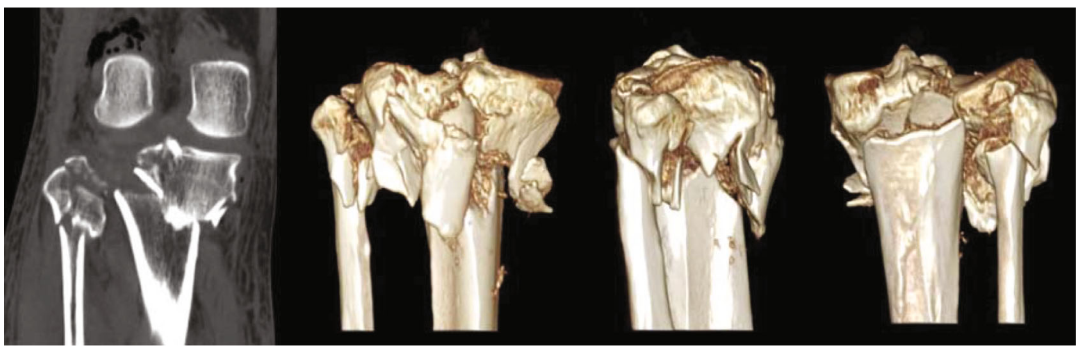

Figure 9: A tibial plateau fracture case with type 1 + type 2 fibular column injury.

requires removal of the screws at 12 to 16 weeks postoperatively. Figure 7 shows a TPF case with type 4 fibular column injury; a positioning screw was placed to maintain the stability of the proximal tibiofibular joint. Delayed dislocation of the superior tibiofibular syndesmosis may require ligament reconstruction [20, 21].

Both extending types (EX1 and EX2) covered the injury information about LCL (PLC) and originated from varus/extension/hypertension injury the same as type 1 avulsion. For EX1, early repair or primary reconstruction brings about a better prognosis [22]. Missed EX1 injury could lead to sustained posterolateral instability, which required arthroscopic or open reconstruction [23, 24]. All avulsion of lateral femoral condyle could be recorded as EX2 of the fibular column which is usually considered LCL avulsion injury. Small and undisplaced bony pieces are usually conservative while large pieces of bone need to be fixed surgically (Figure 8).

Obviously, the setting of six categories in four-column nine-segment classification (Yao classification) can effectively remind orthopedic surgeons to avoid missing various injury patterns from the lateral condyle of the femur to the fibular shaft. It should be noted that the injury type is only a morphological description of the distribution of fracture lines. A certain kind may originate from violence at different levels and in different directions. For example, an undisplaced fibula tip crack fracture can be caused by mild tension or compression violence. Moreover, six kinds of injury types do not exist alone and occasionally coexist. Figure 9 illustrates a TPF case with type 1 + type 2 fibular column injury.

There were several limitations in this study. First, although our sample size is by far the largest, increased samples and multicenter study will lead to a more accurate incidence. Second, the incidence of EX1 has not been revealed for lacking MR or ultrasound data, and MR will provide injury information of the total knee joint more than the posterolateral corner. Third, the relationship between the injury type of the fibular column and the functional recovery of the knee needs further follow-up and summarization.

5. Conclusions

Six injury types in the four-column nine-segment classification covered all patterns of bony and soft tissue injuries of the fibular column and concisely explained the injury mechanism. The classification is helpful for the precise judgement and decision-making of the concomitant fibular column injuries in tibial plateau fractures.

Data Availability

The main object of this study is X-ray and CT image data, and we have provided a typical illustrative diagram. The extra data used to support the findings of the current study are included within the article.

Conflicts of Interest

The authors declare that there is no conflict of interest regarding the publication of this paper.

Authors' Contributions

Xiang Yao, Bin Lv, and MinJie Hu contributed equally to this work and are co-first authors.

Acknowledgments

We thanked Fujun Luan (Figure 3), WenHao Liang (Figure 4), Dong Li (Figure 5), and ZhiGang Wang (Figure 7) for the great support on the schematic images. This study was supported by the Zhenjiang Science & Technology Program (Grant No.: SH2021034).

References

[1] M. Maeseneer, M. Shahabpour, K. Vanderdood, F. Ridder, F. Roy, and M. Osteaux, "Posterolateral supporting structures of the knee: findings on anatomic dissection, anatomic slices and MR images," *European Radiology*, vol. 11, no. 11, pp. 2170–2177, 2001.

[2] J. Schatzker, "Compression in the surgical treatment of fractures of the tibia," *Clinical Orthopaedics and Related Research*, vol. 105, pp. 220–239, 1974.

[3] J. L. Marsh, T. F. Slongo, J. Agel et al., "Fracture and dislocation classification compendium -2007: Orthopaedic Trauma Association classification, database and outcomes committee," *Journal of Orthopaedic Trauma*, vol. 21, 10 Suppl, pp. S1–133, 2007.

[4] C. F. Luo, H. Sun, B. Zhang, and B. F. Zeng, "Three-column fixation for complex tibial plateau fractures," *Journal of Orthopaedic Trauma*, vol. 24, no. 11, pp. 683–692, 2010.

[5] M. Kfuri and J. Schatzker, "Revisiting the Schatzker classification of tibial plateau fractures," *Injury*, vol. 49, no. 12, pp. 2252–2263, 2018.

[6] M. Bozkurt, S. Turanli, M. N. Doral et al., "The impact of proximal fibula fractures in the prognosis of tibial plateau fractures: a novel classification," *Knee Surgery, Sports Traumatology, Arthroscopy*, vol. 13, no. 4, pp. 323–328, 2005.

[7] X. Yao, Y. Xu, J. Yuan et al., "Classification of tibia plateau fracture according to the "four-column and nine-segment"," *Injury*, vol. 49, no. 12, pp. 2275–2283, 2018.

[8] E. G. Meinberg, J. Agel, C. S. Roberts, M. D. Karam, and J. F. Kellam, "Fracture and dislocation classification compendium-2018," *Journal of orthopaedic trauma*, vol. 32, Suppl 1, pp. S1–S170, 2018.

[9] B. H. Cohen, D. F. SF, J. D. Hodax, D. Johnson, J. K. Ware, and P. D. Fadale, "The arcuate fracture: a descriptive radiographic study," *Injury*, vol. 49, no. 10, pp. 1871–1877, 2018.

[10] T. Sillat, M. Parkkinen, J. Lindahl et al., "Fibular head avulsion fractures accompanying operative treated medial tibial plateau fractures," *Skeletal Radiology*, vol. 48, no. 9, pp. 1411–1416, 2019.

[11] H. Chang, Z. Zheng, Y. Yu, and Y. Zhang, "The degree of fracture displacement does not affect the risk for concomitant proximal fibular fractures in tibial plateau fractures," *International Orthopaedics*, 2021.

[12] Z. L. Zheng, Y. Y. Yu, H. R. Chang, H. Liu, H. L. Zhou, and Y. Z. Zhang, "Establishment of classification of tibial plateau fracture associated with proximal fibular fracture," *Orthopaedic Surgery*, vol. 11, no. 1, pp. 97–101, 2019.

[13] J. D. Hodax, B. H. Cohen, D. F. SF, A. D. Sobel, and P. D. Fadale, "Comparison of three fixation techniques for arcuate fractures," *Injury*, vol. 51, no. 2, pp. 478–482, 2020.

[14] S. Vojdani, L. Fernandez, J. Jiao et al., "Novel spiked-washer repair is biomechanically superior to suture and bone tunnels for arcuate fracture repair," *Journal of Orthopaedic Trauma*, vol. 31, no. 3, pp. e81–e85, 2017.

[15] D. J. Cinats and T. Stone, "Comminuted fibular head fractures with posterolateral knee instability: a novel repair technique using a tension-slide device," *Journal of Orthopaedic Trauma*, vol. 35, no. 2, pp. e66–e70, 2021.

[16] J. A. Ogden, "Subluxation and dislocation of the proximal tibiofibular joint," *The Journal of bone and joint surgery*, vol. 56, no. 1, pp. 145–154, 1974.

[17] A. C. Moscon, A. L. Martimbianco, A. D. Junior, and G. C. Gracitelli, "Proximal tibiofibular joint dislocation treated using flexible and permanent syndesmosis fixation," *BMJ Case Reports*, vol. 2018, 2018.

[18] J. A. Porrino, M. L. Richardson, H. Mulcahy, F. S. Chew, and B. Twaddle, "Disruption of the proximal tibiofibular joint in the setting of multi-ligament knee injury," *Skeletal Radiology*, vol. 44, no. 8, pp. 1193–1198, 2015.

[19] M. Oksum and P. H. Randsborg, "Treatment of instability of the proximal tibiofibular joint by dynamic internal fixation with a suture button," *Arthroscopy Techniques*, vol. 7, no. 10, pp. e1057–e1061, 2018.

[20] T. L. M. D. Miller, "New technique of soft tissue reconstruction for proximal tibiofibular joint instability using iliotibial band and biceps femoris longhead autograft," *Techniques in Orthopaedics*, vol. 29, no. 4, pp. 243–247, 2014.

[21] T. J. Dekker, N. N. DePhillipo, M. I. Kennedy, Z. S. Aman, W. W. Schairer, and R. F. LaPrade, "Clinical characteristics and outcomes after anatomic reconstruction of the proximal tibiofibular joint," *Arthroscopy : the journal of arthroscopic & related surgery : official publication of the Arthroscopy Association of North America and the International Arthroscopy Association*, vol. 36, no. 6, pp. 1649–1654, 2020.

[22] J. Tomás-Hernández, J. M. Monyart, J. T. Serra et al., "Large fracture of the anteromedial tibial plateau with isolated posterolateral knee corner injury: case series of an often missed unusual injury pattern," *Injury*, vol. 47, pp. S35–S40, 2016.

[23] P. Liu, X. Gong, J. Zhang, and Y. Ao, "Anatomic, all-arthroscopic reconstruction of posterolateral corner of the knee: a cadaveric biomechanical study," *Arthroscopy : the journal of arthroscopic & related surgery : official publication of the Arthroscopy Association of North America and the International Arthroscopy Association*, vol. 36, no. 4, pp. 1121–1131, 2020.

[24] P. S. Vezeridis, I. D. Engler, M. J. Salzler et al., "Biomechanics following isolated posterolateral corner reconstruction comparing a fibular-based docking technique with a tibia and fibular-based anatomic technique show either technique is acceptable," *Arthroscopy : the journal of arthroscopic & related surgery : official publication of the Arthroscopy Association of North America and the International Arthroscopy Association*, vol. 36, no. 5, pp. 1376–1385, 2020.

Hindawi
BioMed Research International
Volume 2021, Article ID 1308805, 9 pages
https://doi.org/10.1155/2021/1308805

Research Article

A Novel 3D-Printed Device for Precise Percutaneous Placement of Cannulated Compression Screws in Human Femoral Neck Fractures

Cheng Long,[1] **Jin-hai Liu**,[2] **Xiang-ping Chai**,[3] **Xiang-feng Liu**,[3] **and Zhi-xi Duan**[3]

[1]*Department of Orthopedics, Xiangya Hospital, Central South University, No. 87 Xiangya Road, Changsha 410008, China*
[2]*Department of Orthopedics, Qingdao Chengyang Guzhen Orthopedic Hospital, No. 518 Yinhe Road, Chengyang District, Qingdao 266107, China*
[3]*Department of Emergency Medicine, Trauma Center, The Second Xiangya Hospital, Central South University, No. 139 Renmin Road, Changsha, 410011 Hunan, China*

Correspondence should be addressed to Zhi-xi Duan; xiangyadzx@csu.edu.cn

Received 10 April 2021; Accepted 31 May 2021; Published 11 June 2021

Academic Editor: Ying-Qi Zhang

Copyright © 2021 Cheng Long et al. This is an open access article distributed under the Creative Commons Attribution License, which permits unrestricted use, distribution, and reproduction in any medium, provided the original work is properly cited.

Background. The aim of this study was to investigate the application of computer-aided design and 3D printing technology for percutaneous fixation of femoral neck fractures using cannulated compression screws. *Methods*. Using computed tomography data, an individualized proximal femur model was created with a 3D printer. The reduction of the femoral neck fracture and the placement of the cannulated compression screws were simulated on a computer. A 3D printing guide plate was designed to match the proximal femur. After demonstrating the feasibility of the 3D model before the surgical procedure, the guide needles and cannulated compression screws were inserted with the aid of the 3D-printed guide plate. *Results*. During the procedure, the 3D-printed guide plate for each patient matched the bone markers of the proximal femur. With the aid of the 3D-printed guide plate, three cannulated compression screws were accurately inserted into the femoral neck to treat femoral neck fractures. After screw placement, intraoperative X-ray examination showed results that were consistent with the preoperative design. The time taken to complete the procedure in the guide plate group was 35.3 ± 2.1 min, the intraoperative blood loss was 6.3 ± 2.8 mL, and X-ray fluoroscopy was only performed 9.1 ± 3.5 times. Postoperative radiographs showed adequate reduction of the femoral neck fractures. The entry point, entry direction, and length of the three cannulated compression screws were consistent with the preoperative design, and the screws did not penetrate the bone cortex. *Conclusion*. Using computer-aided design and 3D printing technology, personalized and accurate placement of cannulated compression screws can be realized for the treatment of femoral neck fractures. This technique can shorten the time required for the procedure and reduce damage to the femoral neck cortex, intraoperative bleeding, and the exposure of patients and healthcare staff to radiation.

1. Introduction

A femoral neck fracture is the third most common type of fracture in trauma orthopedics, and it accounts for approximately 41% of hip fractures and 3.6% of total fractures [1–3]. There are approximately 1.5 million hip fractures every year globally, and with the aging of the population, this is expected to increase to 6.3 million by 2050 [4]. It is estimated that approximately 30% of hip fractures in the world occur in Asian countries, especially in China [5].

The femoral neck fracture often occurs in elderly patients with osteoporosis, mainly due to low-energy injury [6]. Its incidence is very low in young patients, in whom it occurs mainly due to high-energy trauma. Despite surgical interventions, the reoperation rates for and mortality after this type of fracture remain high [7–9]. Although there are many

Table 1: Patient information.

Group	Number of cases	Gender (M/F)	Age (years/range)	Injury side (right/left)	Garden classification (I, II, III, IV)
3D guide plate group	20	M: 7 F: 13	63.8 ± 16.9 50-93	R: 10 L: 10	6 II, 10 III, 4 IV
Control group	20	M: 9 F: 11	61.3 ± 19.8 45-85	R: 12 L: 8	8 II, 10 III, 2 IV

methods to treat femoral neck fractures, cannulated compression screw fixation remains the mainstream surgical intervention [10–12].

In recent years, computer-aided design and 3D printing technology have become more widely used in the medical field [13]. In particular, considerable progress has been made in the field of orthopedics. At present, these techniques are mainly used for preoperative planning, the 3D printing of guide plates, and personalized implant production [14–16]. 3D-printed guide plates are usually used to guide surgeons to accurately insert internal fixation screws and plates. In this study, we used computer-aided design and 3D printing technology to develop a new type of guide plate for the precise and rapid percutaneous fixation of femoral neck fractures.

2. Materials and Methods

2.1. Patient Information. From February 2019 to February 2020, 40 patients with a femoral neck fracture were operated in our hospital, and they were divided into two groups according to their preferences. Patients were included in the study if they presented with a simple femoral neck fracture without neurovascular injury. They were treated with three cannulated compression screws. Forty patients with femoral neck fractures were included in the study. Twenty patients were treated with 3D-printed guide plate-assisted screw placement (guide plate group), and the remaining 20 were treated with freehand screw placement under a C-arm X-ray fluoroscopy instrument (control group). The guide plate group comprised 7 male and 13 female patients, and the control group comprised 9 male and 11 female patients. Additional information about the patients is provided in Table 1. Patients were excluded if they presented with a pelvic, intertrochanteric, or open fracture. All patients were treated with the same type of cannulated compression screw implant by the same surgical team.

2.2. Digital 3D Model Reconstruction. The anatomical data of the patients were obtained by computed tomography (CT) scanning, and 3D models of the upper femur were reconstructed on the screen using medical digital imaging and an E3D digital medical modeling and design system (http://www.e3d-med.com; E3D Digital Medical and Virtual Reality Research Center, Central South University, Hunan Province, China). The surgeon then used a preoperative planning procedure to design the model. The surgeon chose an appropriate size for the required parts and recorded them. The model was stored as a stereolithography file, which was then sent to a 3D printer. The material of the 3D printing guide is polylactic acid (PLA).

2.3. Operation and Postoperative Follow-Up. Before the operation, the 3D-printed guide plate underwent plasma sterilization. After the femoral neck fracture was reduced by traction, the guide plate was placed percutaneously on the matching area of the proximal femur. With an assistant keeping the fracture stable, the surgeon maintained the position and direction of the guide plate stably with one hand and inserted the guide needle at the designed depth with the other hand. C-arm X-ray fluoroscopy was used to confirm that the insertion direction and guide needle depth were correct. Three cannulated compression screws were then implanted along the guide needle, according to the preoperative design. The position and angle of the three cannulated compression screws were determined by C-arm X-ray fluoroscopy, and the results were compared with the preoperative plan. The patients were followed up every 3 months. All patients were followed up successfully.

2.4. Statistical Analysis. Data were analyzed using Prism 7.0 statistical software (GraphPad, San Diego, CA, USA). Normally distributed data are expressed as the mean ± standard deviation and were analyzed using independent sample Student's t-test. Data that did not conform to a normal distribution were analyzed by the Mann-Whitney U test. $P < 0.05$ was considered to indicate a significant difference between the groups.

3. Results

3.1. Preoperative Data Acquisition, 3D Simulation Reconstruction, Screw Path, and 3D-Printed Guide Plate Design. First, we performed a CT scan of the femoral neck fracture to collect detailed data (Figures 1(a)–1(d)). We then successfully simulated the reduction process of the femoral neck fracture using a computer, and fracture reduction was found to be satisfactory (Figures 1(e)–1(h)). Finally, we correctly evaluated the direction and length of the screw. The design of the 3D-printed guide plate was based on the anatomical characteristics of each individual (Figures 1(i)–1(l)).

3.2. The Accuracy of Computer-Aided Design and 3D-Printed Guide Technology. The 3D-printed guide plate was consistent with the anatomical characteristics of each individual. Under the guidance of the navigation template, the

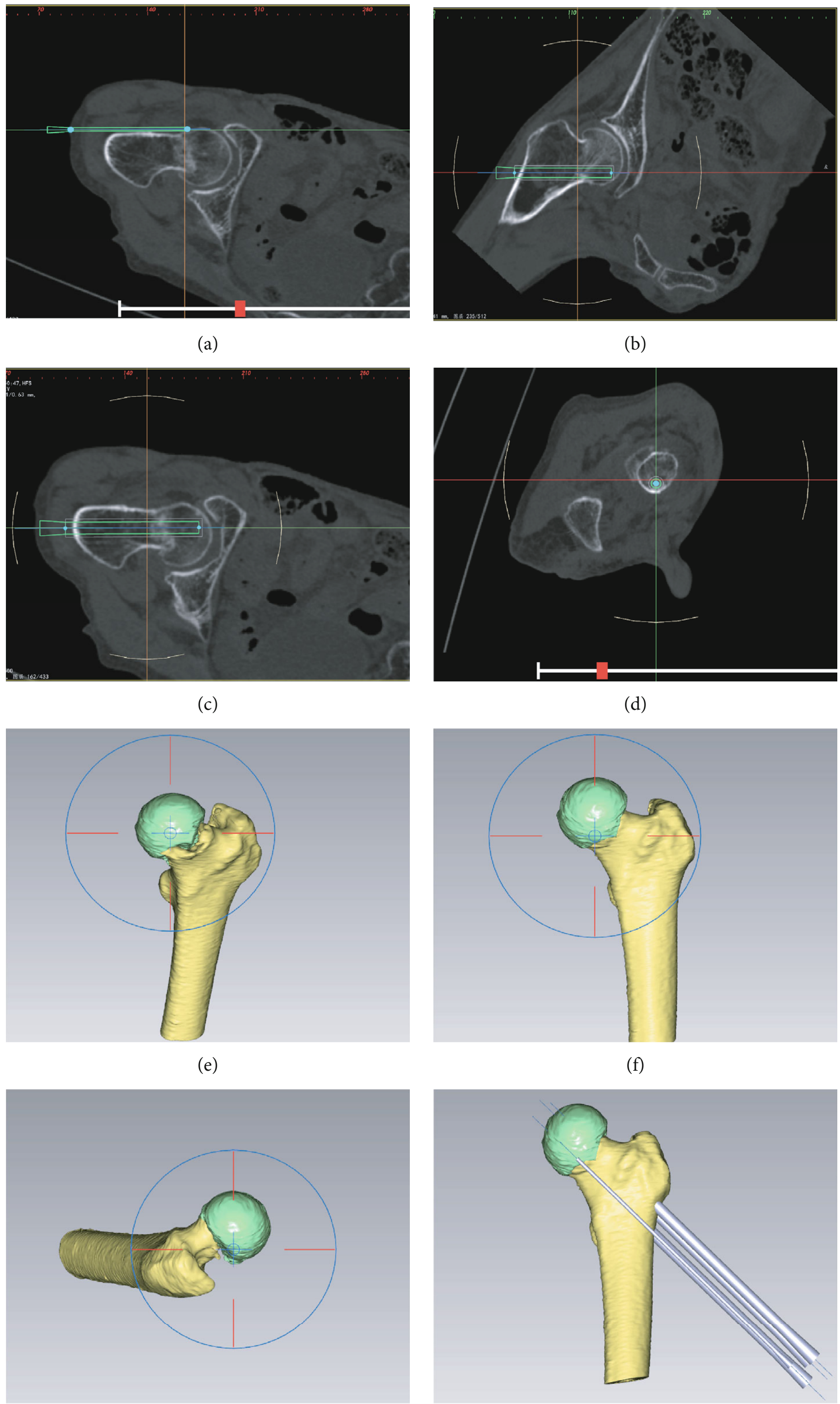

(a) (b) (c) (d) (e) (f) (g) (h)

Figure 1: Continued.

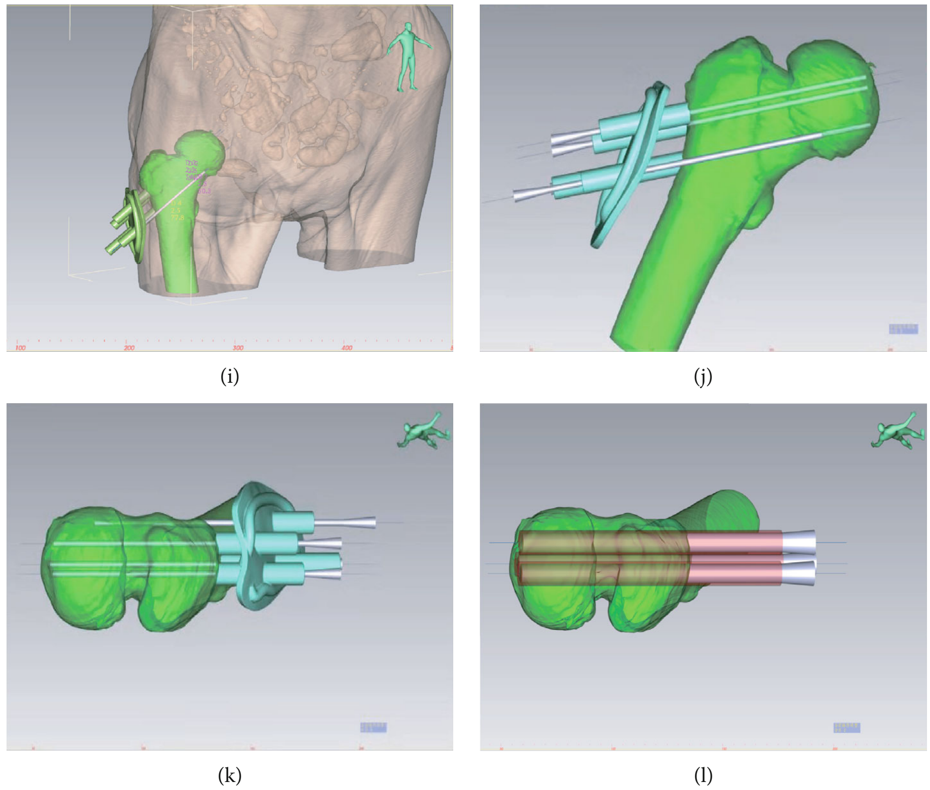

Figure 1: Digital 3D model reconstruction and preoperative planning. (a–d) CT scanning, multiplanar measurements, and reconstruction were performed for femoral neck fractures. (e–h) Computer-aided design and 3D simulation of femoral neck fracture reconstruction. (i–l) Computer-aided design and 3D simulation of the use of a guide plate and the surgical process of inserting three cannulated compression screws.

percutaneous insertion of the guide needle and the intraoperative C-arm fluoroscopy results were consistent with the preoperative design (Figures 2(a)–2(h)). CT scans immediately after the procedure showed that the reduction of the femoral neck fracture was satisfactory and that the position of the three cannulated compression screws was accurate (Figures 2(i)–2(l)). There were 17 cases of anatomical reduction and 3 cases of functional reduction in the guide plate group and 15 cases of anatomical reduction and 5 cases of functional reduction in the control group. The time taken to complete the procedure was significantly less for the guide plate group (35.3 ± 2.1 min) than for the control group (68.1 ± 4.9 min, $P < 0.05$). The amount of intraoperative blood loss was 6.3 ± 2.8 mL in the guide plate group and 21.3 ± 7.1 mL in the control group ($P < 0.05$). The guide plate group required significantly fewer X-ray fluoroscopy images (9.1 ± 3.5) than the control group (20.9 ± 2.8, $P < 0.05$).

3.3. Postoperative Follow-Up Results. All 40 patients were successfully followed up. The average follow-up time was 8 (range, 6–12) months. No avascular necrosis of the femoral head, screw withdrawal, or fractures occurred during the follow-up period (Figures 3(a)–3(f)). At the final follow-up assessment (Figures 3(g)–3(i)), the Harris score for hip joint function was 90.4 ± 3.5 in the guide plate group and 88.2 ± 2.8 in the control group ($P > 0.05$).

4. Discussion

The femoral neck fracture is the third most common type of fracture in traumatology, and various treatment options are available for it [1, 17]. Minimally invasive internal fixation with three cannulated compression screws is widely used to treat this type of fracture. The femoral neck shows good antishear force, antibending force, antirotation ability, and antiaxial stress after this fixation procedure. This procedure can reduce the incidence of nonunion of the femoral neck fracture and avascular necrosis of the femoral head. Moreover, the plane of screw placement is an inverted triangle and has the characteristics of triangular stability [18, 19]. Although this method has many advantages, there are certain challenges in its clinical application. First, it requires specialized surgical skills and extensive clinical experience, and it depends on intraoperative fluoroscopy to confirm that the screw position is accurate [20, 21]. Second, the screw placement process requires multiple fluoroscopy images, which increases the exposure of the patient and the surgeon to radiation. Third, intraoperative drilling and

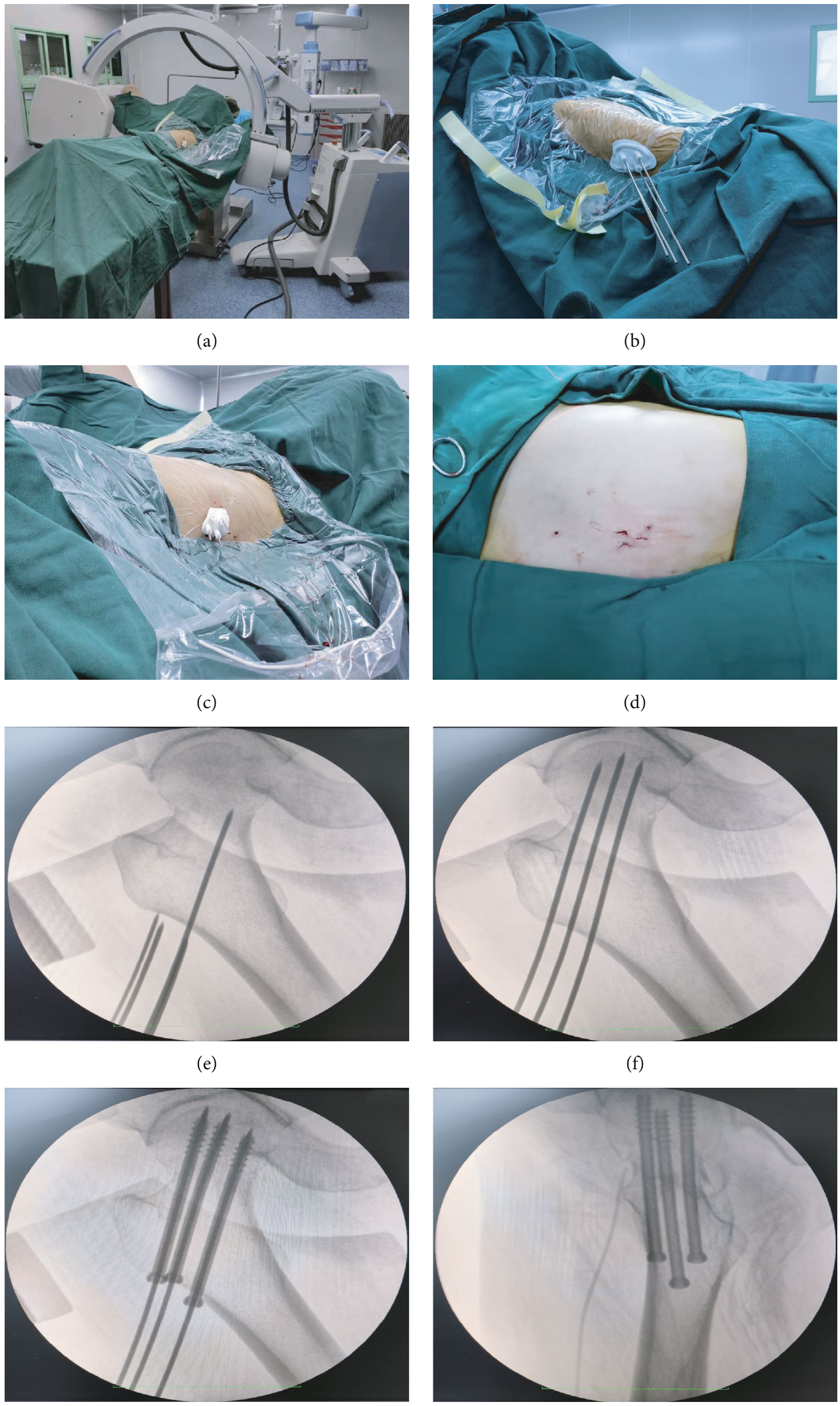
(a) (b) (c) (d) (e) (f) (g) (h)

Figure 2: Continued.

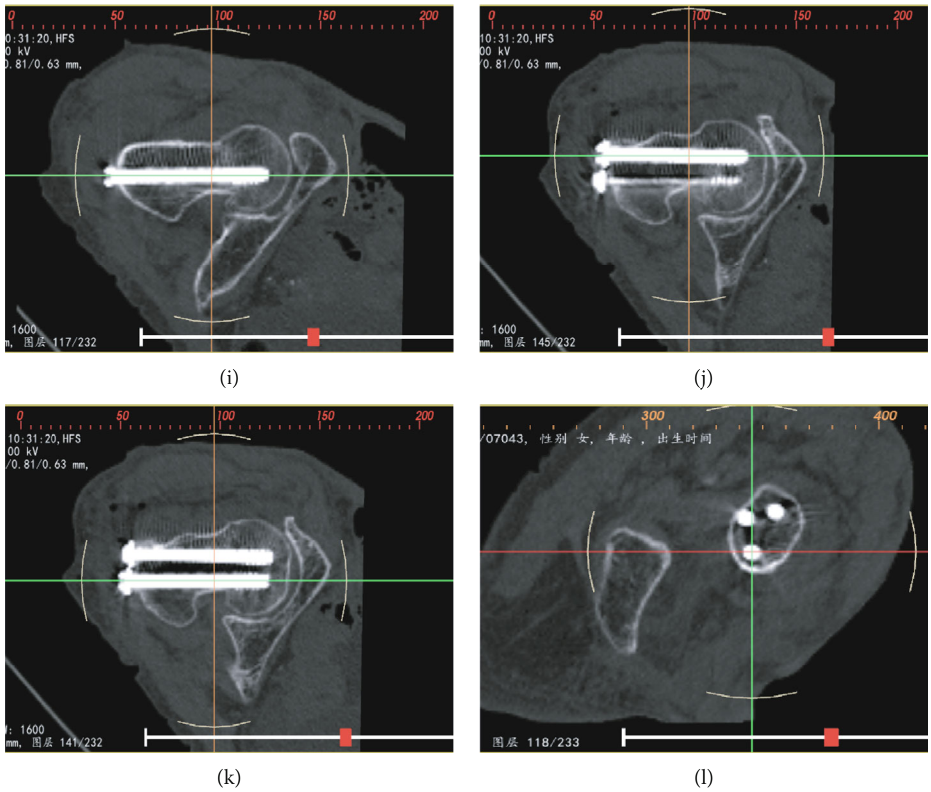

Figure 2: The accuracy of computer-aided design and 3D printing technology for guide plate production. (a–d) The surgical procedure of 3D-printed guide plate-assisted percutaneous needle insertion and cannulated screw placement. (e–h) C-arm X-ray fluoroscopy was used to observe the cannulated compression screw placement. (i–l) Immediate postoperative CT was performed to evaluate fracture reduction and the position of the three cannulated compression screws.

adjustment of the screw channel may affect the blood supply to the femoral head, thus reducing the holding force of the bone on the screw and consequently decreasing the stability of the fixation.

Therefore, a safe and effective method is needed to ensure the accuracy and safety of screw placement. A computer navigation system was once considered to be an acceptable auxiliary screw placement technology. However, the system's shortcomings, such as inconvenient operation, cumbersome registration, and high cost, prevented it from being widely used in clinical practice. With the development of digital medicine, 3D printing technology has become widely used in orthopedics. This technology allows the optimization of preoperative design and the realization of individualized and precise treatments. In addition, it has been reported that 3D-printed personalized guide plates are safe and feasible to use for the treatment of intertrochanteric fractures in adults and of hip diseases in children [16, 22].

In this study, digital orthopedic technology and 3D printing technology were combined in the guide plate group. A 3D-printed guide plate was used to assist in cannulated compression screw fixation of femoral neck fractures. Before the procedure, 3D reconstruction of the fracture site was performed using relevant software, and the resulting model could be rotated and transparently processed to preview the screw placement and adjust the screw path to the optimal path. Therefore, the required length and diameter of the screw could be determined before the procedure. A 1 : 1 fracture model was also printed before the procedure. The navigation template of auxiliary screw placement allowed the surgeon to simulate the procedure on the model, operate skillfully, and evaluate the difficulties and results of the procedure. It is also expected to be helpful for beginners to master the necessary surgical process and skills.

The use of a 3D-printed guide plate to assist the placement of cannulated compression screws for the internal fixation of femoral neck fractures has many advantages. First, it greatly simplifies and optimizes intraoperative procedures. The time taken to complete the procedure was greatly reduced, and the multiple intraoperative fluoroscopies, screw path sounding, and screw selection steps were eliminated. Specifically, the time taken to complete the procedure and the number of intraoperative X-ray fluoroscopy images were significantly less in the guide plate group than in the control group. Second, this procedure is convenient for junior doctors to master, and thus, they are more likely to promote this type of surgery. During the procedure, the guide plate only needs to be placed in the predesigned position, and the screw can be accurately placed without the need for multiple perspectives.

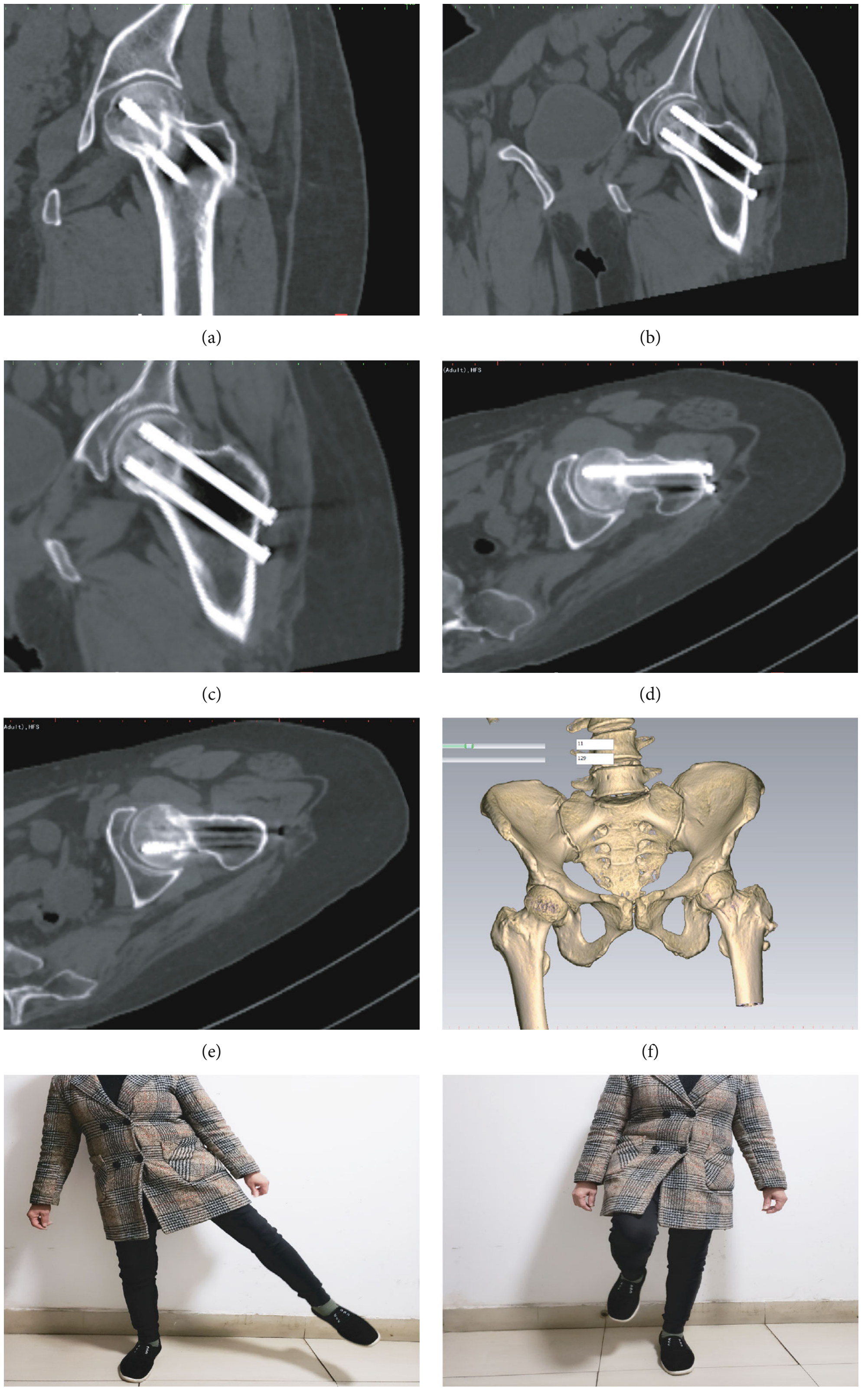

Figure 3: Continued.

(i)

Figure 3: Postoperative follow-up results. (a–f) In the guide plate group, CT images show fracture healing in the final follow-up assessment of a representative 52-year-old female patient. (g–i) The hip function of a representative 52-year-old female patient at the final follow-up assessment.

Third, the biggest characteristic in this study is the positional Kirschner wire in front of the femoral neck and the designed catheter matching on the surface of the lateral femoral, thus guaranteeing the use of the minimally invasive method and the accuracy of the method at the same time. Moreover, because this guide plate-assisted procedure has a short learning curve and is easy to master, it can be performed in relatively poorly equipped hospitals.

5. Conclusion

In conclusion, the use of computer-aided design and a 3D-printed navigation template improved the accuracy of cannulated compression screw implantation for the treatment of femoral neck fractures. It reduced the risk of iatrogenic injury to the femoral neck and vascular system and reduced implantation time, intraoperative bleeding, and X-ray exposure. With further improvements in efficiency and safety, this technology has the potential to be widely adopted.

Data Availability

The data used to support the findings of this study are available from the corresponding author upon request.

Conflicts of Interest

All authors declare no conflicts of interest.

Acknowledgments

This work was supported by the Key Project of Hunan Provincial Science and Technology Innovation (No. 2020SK1014-2).

References

[1] C. Bastard, “Femoral neck fracture,” *La Revue du Praticien*, vol. 69, no. 10, pp. 1124–1128, 2019.

[2] K. G. Thorngren, A. Hommel, P. O. Norrman, J. Thorngren, and H. Wingstrand, “Epidemiology of femoral neck fractures,” *Injury*, vol. 33, Supplement 3, pp. 1–7, 2002.

[3] I. Flóris and É. Belicza, “Analysis of hip fracture care in Hungary between 2004-2009,” *Orvosi Hetilap*, vol. 157, no. 41, pp. 1642–1648, 2016.

[4] B. Abrahamsen, T. van Staa, R. Ariely, M. Olson, and C. Cooper, “Excess mortality following hip fracture: a systematic epidemiological review,” *Osteoporosis International*, vol. 20, no. 10, pp. 1633–1650, 2009.

[5] C. Cooper, The IOF CSA Working Group on Fracture Epidemiology, Z. A. Cole et al., “Secular trends in the incidence of hip and other osteoporotic fractures,” *Osteoporosis International*, vol. 22, no. 5, pp. 1277–1288, 2011.

[6] O. Johnell and J. A. Kanis, “An estimate of the worldwide prevalence and disability associated with osteoporotic fractures,” *Osteoporosis International*, vol. 17, no. 12, pp. 1726–1733, 2006.

[7] C. Klop, P. M. Welsing, C. Cooper et al., “Mortality in British hip fracture patients, 2000-2010: a population-based retrospective cohort study,” *Bone*, vol. 66, pp. 171–177, 2014.

[8] J. J. Roche, R. T. Wenn, O. Sahota, and C. G. Moran, “Effect of comorbidities and postoperative complications on mortality after hip fracture in elderly people: prospective observational cohort study,” *BMJ*, vol. 331, no. 7529, p. 1374, 2005.

[9] S. Mundi, B. Pindiprolu, N. Simunovic, and M. Bhandari, “Similar mortality rates in hip fracture patients over the past 31 years,” *Acta Orthopaedica*, vol. 85, no. 1, pp. 54–59, 2014.

[10] Y. Xia, W. Zhang, Z. Zhang, J. Wang, and L. Yan, “Treatment of femoral neck fractures: sliding hip screw or cannulated screws? A meta-analysis,” *Journal of Orthopaedic Surgery and Research*, vol. 16, no. 1, p. 54, 2021.

[11] L. Li, X. Zhao, X. Yang, X. Tang, and M. Liu, “Dynamic hip screws versus cannulated screws for femoral neck fractures: a systematic review and meta-analysis,” *Journal of Orthopaedic Surgery and Research*, vol. 15, no. 1, p. 352, 2020.

[12] C. Papakostidis, A. Panagiotopoulos, A. Piccioli, and P. V. Giannoudis, “Timing of internal fixation of femoral neck fractures. A systematic review and meta-analysis of the final outcome,” *Injury*, vol. 46, no. 3, pp. 459–466, 2015.

[13] A. Aimar, A. Palermo, and B. Innocenti, “The role of 3D printing in medical applications: a state of the art,” *Journal of Healthcare Engineering*, vol. 2019, Article ID 5340616, 10 pages, 2019.

[14] D. Joung, N. S. Lavoie, S. Z. Guo, S. H. Park, A. M. Parr, and M. C. McAlpine, “3D printed neural regeneration devices,” *Advanced Functional Materials*, vol. 30, no. 1, 2020.

[15] H. Lv, L. Zhang, F. Yang et al., "A novel 3D-printed device for localization and extraction of trabeculae from human femoral heads: a comparison with traditional visual extraction," *Osteoporosis International*, vol. 26, no. 6, pp. 1791–1799, 2015.

[16] S. N. Zheng, Q. Q. Yao, F. Y. Mao et al., "Application of 3D printing rapid prototyping-assisted percutaneous fixation in the treatment of intertrochanteric fracture," *Experimental and Therapeutic Medicine*, vol. 14, no. 4, pp. 3644–3650, 2017.

[17] A. V. Florschutz, J. R. Langford, G. J. Haidukewych, and K. J. Koval, "Femoral neck fractures," *Journal of Orthopaedic Trauma*, vol. 29, no. 3, pp. 121–129, 2015.

[18] K. CCH, A. haseeb, and V. Ajit Singh, "Cannulated screw fixation for femoral neck fractures: a 5-year experience in a single institution," *Malaysian Orthopaedic Journal*, vol. 8, no. 2, pp. 14–21, 2014.

[19] P. Augat, E. Bliven, and S. Hackl, "Biomechanics of femoral neck fractures and implications for fixation," *Journal of Orthopaedic Trauma*, vol. 33, no. 1, Supplement 1, pp. S27–S32, 2019.

[20] J. C. Hoffmann, J. Kellam, M. Kumaravel, K. Clark, M. L. ". C.". Routt, and J. L. Gary, "Is the cranial and posterior screw of the "inverted triangle" configuration for femoral neck fractures safe?," *Journal of Orthopaedic Trauma*, vol. 33, no. 7, pp. 331–334, 2019.

[21] Y. Q. Zhang, S. M. Chang, Y. G. Huang, and X. Wang, "The femoral neck safe zone," *Journal of Orthopaedic Trauma*, vol. 29, no. 5, pp. e178–e182, 2015.

[22] P. Zheng, Q. Yao, P. Xu, and L. Wang, "Application of computer-aided design and 3D-printed navigation template in Locking Compression Pediatric Hip Plate™ placement for pediatric hip disease," *International Journal of Computer Assisted Radiology and Surgery*, vol. 12, no. 5, pp. 865–871, 2017.

Hindawi
BioMed Research International
Volume 2021, Article ID 5554500, 7 pages
https://doi.org/10.1155/2021/5554500

Research Article

The Application of Digital Design Combined with 3D Printing Technology in Skin Flap Transplantation for Fingertip Defects during the COVID-19 Epidemic

Hui Lu,[1,2] **Hanshu Peng**,[3] **Ze Peng**,[2] **Dingxi Liu**,[2,4] **Qimei Wu**,[5] **and Rong Liu**[2,3]

[1]*School of Medicine, Wuhan University of Science and Technology, No. 1, Huangjia Lake University Town, Wuhan 430065, China*
[2]*Institute of Medical Innovation and Transformation, Puren Hospital of Wuhan, 1 Benxi Road, Wuhan 430081, China*
[3]*Department of Orthopedics, Puren Hospital Affiliated to Wuhan University of Science and Technology, 1 Benxi Road, Wuhan 430081, China*
[4]*School of Mechanical Automation, Wuhan University of Science and Technology, 1 Benxi Road, Wuhan 430081, China*
[5]*Wuhan Liu Sanwu Traditional Chinese Medicine Bone Injury Hospital, Xinzhou District, Wuhan 430081, China*

Correspondence should be addressed to Rong Liu; dr_liurong@whu.edu.cn

Received 25 January 2021; Accepted 31 May 2021; Published 9 June 2021

Academic Editor: Ying-Qi Zhang

Copyright © 2021 Hui Lu et al. This is an open access article distributed under the Creative Commons Attribution License, which permits unrestricted use, distribution, and reproduction in any medium, provided the original work is properly cited.

Objective. We aimed to evaluate the advantages of preoperative digital design of skin flaps to repair fingertip defects during the COVID-19 pandemic. We combined digital design with a 3D-printed model of the affected finger for preoperative communication with fingertip defect patients under observation in a buffer ward. *Methods*. From December 2019 to January 2021, we obtained data from 25 cases of 30 fingertip defects in 15 males and 10 females, aged 20-65 years old (mean 35 ± 5 years). All cases were treated by digitally designing preoperative fingertip defect flaps combined with a 3D-printed model. Preoperative 3D Systems Sense scanning was routinely performed, 3-matic 12.0 was used to measure the fingertip defect area ranging from $1.5\,cm \times 3.5\,cm$ to $2.0\,cm \times 5.0\,cm$, and the skin flap was designed. The flap area was $1.6\,cm \times 3.6\,cm$ to $2.1\,cm \times 5.1\,cm$. CURA 15.02.1 was used to set parameters, and the 3D model of the affected finger was printed prior to the operation. Full-thickness skin grafts were taken from donor areas for repair. *Results*. No vascular crises occurred in any of the 25 cases, and all flaps survived. The postoperative follow-up occurred over 3-12 months. All patients were evaluated 3 months after operation according to the trial standard of hand function evaluation of the Chinese Hand Surgery Society. The results showed that 20 cases had excellent outcomes (80%), four cases had good outcomes (16%), and one case had a fair outcome (4%). The excellent and good rate was 96%. *Conclusions*. During the COVID-19 epidemic, fingertip defects were treated with preoperative digital design of fingertip defect flaps combined with 3D printing. Precision design saves surgery time and improves the success rate of surgery and the survival rates of skin flaps. In addition, 3D model simulations improve preoperative communication efficiency, and the personalized design improves patient satisfaction.

1. Introduction

Soft tissue defects of fingertips are one of the most common hand injuries, which can lead to loss of sensation, reduced general hand function, and decreased quality of life [1]. It is essential to repair the soft tissue of fingertips as early as possible, to restore hand function and ensure the quality of life. Clinical practice has shown that early operation to close the wound surface and strengthen functional exercise is beneficial to future recovery of function [2]. However, the appearance of COVID-19 has complicated the traditional treatment of finger defects. In early December 2019, Chen et al. [3] reported the first case of pneumonia caused by the novel coronavirus infection in Wuhan, Hubei Province. On February 11, 2020, the disease caused by the novel coronavirus was officially named COVID-19 (coronavirus disease 2019) [4]. Since December 2019, the COVID-19 outbreak has spread across the country [5] and the world, with human-to-human transmission of the virus [6]. In order to contain the spread of the disease, person-to-person contact should be minimized to avoid transmission.

The treatment of fingertip defects is an emergency operation that should be conducted as soon as possible. During the COVID-19 pandemic, however, hospitalized patients are required to undergo routine pharyngeal swabs, COVID-19 antibody tests, and chest CT scans to rule out COVID-19. While waiting for the results, each patient must enter a buffer ward for observation. Buffer wards are rooms where a patient is observed without contact with other patients and before being treated in a general ward until COVID-19 infection has been ruled out. During the observation period, no substantial treatment for a surgical patient with a fingertip defect can be performed, missing a critical window and decreasing the probability of recovery of finger function. Thus, it is essential to develop techniques to reduce time prior to surgery for fingertip defect patients.

For the past few years, digital design and 3D printing technology have significantly improved the efficiency of doctor-patient communication [7, 8], because they can be used for preoperative planning and intraoperative navigation [9–11]. During the COVID-19 epidemic, skin flaps can be precisely digitally designed for patients under observation, with minimal contact with the patient, saving time typically used for designing flaps in the traditional way during the operation. These flaps can also be customized according to the needs of patients, improving patient satisfaction. The 3D model is printed simultaneously to simulate the operation and allows for thorough preoperative communication with the patient only once or as few times as possible. Such preoperative design avoids incomplete and repeated communication and improves the efficiency of preoperative communication.

In this study, fingertip defects were treated by digitally designing skin flaps preoperatively, combined with a 3D-printed model of the affected finger, for fingertip defect patients under observation in a buffer ward during the COVID-19 pandemic. This procedure saves time during the operation and improves the success rate of the operation and the survival rate of the flap with minimal preoperative contact with the patient, thereby reducing the risk of COVID-19 transmission. At present, there are few reports on the application of digital design combined with 3D printing technology in fingertip defect flap transplantation during the COVID-19 pandemic. In this study, 25 cases of 30 fingertip defect patients were selected, and good postoperative efficacy was obtained.

2. Materials and Methods

2.1. Case Inclusion and Exclusion Criteria. Case inclusion criteria were as follows: (1) patients with negative COVID-19 nucleic acid tests in the outpatient department were rechecked with a nucleic acid test, antibody test, and chest CT examination after hospitalization. Before the examination results were obtained, the patients were temporarily placed in a buffer ward. (2) Physical examination identified the patients as having a fingertip defect. (3) A fingertip defect flap was digitally designed preoperatively. (4) 3D-printed models of the affected finger were used for preoperative communication with patients with fingertip defects.

Exclusion criteria were as follows: (1) patients with old fingertip defects and (2) patients with other diseases who cannot tolerate surgery.

2.2. Materials. There were 25 cases with 30 fingers in the group of 15 males and 10 females aged 20-65 years old (mean 35 ± 5 years). Injured fingers were as follows: index finger in five cases, middle finger in eight cases, ring finger in ten cases, and little finger in two cases. The defect area of fingertips ranged from $1.5\,cm \times 3.5\,cm$ to $2.0\,cm \times 5.0\,cm$. One-stage flap repair was performed after emergency debridement.

2.3. Digital Design and 3D Printing Technology

2.3.1. Scans of Injured Fingers. The 3D Systems Sense software (3D Systems Company, America) was used to assess injured fingers. Geometric resolution was adjusted to the highest level with scanning capacity at the minimum. The scanner was aimed at the patient's hand to accurately capture an image of the hand on the affected side. Uninjured parts of the hand were removed by cutting, materialized to form a 3D hand model, and exported in STL file format. The same procedure was followed for the healthy side of the hand.

2.3.2. Flap Design. The STL file was imported into 3-matic 12.0 (Materialise Company, Belgium). First, the healthy hand model was processed, and "Wrap" and "Smooth" were used to smooth the surface of the model. Using the "Mirror" function, a hand model of the affected side was generated. Then, using the same method for the affected hand model, coincident comparison was made between the affected finger of the generated mirrored hand model of the affected side and that of the affected hand model. The extra part is the missing part of the fingertip. The "Trim" tool in "Design" was used to cut the extra part of the affected hand model except the affected finger, keeping the part of the affected finger that needs to be transplanted. The "Mark" tool was used to mark the part of the fingertip defect that needs to be covered, and "Smooth Marking Border" was used for the marked area to generate smooth edges. The generated surface was selected, and the property bar was checked to identify the area of the selected surface, that is, the area of the skin flap of the donor area. According to the needs of the operation, the same area was marked on the side of the affected finger, and the thickness of the shell was adjusted to 2 mm using the "Hollow" tool to extract the flap in the donor area. With the "Boolean Subtraction" tool, the model of the affected finger was subtracted from the model of the skin flap by Boolean subtraction to obtain a model of the fingertip with the defective skin flap (Figure 1), which was exported in STL file format.

2.3.3. Parameters for Designing the 3D Model. The STL file was imported into CURA 15.02.1 (Ultimaker Company, Netherlands), according to a previous study [12], and prior experience was used to set software parameters. The model "Scale" parameter was set to 0.9, while the scale of the printed model was closer to the real size. Because the finger model

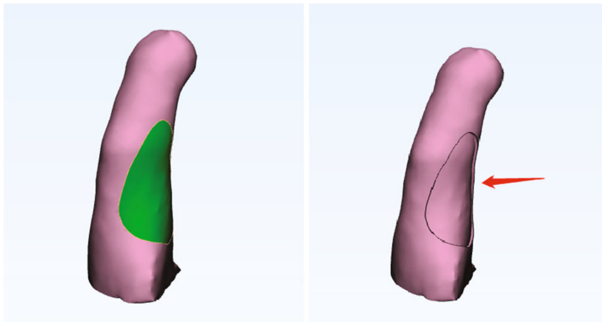

Figure 1: 3-matic 12.0 was used to design grafted skin flaps for fingertip defects. The green region simulates the selected donor area; removing the donor flap by pulling out the shell simulates flap cutting.

was wrapped in the design of the skin flap, the model proportions were a little larger than the actual proportions, so when setting parameters, the proportion should be appropriately reduced. The design was then exported in Gcode file format.

2.3.4. 3D Printing. The Gcode-formatted file was imported into a 3D printer (JGAURORA Company, China). Nozzle temperature was set at 210°C, and the hot bed temperature was set at 50°C. After preheating, the 3D-printed model of the fingertip defect of the defective skin flap was obtained.

2.3.5. Preoperative Communication. The biological skin flap was pasted on the surface of the 3D model and then cut to obtain the area that fits with the donor area of the defect. This is the transplanted skin flap. The root of the simulated grafted skin flap was fixed on the model, and the rotation was used to simulate the flipping of the donor flap during the operation for preoperative communication (Figure 2).

2.3.6. Intraoperative Guidance. The simulated grafted skin flap was removed from the surface of the 3D model, used to cover the donor area of the patient's finger, and marked on the donor area, to accurately obtain the selected area and range of the donor area intraoperatively before surgery.

2.4. Operation Methods

2.4.1. Flap Cut Out. All patients underwent a nucleic acid test, antibody test, and chest CT examination after hospitalization, and the possibility of COVID-19 was excluded. Brachial plexus block anesthesia was performed under a tourniquet, and complete debridement was performed during the operation. The flap was designed on the side of the affected finger, pedicled with the distal end of the digital artery. The distal end of the flap retained 1 cm of soft tissue including the ipsilateral digital vasculature and nerve bundle. The flap area was 1.6 cm × 3.6 cm to 2.1 cm × 5.1 cm. The proximal flap was dissociated in the superficial plane of the vascular nerve bundle from the proximal end to the distal end, the distal 2 cm vascular nerve bundle was dissociated, and the farthest 1 cm vascular nerve bundle was contained in the soft tissue and dissociated with the flap. After the flap was completely dissociated, it was rotated 180° to cover the fingertip defect, and the flap was sutured. Full-thickness skin grafts were taken from donor areas for repair and pressurized bandaging.

2.4.2. Postoperative Management and Follow-Up. Symptomatic supportive treatments such as nerve nutrition, swelling and pain relief, anticoagulation, anti-infection, and antispasticity were routinely conducted. The affected limb was elevated to allow for venous return, and blood circulation was closely observed to prevent and treat vascular crisis. Postoperative wound dressings were actively changed, and drainage strips were removed. Sutures were removed 14 days after the operation, and the plaster cast was removed for external fixation 3 weeks later. The finger joint and wrist joint were strengthened for functional exercise under the guidance of physicians.

A follow-up was conducted within one year after the operation. During the follow-up, the evaluation indexes of the patients' skin flaps were measured and recorded, and the patients were instructed in how to strengthen finger and wrist joints using functional exercises. The standard of hand function evaluation of the Chinese Hand Surgery Society [13] was referenced to comprehensively evaluate the finger flap and function.

3. Results

No vascular crises occurred in 25 cases, and all flaps survived. One patient had superficial necrosis of about 0.4 cm × 0.4 cm at the distal end of the skin flap, which gradually healed after the dressing was changed. The postoperative follow-up was 3-12 months. The skin flaps were soft in texture and full in appearance, with good elasticity, no bloat, and color close to normal skin color; partial superficial sensation was restored; and there were no complications such as interphalangeal joint motion disorder or pain in the donor area [14]. The two-point resolution of the skin was 4-8 mm, with an average of 5.1 mm. All patients were evaluated 3 months after the operation according to the trial standard of hand function evaluation of the Chinese Hand Surgery Society. The results showed that outcomes in 20 cases were excellent (80%), four cases were good (16%), and one case was fair (4%). The excellent and good rate was 96%.

3.1. Typical Case. The patient (male, 40 years old) was admitted to the hospital due to soft tissue defect of the left middle finger (Figure 3(a)). Debridement treatment was performed in the first stage, and after 2 days, surgery was performed to repair the wound. The flap was removed according to the preoperative design (Figure 3(b)). The lateral flap of the finger covered the defect of the fingertip of the middle finger, and the blood supply of the flap was good (Figure 3(c)). Full-thickness skin grafts were taken from the donor area for repair and pressurized bandaging (Figure 3(d)). After 6 months of the postoperative follow-up, the skin flap was soft in texture and full in shape, had good elasticity, and was without bloat, and the skin color was close to normal. Some superficial sensation recovered, and no complications such as interphalangeal joint motion disorder and pain at the donor site were found (Figures 3(e) and 3(f)).

Figure 2: The root of the simulated grafted flap is fixed on the model, and the flipping of the donor flap during the operation is simulated for preoperative communication.

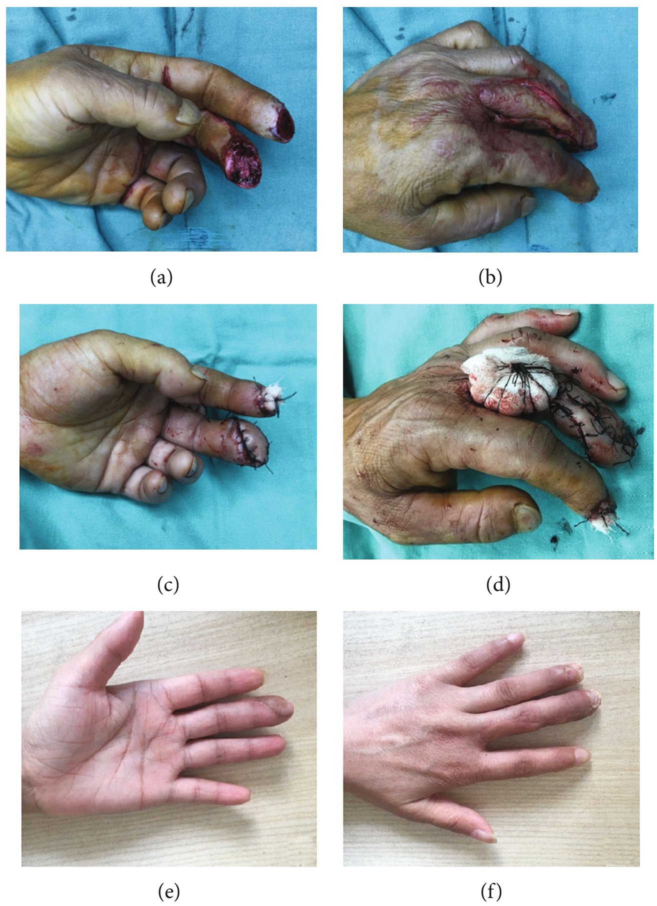

Figure 3: Progression of fingertip replacement prior to surgery and 6 months after surgery: (a) soft tissue defect of the left middle finger before surgery; (b) design of a lateral finger flap; (c) lateral finger flap covering the fingertip defect of the middle finger; (d) full-thickness skin grafts were taken from the donor area for repair and pressurized bandaging; (e, f) good appearance of the skin flap at 6-month follow-up after surgery.

4. Discussion

4.1. Research Status of Fingertip Defect Flap Transplantation. Fingertip skin defects are a common hand trauma, and there are various repair methods, each with advantages and disadvantages [15, 16]. Treatment methods include occluded dressing, local flap transplantation of the same or different fingers, and free flap transplantation [17–22]. Since the 1960s, local advance flap transplantation has been a common method to repair fingertip defects [23]. Fingertip defect flap transplantation technology is constantly optimized and improved based on prior methods, and various new methods emerge, promoting further development. At present, the reverse digital artery island flap, adjacent finger island flap, adjacent finger pedicled flap, dorsal finger fascia flap, or free toe lateral flap are commonly used in clinical repair [24–27], with good curative effect, and traditional surgical techniques have become increasingly mature.

4.2. Application of Digital Design Combined with 3D Printing Technology in Skin Flap Transplantation of Fingertip Defects. In recent years, applications of 3D printing technology in the field of medicine have been greatly developed. At present, many domestic universities, medical industry units, and scientific research institutions are constantly increasing investment in the field of 3D printing technology research and have made relatively big breakthroughs. However, there are few reports on the application of 3D printing technology in fingertip defect flap transplantation. Xu et al. [28] collected CT data of hands and feet from seven patients with thumb defects and used digital design combined with 3D printing technology to the select donor area for thumb reconstruction, realizing accurate, personalized, and optimized selection of the donor area of thumb defects. He et al. [29] included 13 cases of proximal interphalangeal joint defects of 13 fingers and simulated the digital test method of repairing facet joint defects with autografts of toe joints and realized accurate reconstruction of facet joints through 3D printing navigation technology, so as to achieve better joint movement function. Zhang et al. [30] selected 60 patients with fingertip defects, 30 with routine abdominal skin flap to repair surgery and 30 with regular 3D design improvement based on the dorsal fascia pedicle retrograde island flap to repair surgery. Through contrast research, Zhang et al. showed that 3D design improved the dorsal fascia pedicle retrograde island flap to repair fingertip defects with better clinical effect, convenient operation, and higher survival rate of the skin flap. In addition, the flap was tolerant to cold, and the flap recovered better after the operation. Mo et al. [31] selected 18 cases of thumb and finger skin defects repaired by free transplantation of toe mini flaps. The 3D images of blood supply in donor areas and defect parameters in recipient areas were analyzed by computer-aided anatomical modeling. Digital 3D reconstruction technology guided surgical design of the donor area, providing a reliable basis for designing a preoperative surgical plan and intraoperative treatment of vascular variation. This procedure reduced the risk during surgery and improved the skin flap survival rate.

At present, preoperative design of fingertip defect flap transplantation is mainly based on the subjective judgment of the surgeon. In traditional procedures, the surgeon covers the affected finger with thin paper or rubber gloves. Based on the experience of the surgeon, the flap area of the donor area is estimated, and the area fitted to the defect area is obtained after cutting the sample cloth. The sample cloth is pasted on the side of the affected finger, and the donor area is marked along the edge of the sample cloth, to design the surgical method and perform the operation. There are some problems in this traditional flap design, such as inaccuracy of donor flap design. The digital surgical design scheme of fingertip defect flap transplantation has thus been adopted, allowing the design to be carried out in a virtual software environment according to the specific injuries of the patients. After printing the 3D physical model of fingertip defects of the defect flap, the biological skin flap is pasted on the surface of the 3D model and then cut to obtain the area that fits with the donor area of the defect. This method can effectively solve the lack of accuracy, scientific basis, and standardization due to subjective experience of previous operations and of the operator in the traditional method. It also effectively avoids a mismatch between the actual cut skin flap and the amputated finger. At the same time, by fixing the root of the simulated grafted skin flap on the model and rotating to simulate turnover of the donor flap during the operation, preoperative communication is more visual and intuitive, which can effectively promote the doctor-patient relationship.

In this study, digital surgical design was adopted to preoperatively design accurate and personalized fingertip defect grafted flaps, according to the specific injuries of different affected fingers. The preoperative surgical design allowed for visualization, which was conducive to smooth operation, reduced unnecessary loss of donor area, and made the selection range of the donor area more accurate, thus improving surgical efficiency. A total of 25 cases were treated with digital design combined with 3D printing defects in the fingertip flap transplantation preoperative design guidance. Intraoperative-specific operation implementation guidance improved accuracy and reduced injury, and after the operation, the repaired finger had cold resistance and the new skin felt good, which supported patient satisfaction.

4.3. Advantages and Disadvantages of Digital Design Combined with 3D Printing Technology during the COVID-19 Epidemic. The main advantages of digital design combined with 3D printing during the COVID-19 epidemic are as follows: (1) the use of digital skin flap design for patients in the observation period prior to surgery allows for accurate design of the skin flap in advance with less patient contact, saving time typically required for designing the skin flap in the traditional way during the operation. (2) Designing the flap in advance saves operation time and reduces the time of tourniquet binding on the affected limb, restoring blood supply to the affected finger as soon as possible and improving the survival rate of the flap. (3) Personalized skin flaps can be designed to meet the needs of patients and improve patient satisfaction. (4) Printing a 3D model to simulate surgery is visual and intuitive. It can result in thorough preoperative communication with patients once or as few times as possible, avoiding incomplete and repeated communication and improving efficiency.

The main disadvantages of digital design combined with 3D printing during the COVID-19 epidemic are as follows: (1) it increases the workload of clinicians, and clinicians need to spend time to learn software operations. (2) 3D printing is high cost, making it difficult to popularize in clinical practice.

4.4. The Improvement of Digital Design Combined with 3D Printing Technology. At present, the application of digital design combined with 3D printing technology in fingertip defect flap transplantation is relatively rare. It has certain advantages in the aspects of skin flap precision, personalized preoperative design, and preoperative communication. However, for the blood vessels and nerves in the flap transplantation, it is hard to carry out effective preoperative simulation, so more technical means are still needed. Mathes and Neligan [32–34] suggested that CTA (CT angiography) can be used to distinguish the soft tissue plane and clearly show the path of inferior abdominal wall perforating vessels in subcutaneous tissue, subfascial tissue, and intramuscular tissue, which can better guide microsurgery. Combined with CTA technology, microsurgery can be used to locate the route of the donor artery and the starting point of the vessel pedicle, avoid unnecessary damage to the donor area, and improve the survival rate of the donor flap. To solve the problem of poor sensation of skin flap repair, Yang et al. [35] adopted the method of the retrograde island flap with cutaneous branch of the proper finger nerve and digital artery to treat soft tissue defects of the same finger. Feeling in the fingertip recovered well after operation, and the shape was appropriate. In cases where other flaps are not suitable, the reverse island flap containing the cutaneous branch of the proper digital nerve and the digital artery is an alternative method to repair soft tissue defect of the fingertip.

5. Conclusion

COVID-19 has complicated the traditional treatment of patients with fingertip defects. Treatment of fingertip defects is an emergency operation that should be conducted as soon as possible. During the COVID-19 pandemic, the time to surgery for patients with fingertip defects is extended. In order to save the treatment time of patients with fingertip defects as much as possible, preoperative digital design of fingertip defect flaps was adopted for patients in the observation period. Preoperative communication was conducted in combination with a 3D-printed model of the affected finger to treat fingertip defects, to achieve the purpose of early treatment with as little patient contact as possible to reduce the risk of transmission. The precise design of the skin flap can save operation time and improve the operation success rate and the survival rate of skin flaps. The efficiency of preoperative communication was improved by printing 3D models to simulate surgery, and the satisfaction of patients was improved by personalized design of skin flaps, providing application value in clinical treatment.

Data Availability

All data were collected from the Department of Hand and Foot Microsurgery, Puren Hospital, Wuhan City, Hubei Province, China.

Consent

Written informed consent was obtained from the patients for their anonymized information to be published in this article.

Conflicts of Interest

The authors declare no potential conflicts of interest with respect to the research, authorship, and/or publication of this article.

Authors' Contributions

Hui Lu and Hanshu Peng contributed equally to this work. The experiment was designed by Rong Liu, Hui Lu, and Hanshu Peng. The experiment was implemented by Hui Lu and Hanshu Peng. The experiment was evaluated by Rong Liu and Qimei Wu. The data was collected by Hui Lu, Ze Peng, Dingxi Liu, and Qimei Wu.

Acknowledgments

This work was supported in part by the Hubei Provincial Natural Science Foundation Committee General Project (2020CFB548) (Research and development of 3D printing rehabilitation AIDS design key technology based on topology optimization technology) and Science and Technology Support Plan Project of Guizhou Province in 2021 (202158413293820389) (Development and Industrialization of Adaptive Implant Devices for Bone Defect Regeneration in Children).

References

[1] L.-W. Lok, W.-L. Chan, and Y.-K. Lau, "Functional outcomes of antegrade homodigital neurovascular island flaps for fingertip amputation," *The Journal of Hand Surgery*, vol. 22, no. 1, pp. 39–45, 2017.

[2] L. Wang and X. Gao, *Orthopedic surgery*, People's Medical Publishing House, Beijing, China, 1989.

[3] N. Chen, M. Zhou, X. Dong et al., "Epidemiological and clinical characteristics of 99 cases of 2019 novel coronavirus pneumonia in Wuhan, China: a descriptive study," *The Lancet*, vol. 395, no. 10223, pp. 507–513, 2020.

[4] D. Wang, B. Hu, C. Hu et al., "Clinical characteristics of 138 hospitalized patients with 2019 novel coronavirus-infected pneumonia in Wuhan, China," *JAMA*, vol. 323, no. 11, pp. 1061–1069, 2020.

[5] Q. Li, X. Guan, P. Wu et al., "Early transmission dynamics in Wuhan, China, of novel coronavirus-infected pneumonia," *The New England Journal of Medicine*, vol. 382, no. 13, pp. 1199–1207, 2020.

[6] H. Zhang, Z. Kang, H. Gong et al., "The digestive system is a potential route of 2019 nCoV infection: a bioinformatics analysis based on single-cell transcriptomes," *BioRxiv*, 2020.

[7] R. Partridge, N. Conlisk, and J. A. Davies, "In-lab three-dimensional printing: an inexpensive tool for experimentation and visualization for the field of organogenesis," *Organogenesis*, vol. 8, pp. 22–27, 2012.

[8] J. S. Mulford, S. Babazadeh, and N. Mackay, "Three-dimensional printing in orthopaedic surgery: review of current and future applications," *ANZ Journal of Surgery*, vol. 86, no. 9, pp. 648–653, 2016.

[9] X. Wang, S. Xu, S. Zhou et al., "Topological design and additive manufacturing of porous metals for bone scaffolds and orthopaedic implants: a review," *Biomaterials*, vol. 83, pp. 127–141, 2016.

[10] S. Z. Zhong, "Exploration of medical 3D printing technology," *Chinese Journal of Orthopaedic Trauma*, vol. 19, no. 2, pp. 138-139, 2017.

[11] J. Wieding, A. Wolf, and R. Bader, "Numerical optimization of open-porous bone scaffold structures to match the elastic

properties of human cortical bone," *Journal of the Mechanical Behavior of Biomedical Materials*, vol. 37, pp. 56–68, 2014.

[12] B. Zhu, "Research on Pro/E-Cura 3D printing process technology," *Science and Technology Outlook*, vol. 17, pp. 149–149, 2014.

[13] P. Shengde, G. Yudong, and S. De, "The trial standard of upper extremity function evaluation of hand surgery society of Chinese medical association," *Chinese Journal of Hand Surgery*, vol. 16, no. 3, pp. 130–135, 2000.

[14] W. Wang, L. Zongbao, Y. Wang et al., "A long-term follow-up report on the repair of soft tissue defect of finger tip with digital artery reverse island flap," *Chinese Journal of Hand Surgery*, vol. 28, no. 3, pp. 142-143, 2012.

[15] Z. Feiya, W. Gao, J. Wu et al., "Reconstruction of finger tip defect with double subcutaneous pedicle V-Y advanced flap and its curative effect," *Chinese Journal of Hand Surgery*, vol. 26, no. 3, pp. 162–164, 2010.

[16] H. Jingliang, X. Zhenrong, L. Yanwen et al., "A single perforator micro flap of posterior interosseous artery was used to repair finger skin defect," *Chinese Journal of Hand Surgery*, vol. 22, no. 5, pp. 267–269, 2006.

[17] R. Adani, I. Marcoccio, L. Tarallo, and U. Fregni, "The reverse heterodigital neurovascular island flap for digital pulp reconstruction," *Techniques in Hand & Upper Extremity Surgery*, vol. 9, no. 2, pp. 91–95, 2005.

[18] Y. Lee, S.-H. Woo, Y.-W. Kim, Y. H. Lee, and G. H. Baek, "Free flaps for soft tissue reconstruction of digits," *Hand Clinics*, vol. 36, no. 1, pp. 85–96, 2020.

[19] J. B. Tang, "Fingertip repair methods: choices for different fingers and sides emphasizing sensation," *Journal of Hand Surgery*, vol. 44, no. 10, pp. 1109–1111, 2019.

[20] J. B. Tang, D. Elliot, R. Adani, M. Saint-Cyr, and F. Stang, "Repair and reconstruction of thumb and finger tip injuries: a global view," *Clinics in Plastic Surgery*, vol. 41, no. 3, pp. 325–359, 2014.

[21] P. Tos and R. Adani, "Finger amputations and pulp defects distal to the distal interphalangeal joint," *Journal of Hand Surgery*, vol. 44, no. 10, pp. 1105-1106, 2019.

[22] H. Wang, X. Yang, C. Chen, Y. Huo, B. Wang, and W. Wang, "Modified heterodigital neurovascular island flap for sensory reconstruction of pulp or volar soft tissue defect of digits," *The Journal of Hand Surgery*, vol. 45, no. 1, pp. 67.e1–67.e8, 2020.

[23] J. Chen, "Research progress in the treatment of finger wound," *Chinese Journal of Trauma*, vol. 34, no. 7, pp. 663–669, 2018.

[24] Z. Gao, Z. Jingliang, L. Yanwen et al., "Fingertip defect was repaired with free nerve flap of foot toe peroneal artery," *Chinese Journal of Hand Surgery*, vol. 31, no. 5, p. 398, 2015.

[25] L. Qichao, B. Chaohui, W. Zhu et al., "Island flap of dorsal branch of proper digital artery of long pedicled adjacent finger to repair lateral tissue defect of middle and distal finger," *Chinese Journal of Hand Surgery*, vol. 31, no. 5, pp. 340–342, 2015.

[26] X. Wang, C. Jiansheng, G. Wu et al., "The dorsal finger nerve fascia flap was used to repair the skin defect at the end of multiple fingers," *Chinese Journal of Hand Surgery*, vol. 28, no. 6, p. 360, 2012.

[27] C. Lefeng, Z. Zhenwei, Y. Chuhong et al., "Reverse island flap of proximal radial digital artery of middle finger to repair the defect of thumb tip," *Chinese Journal of Hand Surgery*, vol. 30, no. 1, pp. 44–46, 2014.

[28] J. Xu, G. D. Zhang, and H. T. Tan, "Application of digital design combined with 3D printing technology in thumb reconstruction," *Journal of Clinical Anatomy*, vol. 33, no. 5, pp. 541–544, 2015.

[29] Z. He, J. Xu, Z. Guodong et al., "3D printing technology assisted autogenous phalangeal joint transplantation to accurately repair facet joint defects," *Chinese Journal of Tissue Engineering Research*, vol. 23, no. 31, pp. 4932–4938, 2019.

[30] Z. Li, X. Shuijun, and H. Zhu, "Clinical study of repairing finger tip defect with 3D modified retrograde island flap of dorsal finger fascia pedicle," *Shenzhen Journal of Integrated Traditional and Western Medicine*, vol. 29, no. 21, pp. 123-124, 2019.

[31] M. Yongjun, H. Tan, K. Yang et al., "Application of 3D technique in the reconstruction of thumb and finger defects by transplantation of toe miniature skin flap," *Chinese Journal of Microsurgery*, vol. 20, no. 3, pp. 294–297, 2015.

[32] D. Mathes and P. Neligan, "Current techniques in preoperative imaging for abdomen-based perforator flap microsurgical breast reconstruction," *Journal of Reconstructive Microsurgery*, vol. 26, no. 1, pp. 003–010, 2010.

[33] R. D. Katz, M. A. Manahan, A. N. Rad, J. I. Flores, N. K. Singh, and G. D. Rosson, "Classification schema for anatomic variations of the inferior epigastric vasculature evaluated by abdominal CT angiograms for breast reconstruction," *Microsurgery*, vol. 30, no. 8, pp. 593–602, 2010.

[34] W. M. Rozen and M. W. Ashton, "The "limited rectus sheath incisions" technique for DIEP flaps using preoperative CT angiography," *Microsurgery*, vol. 29, no. 7, pp. 525–528, 2009.

[35] L. Yang, L. Hongjun, Z. Wenzhong et al., "Repair of soft tissue defect of the same finger with reverse island flap of digital artery with cutaneous branch of proper finger nerve," *Chinese Journal of Hand Surgery*, vol. 33, no. 4, pp. 307–309, 2017.

Hindawi
BioMed Research International
Volume 2021, Article ID 5542595, 8 pages
https://doi.org/10.1155/2021/5542595

Research Article

Screws Fixation for Oblique Lateral Lumbar Interbody Fusion (OL-LIF): A Finite Element Study

Qinjie Ling,[1] **Huanliang Zhang**,[2] **and Erxing He**[1]

[1]Dept of Spinal Surgery, The First Affiliated Hospital of Guangzhou Medical University, 151 Yanjiang West Road, Guangzhou, Guangdong, China 510120
[2]MOE Key Laboratory of Disaster Forecast and Control in Engineering, Institute of Applied Mechanics, Jinan University, Guangzhou, Guangdong, China 510632

Correspondence should be addressed to Erxing He; heerxing717@163.com

Received 15 April 2021; Accepted 10 May 2021; Published 17 May 2021

Academic Editor: Ying-Qi Zhang

Copyright © 2021 Qinjie Ling et al. This is an open access article distributed under the Creative Commons Attribution License, which permits unrestricted use, distribution, and reproduction in any medium, provided the original work is properly cited.

Background. The combination of screw fixation and cage can provide stability in lumbar interbody fusion (LIF), which is an important technique to treat lumbar degeneration diseases. As the narrow surface cage is developed in oblique lateral lumbar interbody fusion (OL-LIF), screw fixation should be improved at the same time. We used the finite element (FE) method to investigate the biomechanics response by three different ways of screw fixation in OL-LIF. *Methods*. Using a validated FE model, OL-LIF with 3 different screw fixations was simulated, including percutaneous transverterbral screw (PTVS) fixation, percutaneous cortical bone trajectory screw (PCBTS) fixation, and percutaneous transpedical screw (PPS) fixation. Range of motion (ROM), vertebral body displacement, cage displacement, cage stress, cortical bone stress, and screw stress were compared. *Results*. ROM in FE models significantly decreased by 84-89% in flexion, 91-93% in extension, 78-89% in right and left lateral bending, and 73-82% in right and left axial rotation compared to the original model. The maximum displacement of the vertebral body and the cage in six motions except for the extension of model PTVS was the smallest among models. Meanwhile, the model PTVS had the higher stress of screw-rods system and also the lowest stress of cage. In all moments, the maximum stresses of the cages were lower than their yield stress. *Conclusions*. Three screw fixations can highly restrict the surgical functional spinal unit (FSU). PTVS provided the better stability than the other two screw fixations. It may be a good choice for OL-LIF.

1. Introduction

Screw fixation with cage in lumbar interbody fusion (LIF) is a key technique to treat lumbar disease degeneration. Wide surface cages were used in some minimally invasive LIF, such as oblique lumbar interbody fusion (O-LIF), direct/extreme lateral interbody fusion (DLIF/XLIF), and anterior lumbar interbody fusion (ALIF). However, injuries to the paraspinal nerves and vessels sometimes occur [1, 2]. Currently, an endoscopic technique through Kambin's triangle lumbar interbody fusion named as oblique lateral lumbar interbody fusion (OL-LIF) was introduced [3]. The safety and effectivity of the technique have been proved [4]. OL-LIF was a different form O-LIF, of which the approach was expanded via posterior retraction of the psoas for disc exposure [5]. Instead of the wide surface cage, the narrow surface cage was used by OL-LIF for inserting to the intervertebral space through an endoscopic working tunnel. Biomechanical evaluation showed that a narrow surface cage with 9 mm width was recommended in OL-LIF [6]. When a small cage was used, the demand of a screw-rods system for function spinal unit (FSU) stability was increased. The way of screw fixation in FSU was studied. One of them was transverterbral screws (TVS), also called transdiscal screws or transpedicular-transdiscal screws [7–9]. TVS was used to treat L5-S1 spondylolisthesis [7, 8, 10, 11] and thoracic interbody fusion

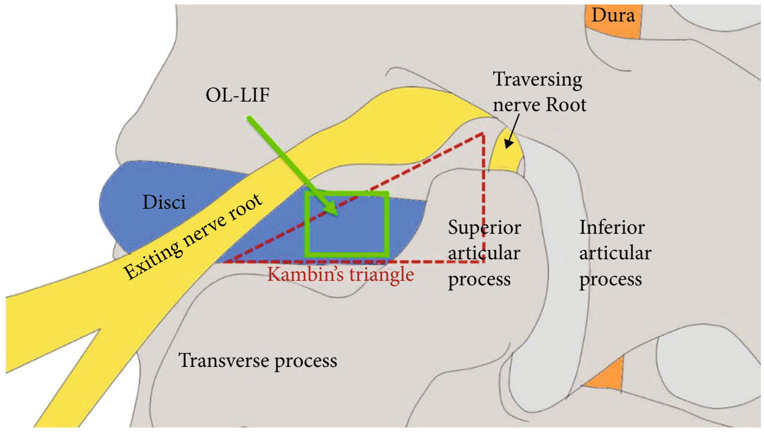

Figure 1: The surgical approach of endoscopic OL-LIF (direction of approach and surrounding anatomy: solid rectangle line was the endoscopic approach of OL-LIF and broken triangle line was the boundary of Kambin's Triangle. OL-LIF: oblique lateral lumbar interbody fusion).

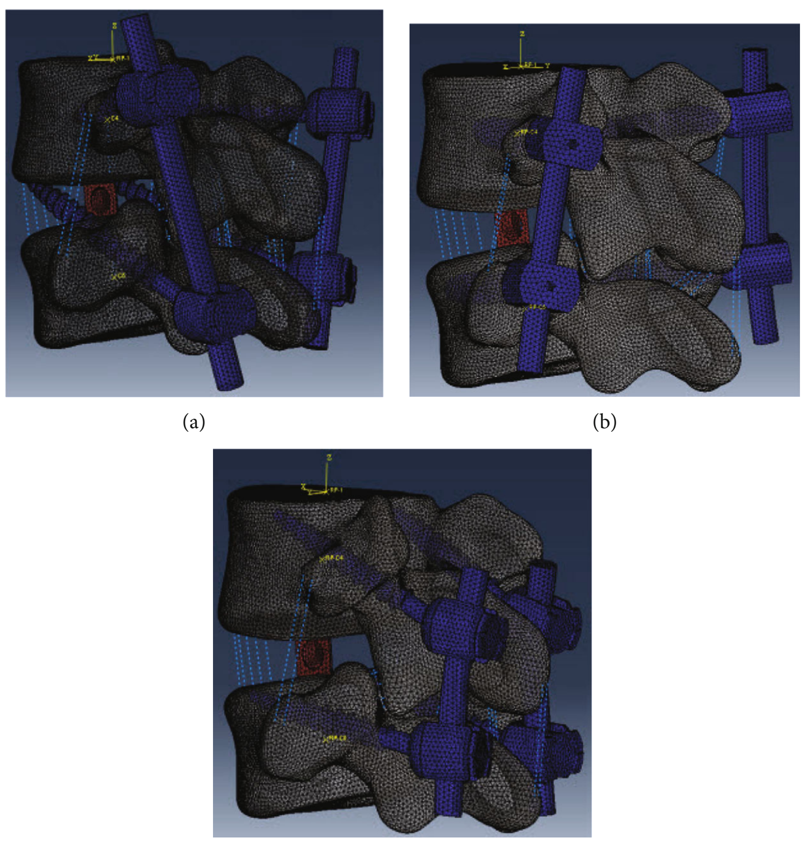

(a) (b)

(c)

Figure 2: Endoscopic OL-LIF models with different screw fixation in Abaqus 6.14-4. (a) Model PTVS. (b) Model PCBTS. (c) Model PPS (PCBTS: percutaneous transverterbral screws fixation; PCBTS: percutaneous cortical bone trajectory screws; PPS: fixation and percutaneous transpedical screws).

[12]. Due to the multiple cortical bones across, FSU had more stability than that fixed by traditional transpedical screws (PS) and a high fusion rate was observed [12]. With the help of the SpineAssist miniature system [13] and the O-arm image guidance system [12], percutaneous transverterbral screws (PTVS) could be applied in the clinical setting. Similarly, cortical bone trajectory screw (CBTS) fixation was considered to have similar or even more stability than pedicle screws. Percutaneous cortical bone trajectory screws (PCBTS) have been applied well in LIF recently [14, 15].

Table 1: Parameters of the various tissues of the lumbar spine. [5].

Tissues	Modulus (MPa)	Poisson's ratio	Element type	Thickness
Cortical bone	12000	0.3	Shell	1 mm
Cancellous bone	100	0.2	Solid	/
Bony endplate	12000	0.3	Shell	1 mm
Cartilaginous endplate	23.8	0.4	Shell	0.8 mm
Facet	35	0.4	Shell	0.2 mm
Titanium (Ti-6Al-4V)	110000	0.3	Solid	/
PEEK (polyetheretherketone)	3700	0.3	Solid	/

Table 2: Property of seven ligaments of the lumbar spine. [5].

Ligament	Strain: ε (%)	Stiffness: k (N/mm)	ε (%)	k (N/mm)	ε (%)	k (N/mm)	ε (%)	k (N/mm)
ALL			$0 < \varepsilon < 12.2$	347	$12.2 < \varepsilon < 20.3$	787	$20.3 < \varepsilon$	1864
PLL			$0 < \varepsilon < 11.1$	29.5	$11.1 < \varepsilon < 23$	61.7	$23 < \varepsilon$	236
CL			$0 < \varepsilon < 25$	36	$25 < \varepsilon < 30$	159	$30 < \varepsilon$	384
ITL	$\varepsilon < 0$	$k = 0$	$0 < \varepsilon < 18.2$	0.3	$18.2 < \varepsilon < 23.3$	1.8	$23.3 < \varepsilon$	10.7
FL			$0 < \varepsilon < 5.9$	7.7	$5.9 < \varepsilon < 49$	9.6	$49 < \varepsilon$	58.2
SSL			$0 < \varepsilon < 20$	2.5	$20 < \varepsilon < 25$	5.3	$25 < \varepsilon$	34
ISL			$0 < \varepsilon < 20$	1.4	$13.9 < \varepsilon < 20$	1.5	$20 < \varepsilon$	14.7

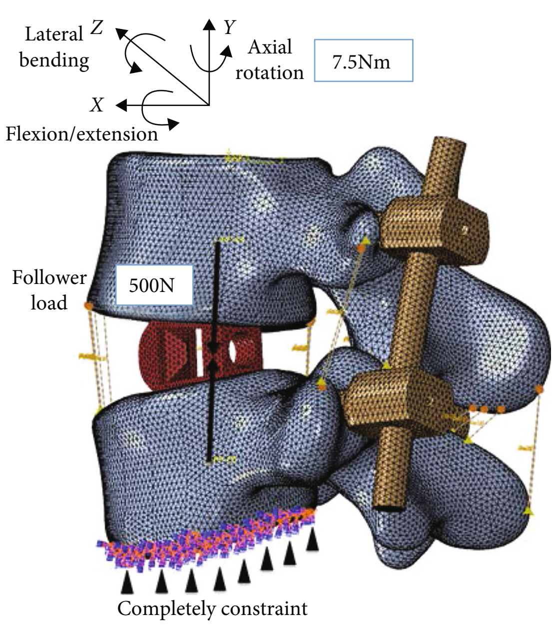

Figure 3: Loading and boundary conditions of the surgical model.

However, which screw fixation has the most stability among PTVS, PCBTS, and percutaneous pedicle screws (PPS) have not been discussed.

Since 1973, Belytschko et al. [16] first developed a two-dimensional finite element (FE) model of the lumbar disc; FE analysis has become an effective method to study the biomechanics of the human spine. Compared with the in vitro cadaveric study, FE analysis had some advantages: lower economic cost, the easier to repeat the experiment, and better to predict the in vivo bone and spinal implant stress [17, 18]. Cage and screw fixation combination has been prove to achieve adequate vertebral stability in LIF [19, 20]. Recently, a novel narrow surface cage has been introduced to OL-LIF [6]. The result suggested that a 9 mm width cage was recommended in such minimally spinal surgery [6]. However, ways in screw fixation with the endoscopic cage for LIF have not been studied. The aim of this FE study was to evaluate three percutaneous screw fixations in biomechanics. The result can provide engineering evidence for the surgeon to improve the minimally invasive spinal surgery.

2. Materials and Methods

2.1. FE Model Development. The study was approved by the authors' affiliated institutions ethics committee. A FE software ABAQUS 6.14-4 (Dassault Systèmes, Vélizy-Villacoublay, France) was used to create a FE model of the L4-L5 functional spinal unit (FSU). The mesh sensitivity test and model validation have been done in previous study; the result of which is in a good agreement with other published experiments [6]. To simulate endoscopic OL-LIF (Figure 1), the disc of L4-L5 FSU and cartilage endplate were removed. Osteotomy was not needed in OL-LIF. Cortical bone and bony endplates were with 1 mm thickness. The thickness of facet joints in the contact area was 0.2 mm. The tangential behavior in contact was considered smooth, and normal behavior was described as a penalty algorithm. Seven major ligaments, the anterior longitudinal ligament (ALL), posterior longitudinal ligament (PLL), flaval ligament (FL), facet capsular ligament (CL), intertransverse ligament (ITL), interspinous ligament (ISL), and supraspinous ligament (SSL),

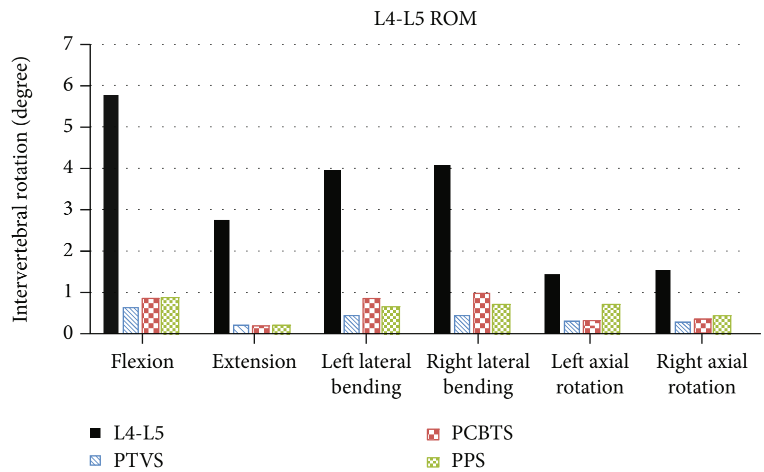

FIGURE 4: ROM of different FEA models (grey column: original model; blue column: PTVS; red column: PCBTS; green column: PPS).

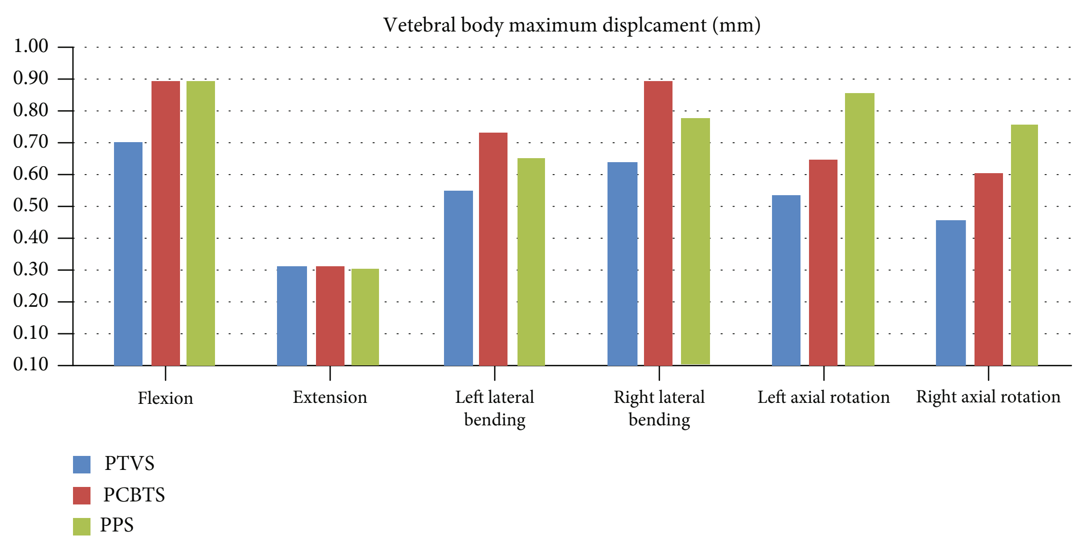

FIGURE 5: Vertebral body maximum displacement (mm) (blue column: PTVS; red column: PCBTS; green column: PPS).

were defined as axial connectors. The mechanical behaviors of all ligaments were described as nonlinear stress–strain curves. A peek cage with 9 mm width narrow surface and 11 mm height was inserted to the intervertebral space through Kambin's triangle by endoscopic approach [6]. Screws and rods were simulated as homogeneous linear elastic titanium (Ti-6Al-4V). Three different screw fixations (PTVS, PCBTS, and PPS) were assembled in the surgical models, respectively (Figure 2). The contact between screw heads and rods was defined as tied, where relative movement was forbidden. Additionally, contact between the screw and bone was simulated fully tied. The material properties of FE models can be seen in Tables 1 and 2.

2.2. Boundary and Loading Conditions. The inferior endplate of L5 was fully constrained. 500 N upper body weight in the lumbar spine was simulated by a compressive follower load with path through the centroids of two vertebral bodies (Figure 3). The moment of 7.5 Nm was applied on the superior endplate of L4 to test the motions of L4-L5 FSU in flexion, extension, lateral bending, and axial rotation (Figure 3).

3. Results

3.1. ROM and Displacement. Compared with the original model, ROMs of the three surgical models were significantly decreased by 84-89% in flexion, 91-93% in extension, 78-89% in right and left lateral bending, and 73-82% in right and left axial rotation (Figure 4). Model PTVS had the lowest ROM in five motions except in extension. In extension, the difference among surgical models was no more than 2%. The biggest difference happened in the right lateral bending between PTVS and PCBTS.

Among the models, the maximum displacement of the vertebral body and of the cage in model PTVS was the lowest in five moments, except that the extension was similar (Figures 5 and 6). Model PCBTS had the highest maximum displacement of the vertebral body in lateral bending, while

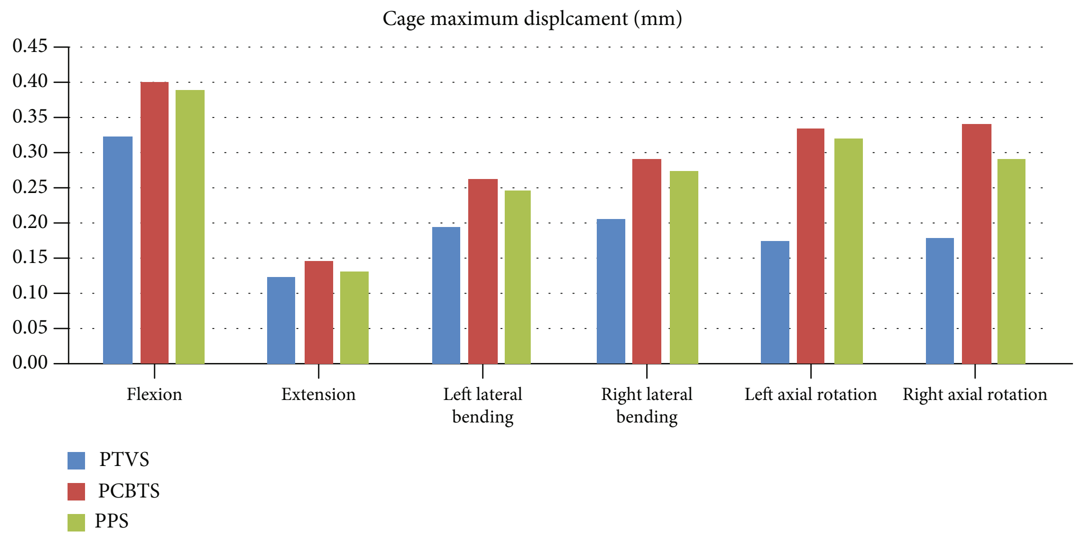

Figure 6: Cage maximum stress (MPa) (blue column: PTVS, red column: PCBTS, green column: PPS).

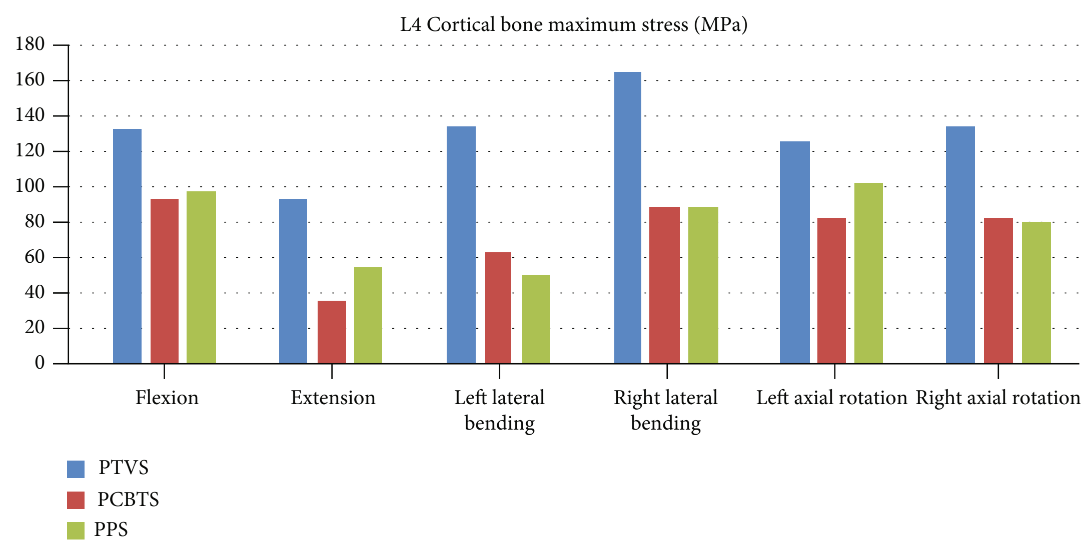

Figure 7: L4 cortical bone maximum stress (MPa) (blue column: PTVS, red column: PCBTS, green column: PPS).

the model PPS had in axial rotation (Figure 5). Model PCBTS also had the highest maximum displacement of the cage in all motions (Figure 6). The differences between model PCBTS and PPS were not obvious (Figure 6). Cages had the biggest displacement in flexion that model PTVS had 0.32 mm cage maximum displacement less than 0.40 mm for model PCBTS and 0.39 mm for model PPS (Figure 6).

3.2. The Maximum Equivalent von Mises Stress. The maximum stress of the L4 cortical bone in model PTVS was larger than the other two models in all moments (Figure 7). The largest stress was 132 MPa in PTVS in right lateral bending (Figure 7). The difference between PCBTS and PPS was not obvious. PCBTS had the lowest stress 36 MPa in extension among the models (Figure 7). The maximum stress of the L5 cortical bone was the largest in flexion and in left lateral bending in model PTVS, while it was the largest in extension and in right lateral bending in model PCBTS and was largest in left/right axial rotation in model PPS (Figure 8). In flexion, cage suffered the highest stress, which in PTVS was 57 MPa, in PCBTS was 82 MPa, and in PPS was 85 MPa. Among the models, the cage maximum stress of model PTVS was the smallest in five moments except for extension (Figure 9). Screw and rod maximum stress of model PTVS was the largest among the models in all motions; those were obvious in flexion, left lateral bending, and left/right axial rotation. In model PTVS, screw fixation maximum stress was 307 MPa, larger than 224 MPa for model PCBTS and 209 MPa for model PPS (Figure 10).

4. Discussion

Stability of the lumbar spine refers to the ability of the lumbar to cope with the physiological load of daily life, which is

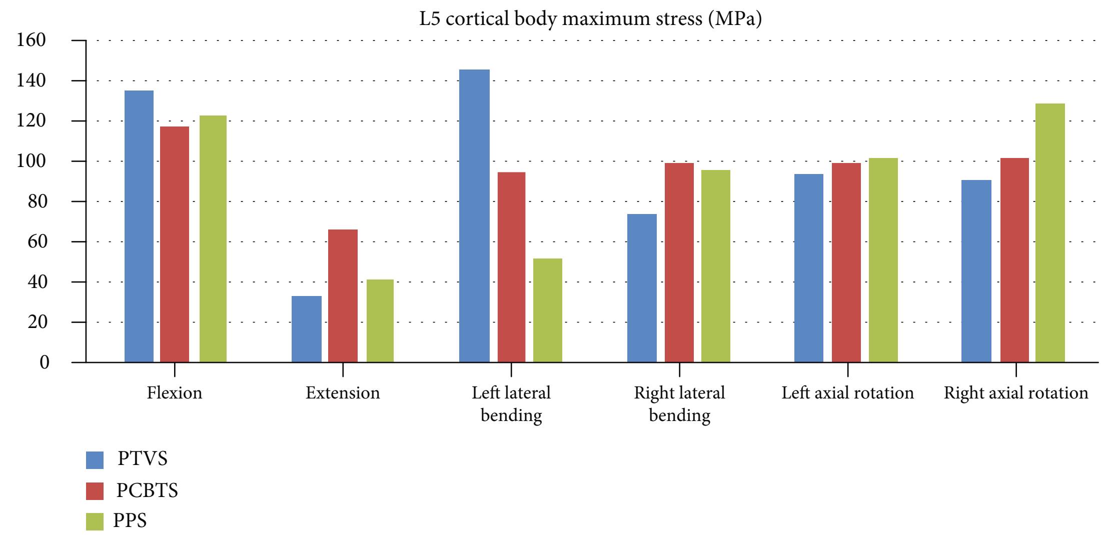

Figure 8: L5 cortical bone maximum stress (MPa) (blue column: PTVS; red column: PCBTS; green column: PPS).

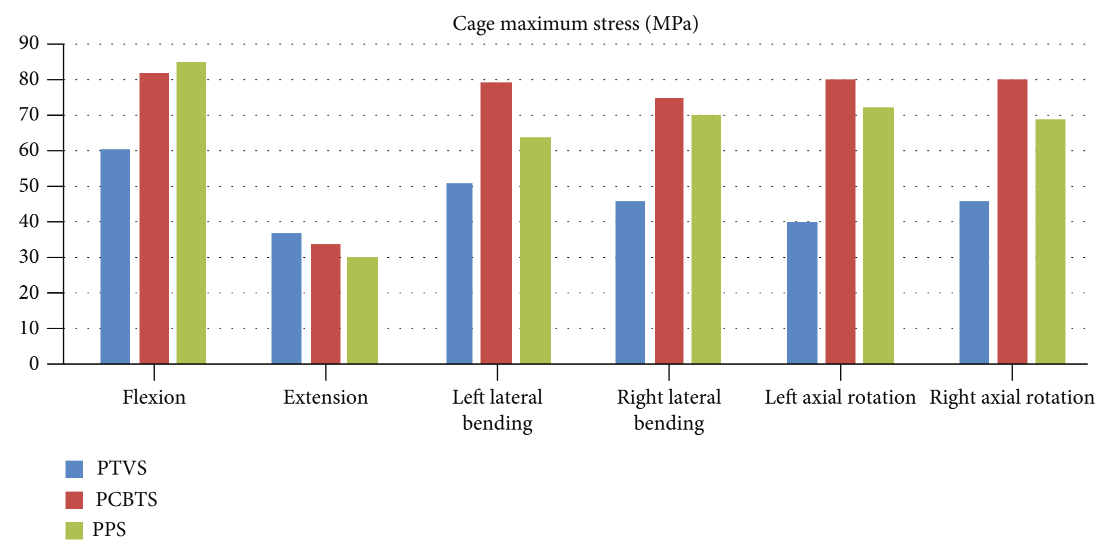

Figure 9: Cage maximum displacement (mm) (blue column: PTVS; red column: PCBTS; green column: PPS).

mainly maintained by the lumbar intervertebral disc, facet joint, intervertebral ligaments, and muscles. LIF with screw-rods system combined with cage can provide a strong stability for the lumbar segment and create an environment for the transplanted bone tissue for solid fusion. The way of screw fixation and the size of the cage both affect the stability of postoperative FSU. As the minimally invasive spinal surgery developed, the size of the cage got smaller than before to match the endoscopic working tunnel. When the cage changed, the screws should be enhanced. PTVS, PCBTS, and PPS have actually been put on the professional treatment of spinal disease. This study utilized a finite element method to assess the biomechanics of three screw fixations in endoscopic LIF. The result provided engineering evidence to the surgeon for reference in the clinical setting.

The ROM and the maximum displacement of the FE model can directly reflect the stability of the postoperative model. The smaller the ROM and displacement of FE model were, the greater the limit of the model activity, and the better the stability of the postoperative model. A solid stability of the postoperative FSU is good for intervertebral bone fusion because the micromotion of the cage in the intervertebral space can hinder bone fusion [21, 22]. In this study, the bottom of L5 was completely constricted and the maximum displacement of the model occurred in the anterior upper side of the L4 vertebral body. The displacement of the L4 vertebral body can mirror the ROM of the surgical model. A smaller L4 displacement resulted in lower ROM of FSU and higher stability of model. Displacement of L4 in six motions except extension of model PTVS was smaller than that of model PCBTS and model PPS (Figure 5). Similarly, the displacement of cage in six motions except the extension of the cage in model PTVS was smallest among the three models (Figure 6). Therefore, the model PTVS had the best stability

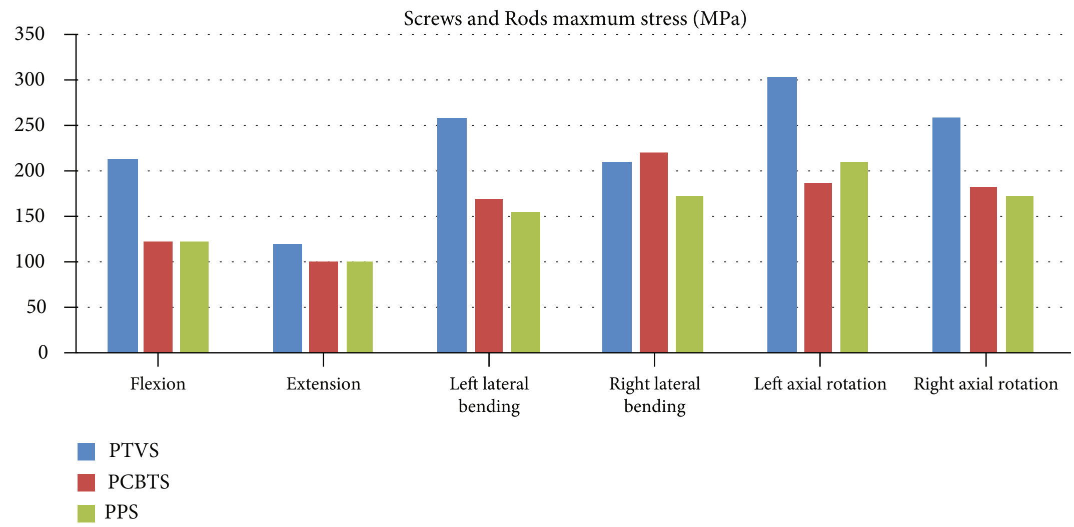

Figure 10: Screws and rods maximum stress (MPa) (blue column: PTVS; red column: PCBTS; green column: PPS).

among the models. The difference of extension among models was small, which agreed with the clinical setting because of the obstruction of the upper and lower articular process, lamina, spinous process, and ligaments. PTVS can effectively restrict the movement of the vertebral body by traversing multiple layers of the cortical bone (posterior pedicle cortex of L5, superior cortex of L5, and inferior cortex of L4), strongly fixing the anterior, middle, and posterior columns of L4-L5.

In LIF, after discectomy, the stability of FSU was mainly maintained by the cage and screw-rods system in addition to the facet joint and posterior osseous ligament complex. The stress of the cage was inversely proportional to that of the screw-rods system. The smaller the stress of cage, the greater the stress experienced by the screw-rods system, especially in minimally invasive LIF. In flexion, PTVS prevented L4 from moving downward and shared the pressure caused by L4, so the strain and stress of the cage were reduced (Figures 6 and 9). On the one hand, the proper pressure of the cage could prevent the movement of the implanted bone tissue and cage, which was good for interveterbral bone fusion. On the other hand, the cage maximum stress was no more than the yield stress 95 MPa [23] and that it would not cause fatigue rupture due to excessive stress. According to Wolff's law, the bone tissue has the ability to adapt to the mechanical environment. Proper stress can stimulate the growth of the bone tissue.

The contact area between the PTVS and the cortical bone of the vertebral body was small, so it was easy to cause local contact stress concentration. However, the stress concentration was not obvious from the result of calculation. The stress distribution of PTVS is more even than that of the other two fixations. The maximum stress of the PTVS was distributed more evenly in the screw body, while those of the PCBTS and PPS were distributed at the junction between the screw body and the screw head. PTVS has a longer body than PCBTS and PPS. Longer screw in the vertebral body could provide a better fatigue test, which could a bear better circulating load [24]. Using the large diameter screw may provide a better fatigue test, and the fusion cage could be considered omitted.

From the discussion above, it can be found that PTVS had the better stability than the other two screw fixations. Crossing the multiple layers of the cortical bone, PTVS effectively constrained the FSU sharing load stress with cage. With PTVS, the narrow surface cage in LIF was hardly destroyed. In the future, when the material of the screw improves and the fatigue test was passed, maybe there is no need for using the cage in LIF.

4.1. Limitations of This Study. The model of this study selected a FSU and did not simulate the whole lumbar vertebral model. The effect on the postoperative adjacent lumbar intervertebral disc was not considered. Cyclic load on the lumbar was not taken into account. Some components were simplified, e.g., the ligaments were modeled as an axial connector. The bone graft and postoperative residual annular fibrous were not constructed in the models because until bone fusion neither of these structures could provide immediate mechanical support after surgery. The cage was also simplified to remove the serrated surface. In our future study, the fatigue failure test of screws and cage will be investigated.

5. Conclusion

This study used a finite element method to develop three surgical models to simulate OL-LIF. The result showed PTVS restricted the model most displacement among models. Postoperative PTVS could provide strong stability for FSU immediately. PTVS combined with a narrow surface cage may be a good choice for OL-LIF.

Data Availability

The processed data required to reproduce these findings cannot be shared at this time as the data also forms part of an ongoing study.

Conflicts of Interest

The authors declare that they have no conflicts of interest.

References

[1] J. Inamasu and B. H. Guiot, "Vascular injury and complication in neurosurgical spine surgery," *Acta Neurochirurgica*, vol. 148, no. 4, pp. 375–387, 2006.

[2] J. R. Joseph, B. W. Smith, F. La Marca, and P. Park, "Comparison of complication rates of minimally invasive transforaminal lumbar interbody fusion and lateral lumbar interbody fusion: a systematic review of the literature," *Neurosurgical Focus*, vol. 39, no. 4, article E4, 2015.

[3] H. Abbasi and A. Abbasi, "Oblique lateral lumbar interbody fusion (OLLIF): technical notes and early results of a single surgeon comparative study," *Cureus*, vol. 7, no. 10, article e351, 2015.

[4] A. T. Yeung and P. M. Tsou, "Posterolateral endoscopic excision for lumbar disc herniation: surgical technique, outcome, and complications in 307 consecutive cases," *Spine*, vol. 27, no. 7, pp. 722–731, 2002.

[5] R. J. Mobbs, K. Phan, G. Malham, K. Seex, and P. J. Rao, "Lumbar interbody fusion: techniques, indications and comparison of interbody fusion options including PLIF, TLIF, MI-TLIF, OLIF/ATP, LLIF and ALIF," *Journal of Spine Surgery*, vol. 1, no. 1, pp. 2–18, 2015.

[6] Q. Ling, E. He, H. Zhang, H. Lin, and W. Huang, "A novel narrow surface cage for full endoscopic oblique lateral lumbar interbody fusion: a finite element study," *Journal of orthopaedic science: official journal of the Japanese Orthopaedic Association*, vol. 24, no. 6, pp. 991–998, 2019.

[7] W. A. Abdu, R. G. Wilber, and S. E. Emery, "Pedicular transvertebral screw fixation of the lumbosacral spine in Spondylolisthesis," *Spine (Phila Pa 1976)*, vol. 19, pp. 710–715, 1994.

[8] A. Minamide, T. Akamaru, S. T. Yoon, T. Tamaki, J. M. Rhee, and W. C. Hutton, "Transdiscal L5–S1 screws for the fixation of isthmic spondylolisthesis: a biomechanical evaluation," *Clin Spine Surg*, vol. 16, no. 2, pp. 144–149, 2003.

[9] A. M. Wu, J. A. Harris, J. C. Hao, S. M. Jenkins, Y. L. Chi, and B. S. Bucklen, "Biomechanical properties of posterior transpedicular-transdiscal oblique lumbar screw fixation with novel trapezoidal lateral interbody spacer: an in vitro human cadaveric model," *European Spine Journal*, vol. 26, no. 11, pp. 2873–2882, 2017.

[10] C. A. Logroscino, F. C. Tamburrelli, L. Scaramuzzo, G. R. Schirò, S. Sessa, and L. Proietti, "Transdiscal L5-S1 screws for the treatment of adult spondylolisthesis," *European Spine Journal*, vol. 21, no. S1, pp. 128–133, 2012.

[11] I. Collados-Maestre, A. Lizaur-Utrilla, T. Bas-Hermida, E. Pastor-Fernandez, and V. Gil-Guillen, "Transdiscal screw versus pedicle screw fixation for high-grade L5-S1 isthmic spondylolisthesis in patients younger than 60 years: a case–control study," *European Spine Journal*, vol. 25, no. 6, pp. 1806–1812, 2016.

[12] E. W. Nottmeier and S. M. Pirris, "Placement of thoracic transvertebral pedicle screws using 3D image guidance," *Journal of Neurosurgery. Spine*, vol. 18, no. 5, pp. 479–483, 2013.

[13] C. Birkenmaier, O. Suess, M. Pfeiffer, R. Burger, K. Schmieder, and B. Wegener, "The European multicenter trial on the safety and efficacy of guided oblique lumbar interbody fusion (GOLIF)," *BMC Musculoskeletal Disorders*, vol. 11, no. 1, p. 199, 2010.

[14] S. Orita, K. Inage, G. Kubota et al., "One-year prospective evaluation of the technique of percutaneous cortical bone trajectory spondylodesis in comparison with percutaneous pedicle screw fixation: a preliminary report with technical note," *J Neurol Surg A Cent Eur Neurosurg*, vol. 77, no. 6, pp. 531–537, 2016.

[15] H.-M. Huang, C.-H. Chen, H.-C. Lee et al., "Minimal invasive surgical technique in midline lumbar inter-body fusion: a technique note," *Journal of Clinical Neuroscience*, vol. 55, pp. 103–108, 2018.

[16] T. B. Belytschko, T. P. Andriacchi, A. B. Schultz, and J. O. Galante, "Analog studies of forces in the human spine: computational techniques," *Journal of Biomechanics*, vol. 6, no. 4, pp. 361–371, 1973.

[17] U. M. Ayturk and C. M. Puttlitz, "Parametric convergence sensitivity and validation of a finite element model of the human lumbar spine," *Computer Methods in Biomechanics and Biomedical Engineering*, vol. 14, no. 8, pp. 695–705, 2011.

[18] M. Dreischarf, T. Zander, A. Shiraziadl et al., "Comparison of eight published static finite element models of the intact lumbar spine: predictive power of models improves when combined together," *Journal of Biomechanics*, vol. 47, no. 8, pp. 1757–1766, 2014.

[19] W. Cho, C. Wu, A. A. Mehbod, and E. E. Transfeldt, "Comparison of cage designs for transforaminal lumbar interbody fusion: a biomechanical study," *Clinical biomechanics (Bristol, Avon)*, vol. 23, no. 8, pp. 979–985, 2008.

[20] P. P. Tsitsopoulos, H. Serhan, L. I. Voronov et al., "Would an anatomically shaped lumbar interbody cage provide better stability? An in vitro cadaveric biomechanical evaluation," *Journal of Spinal Disorders & Techniques*, vol. 25, no. 8, pp. E240–E244, 2012.

[21] Y. M. Lu, W. C. Hutton, and V. M. Gharpuray, "Do bending, twisting, and diurnal fluid changes in the disc affect the propensity to prolapse? A viscoelastic finite element model," *Spine (Phila Pa 1976)*, vol. 21, no. 22, pp. 2570–2579, 1996.

[22] A. Polikeit, S. J. Ferguson, L. P. Nolte, and T. E. Orr, "Factors influencing stresses in the lumbar spine after the insertion of intervertebral cages: finite element analysis," *European Spine Journal*, vol. 12, no. 4, pp. 413–420, 2003.

[23] J. K. Biswas, M. Rana, S. Majumder, S. K. Karmakar, and A. Roychowdhury, "Effect of two-level pedicle-screw fixation with different rod materials on lumbar spine: a finite element study," *Journal of orthopaedic science: official journal of the Japanese Orthopaedic Association.*, vol. 23, no. 2, pp. 258–265, 2018.

[24] Y. T. Akpolat, S. İnceoğlu, N. Kinne, D. Hunt, and W. K. Cheng, "Fatigue performance of cortical bone trajectory screw compared With standard trajectory pedicle screw," *Spine (Phila Pa 1976)*, vol. 41, no. 6, pp. E335–E341, 2016.

Hindawi
BioMed Research International
Volume 2021, Article ID 6620746, 6 pages
https://doi.org/10.1155/2021/6620746

Research Article

Treating Lumbar Fracture Using the Mixed Reality Technique

Jiaheng Li,[1] Hexing Zhang,[1] Qiang Li,[1] Shuangqi Yu,[2] Wei Chen,[2] Song Wan,[2] Dong Chen,[2] Rong Liu ,[3] and Fan Ding [2]

[1]*Wuhan University of Science and Technology School of Medicine, Qingling Rd. 1#, Wuhan, 430000 Hubei, China*
[2]*Department of Spine Surgery, Wuhan Puren Hospital, Wuhan University of Science and Technology, Benxi Rd. 1#, Wuhan, 430033 Hubei, China*
[3]*Institute of Medical Innovation and Transformation, Puren Hospital Affiliated to Wuhan University of Science and Technology, Department of Orthopedics, Puren Hospital Affiliated to Wuhan University of Science and Technology, Benxi Rd. 1#, Wuhan, 430033 Hubei, China*

Correspondence should be addressed to Rong Liu; dr_liurong@whu.edu.cn and Fan Ding; spine_dingfan@163.com

Received 2 January 2021; Revised 16 March 2021; Accepted 20 March 2021; Published 30 March 2021

Academic Editor: Ying-Qi Zhang

Copyright © 2021 Jiaheng Li et al. This is an open access article distributed under the Creative Commons Attribution License, which permits unrestricted use, distribution, and reproduction in any medium, provided the original work is properly cited.

The mixed reality (MR) technique has recently been widely used in the orthopedic surgery with satisfactory results reported. However, few studies have focused on the application of MR in the Lumbar fracture (LF). In this retrospective study, our aim is to analyze some findings by investigating the feasibility of MR applied to lumbar fracture treatment. Posterior vertebrectomy has been operated on 7 patients. The MR–based intraoperative three-dimensional image-guided navigation system (MITINS) was used to assist implantation of pedicle screws. The feasibility and safety of pedicle screw implantation were assessed by postsurgery radiography. The visual analog scale (VAS) and Oswestry Disability Index (ODI) were used to assess the pain level and recovery situation before and after surgery. 57 pedicle screws were safely and precisely placed into three-dimensional lumbar models by using MITINS. No screw was found outside the pedicle of the models, and it was not necessary for the X-ray to provide extra locative information during the operation with the use of MITINS. In summary, the application of MITINS is feasible, safe, and accurate while the lumbar fracture surgery is processing, providing satisfactory assistance for spine surgeons.

1. Introduction

With aging of the population, the incidence of osteoporosis has increased significantly [1]. Fractures associated with osteoporosis have become a challenging problem in elderly people. And lumbar fracture is the commonest form of the senile osteoporosis fracture [2]. During the treatment of lumbar fracture, if the fracture is only slightly compressed, conservative treatment or vertebral plasty is usually sufficient. However, if the fracture is severely compressed, or if the type of fracture is burst fracture, open surgery is required [3]. As vertebral degeneration and anatomical variation are very common in the elderly people, the additional problems associated with implanting pedicle screws during an operation are becoming more noteworthy [4].

Recently, digital techniques have been widely applied in orthopedic surgery. With the assistant of clinical real-time position and visualization obtained from such approaches, surgical accuracy has been significantly improved [5]. For example, when we want to improve the safety of lumbar pedicle screw implanting in elderly patients, personalized three-dimensional printing technology makes the implanting of lumbar pedicle screw in patients with severe degeneration or anatomical variation simpler, safer, and more accurate [6]. Computed tomography-guided (CT-guided) navigation and fluoroscopy-based computer navigation systems have also been used to place pedicle screws [7]. Despite these systems that improved the safety and accuracy of the pedicle screw placement [8], the problem of inherent spatial and temporal separation still makes it a tough challenge for spine surgeons. The mixed reality (MR) technique, which is to integrate the real vision and the virtual image, offers a solution that MR can provide efficacy and applicability during the guidance of the surgery, and MR can resolve vision deficiencies during the process of synchronizing virtual images and real operative sights. Our aim was to evaluate a new surgical navigation system based on the MR approach and MITINS while inserting pedicle screws into the elderly patients, which can assess its safety and accuracy during the treatment of lumbar fracture.

2. Materials and Methods

2.1. Patient Eligibility. From April 2017 to August 2018, 7 lumbar fracture patients who received open surgery by MITINS were selected and assessed retrospectively. Ethical approval and informed data were obtained from each patient. Inclusion criteria were as follows: (1) definitely diagnosed with lumbar fracture, (2) diagnosed with severe decompression and nerve deficiency, (3) over eighteen years old and in full possession of their mental faculties, (4) being able to receive surgery, and (5) MITINS was used during each operation. Excluded criteria were as follows: (1) unable to tolerate surgery, 2) diagnosed with severe diabetes, (3) diagnosed with serious anemia, and (4) diagnosed with severe lung and heart disease.

2.2. Operative Strategy and the Rehabilitation Protocol. Firstly, fracture-type fixation approaches were analyzed by CT data. Next, the 3D model of the lumbar fracture was constructed, which is built by using MIMICS 10.1 software, then producing 3D printing. Multiple angle views of the lumbar could be seen. A proper stereoscopic and apparent visualization of the lumbar anatomic was completed. We could also achieved an ideal trajectory insertion by eliminating the structural hierarchy. All patients were treated by the same senior surgeon. The operation was performed under general anesthesia. Pedicle screws were inserted into the 3D-printed lumbar model with the assistance of MITINS. Three marks were identified on the preoperative model, and relevant location information was transferred to the computer. The 3D position of the operated vertebrae was determined by three-point registration. By modifying positioning sensors, an optimal registration can be achieved between virtual image and 3D-printed model. Subsequently, the pedicle screws could be placed with the assistant of the MR navigation system from the preoperatively defined ideal pedicle entry point to the terminal point. The subsequent reduction operation procedure was performed as a typical process that a connecting rod was used, and the lateral displacement was relocated by rotating the rod [9]. Anterior dislocation was corrected by lifting the rod, and the vertebral body height was recovered by stretching. Ultimately, the bone graft procedure was completed with titanium cages (Figures 1 and 2).

The rehabilitation protocol was used comprised: 20% mannitol was used for the first 3 days postoperatively, fully drain for 48 hours, followed by removal of the drainage system. The straight leg raising exercise was encouraged after the removal of the drainage system.

2.3. Evaluation Index. The accuracy and safety of the pedicle screw insertion were assessed using the postsurgery radiography. The visual analog scale (VAS) and Oswestry Disability Index (ODI) were used to assess the pain level and recovery situation before and after surgery.

2.4. Statistical Analysis. Nonparametric data was analyzed using the Wilcoxon rank sum test: $P < 0.05$ was regarded as statistically significant. Statistical Product and Service Solutions (SPSS 15.0.1) software was used for statistical analysis.

2.5. Disadvantage of the Application of MR in Lumbar Fracture. However, some limitations of the application of MR in lumbar fracture surgery should be highlighted. First of all, although it can save the expenditure of the complications due to the anatomical and spatial misjudgment of visual limitation of the traditional imaging method, the cost of MR itself is more expensive than the traditional method under the condition of good control of complication after surgery. Secondly, there is a defect of simulation of soft tissues in the MR technique. Thirdly, the effect of navigation during surgery is limited by the factor of light. And different patient postures were needed depending on the operation area, virtual images ,operating table and surgical instruments.

For the surgeon, limitations of MR in lumbar fracture surgery should not be neglected. Firstly, visual discomfort may occur due to the fusion of the real world and the virtual images. Secondly, special training is necessary for the surgeons to tolerate the eye strain induced by the procedure.

3. Results and Discussion

In the present study, 7 patients were received surgery by the assistance of MITINS. After long-term follow-up of the 7 patients, which the period was from 12 to 18 months, the average time is (14.7 ± 1.4) months. 57 pedicle screws (7 patients) were safely and precisely placed into the three-dimensional lumbar models by the assistance of MITINS (Figure 3). No screw was found outside the pedicle of the models, and it was not necessary for the X-ray to provide extra locative information during the operation with the use of MITINS. After surgery, general evaluation of alleviated pain level was assessed by VAS and ODI among all the patients ($P < 0.05$) (Table 1).

With the increase of population, osteoporosis has become an increased dominant disease in the elderly people. It is characterized as a high-risk disease with bone mass decreasing,bone microstructure destroyerd and bone brittleness increasing. [10]. It has been reported that approximately 40% of postmenopausal women are suffering from osteoporotic fractures, and the complications associated with such fractures, including lower limb deep vein thrombosis, bedsores, and urinary tract infections, pose serious threats to the health of the elderly people [11]. Therefore, clarifying the essence and mechanism of fracture cure and carrying out accurate treatment of fractures are major unsolved problems of spine surgery which could produce considerable significance to the society.

Osteoporotic lumbar fracture is very common in the elderly people, and for the lumbar fracture with nerve deficiency, pedicle fixation is widely used. However, due to the serious spine degenerative problem in the elderly people, the consistent and accurate insertion of lumbar pedicle screws i still a challenge for spine surgeons. Compared to the younger group, it is thought that the risk of the failure and nerve injury of posterior pedicle screw placement is

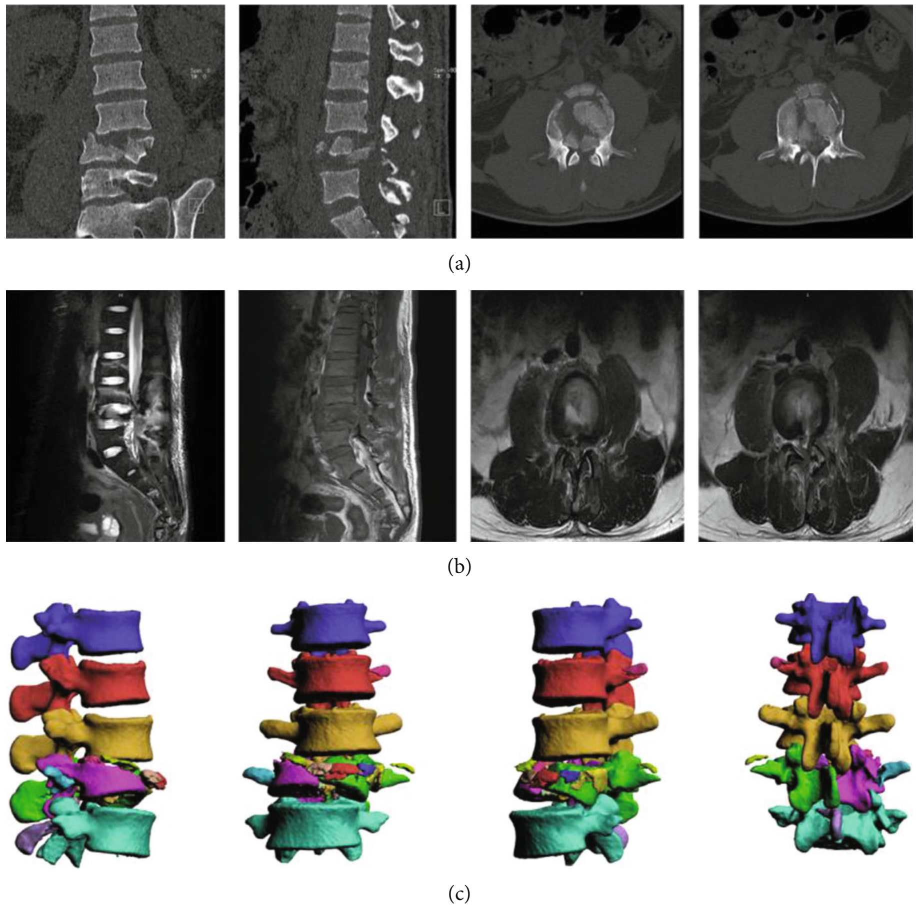

Figure 1: A typical UPA case. A 65-year-old man with LF (L2-L4). (a) CT of lumber presurgery. (b) MRI images of the injured lumbar in the sagittal and the coronal plane. (c) Three dimensional CT images of lumbar.

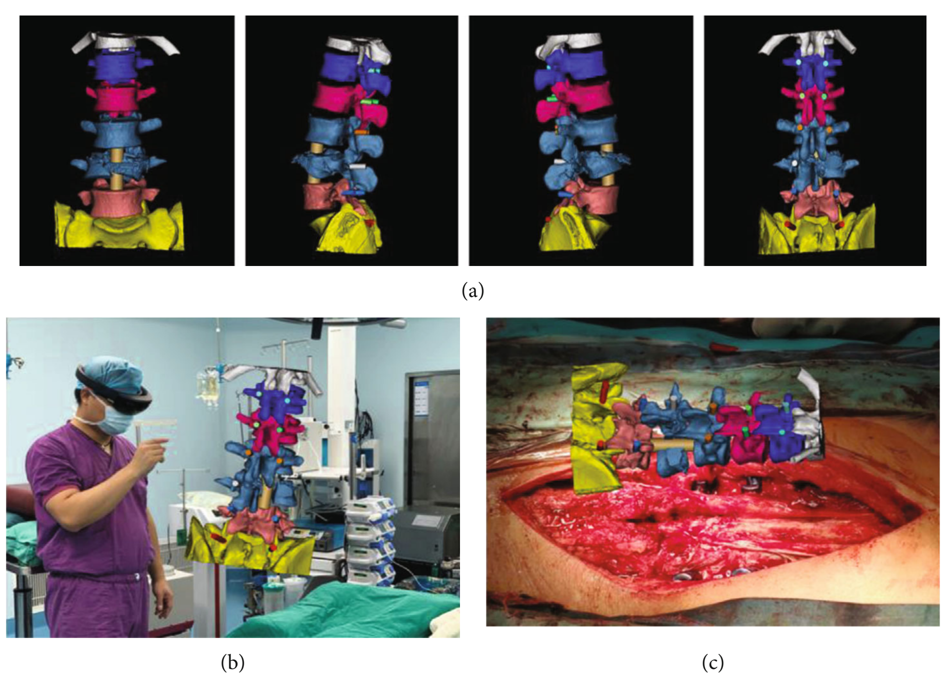

Figure 2: Spine operation of the case identified in Figure 1, performed with the assistance of MITINS. (a) A preoperation surgical demonstration. (b, c) Application of MITINS in the LF operation.

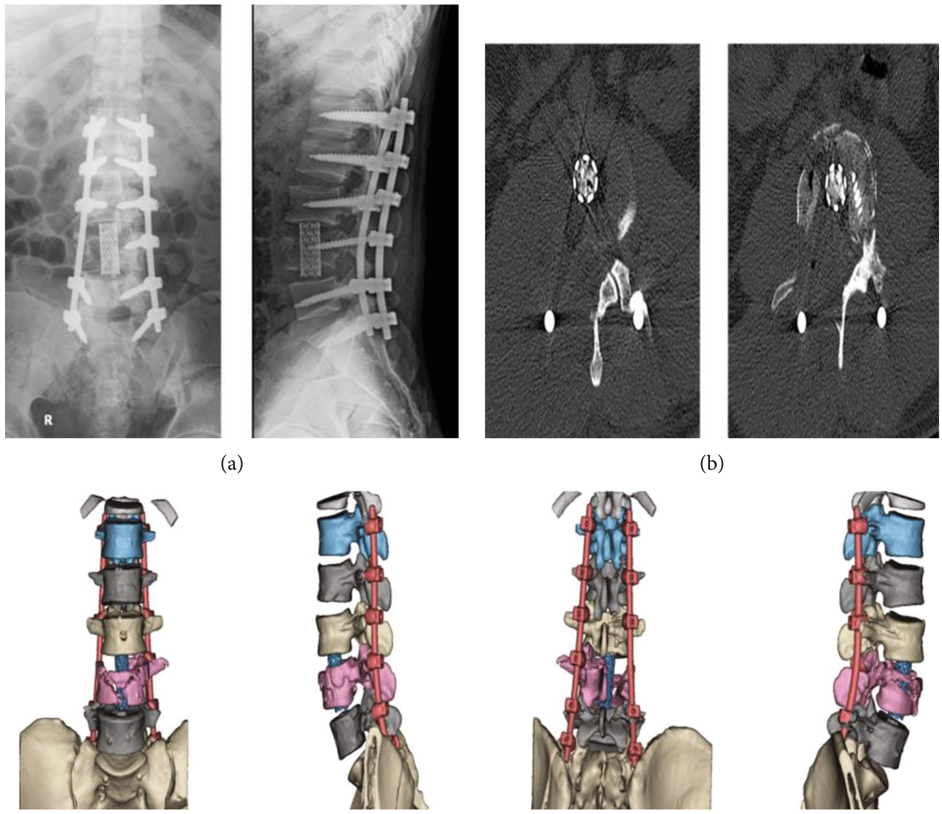

(a) (b)

(c)

Figure 3: The X-rays and CT results of the abovementioned case identified in Figure 1. (a) X-rays of lumber postsurgery. (b) CT of lumber postsurgery. (c) Three dimensional CT images of lumber postsurgery.

Table 1: VAS and ODI of the included patients.

	VAS	ODI
Presurgery	74.4 ± 4.4	82.7 ± 6.2
3 months after surgery	44.7 ± 4.3	45.7 ± 4.7
6 months after surgery	24.2 ± 2.2	27.4 ± 3.2
12 months after surgery	18.4 ± 2.9	16.4 ± 2.6

significantly higher in the elderly people [12]. However, for burst lumbar fractures and patients with symptoms of severe nerve injury, open surgery still makes an indispensable role for fully decompression of vertebral canal. Pedicle screw placement is also needed to secure the stable internal fixation.

Recently, many ways of inserting pedicle screws in elderly people have been evaluated, including the plate guiding technique, the surgical navigation assistance (SNS), and the surgical robot assistance (SRS) [13, 14]. The plate guiding technique is only suitable for the ordinary lumbar fracture. For burst lumbar fracture, the efficacy of the technique is partial [15]. While SNS and SRS are both feasible methods for spine surgery, there are still some disadvantages. For example, innate waste of manpower and time and extending the duration of operations both make it inevitably difficult to apply to clinical application widely.

The MR-based technique has been used successfully in cervical pedicle screw placement [16]. Preoperative discussion is also an advantage of the MR technique. It can provide the optimized planning of surgical procedures, as its unique displaying approach enables images in the computer to be integrated to the holographic vision which is much closer to the real vertebrae situation [17]. In conventional surgical assistance procedures, such as computer tomography and magnetic resonance imaging, the image data was separated from the surgical site. This brings additional difficulties to spine surgeons to speculate the vertebrae situation, who need connect the information from CT and MRI to the real surgical findings, which requiring strong capacity of visual processing to compensate for the lack of depth perception or the limitation of processing of visualization. Fortunately, using the MR technique, surgeons can easily and effectively acquire good stereoscopic vision in the operation area, instead of shifting their attention to the separate visualization of relevant structures [18]. In the present research, 57 pedicle screws (7 patients) were safely and precisely placed into the lumbar three-dimensional models under MITINS. No screw was found outside the pedicle of the model under the guidance of MITINS. All patients obtained obvious alleviated pain in VAS and ODI after surgery ($P < 0.05$), indicating that the MR technique is feasible, safe, and accurate for the treatment of lumbar fracture.

To the best of our knowledge, this is the first study to report use of the MR technique in lumbar fracture surgery. System components of MITINS consist of trakSTAR,electromagnetic transmitter,and sensors,which is an important support for further combination of deeper obscurez surgery image with more visible and integrated vision. However, some limitations of the application of MR in lumbar fracture surgery should be highlighted. Firstly, special training is necessary for the surgeons to tolerate the eye strain induced by the procedure. Secondly, visual discomfort may occur due to the fusion of the real world and the virtual images. Thirdly, different patient postures were needed depending on the operation area, virtual images, operating table and surgical instruments. Fourthly, this is a small case study that includes no controls.

4. Conclusions

The use of MITINS in lumbar fracture surgery is feasible, safe, and accurate, providing satisfactory assistance for spine surgeons.

Data Availability

The data used to support the findings of this study are available from the corresponding author upon request.

Conflicts of Interest

The authors declare that there is no conflict of interest regarding the publication of this paper.

Authors' Contributions

Jiaheng Li, Hexing Zhang and Qiang Li contributed equally to this work.

Acknowledgments

This work was supported in part by the National Nature Science Foundation of China (No. 81601934), Health Research Project of Metallurgical Safety and Health Branch of Chinese Society of Metals (No. JKWS201824), Foundation of Health Commission of Hubei Province (Nos. WJ2018H0093 and WJ2019M023), Natural Science Foundation of Hubei Province (No. 2016CFB664), Combined Foundation of Hubei Provincial Health Commission and Wuhan University of Science and Technology (No. WJ2019H223), and Scientific Research Fund of Wuhan Health Commission (Nos. WX15B11 and WX17Q32).

References

[1] M. Liu, P. Li, D. Z. Ma et al., "Treatment of severe throracolumar fractures with posterior decompression, subtotal vertebrectomy, intervertebral fusion and internal fixation through unilateral pedicle," *Chin J Orthop Trauma*, vol. 18, no. 12, pp. 1100–1104, 2016.

[2] R. A. Lindtner, M. Mueller, R. Schmid et al., "Monosegmental anterior column reconstruction using an expandable vertebral body replacement device in combined posterior-anterior stabilization of thoracolumbar burst fractures," *Archives of Orthopaedic and Trauma Surgery*, vol. 138, no. 7, pp. 939–951, 2018.

[3] U. J. Spiegl, B. M. Devitt, I. Kasivskiy et al., "Comparison of combined posterior and anterior spondylodesis versus hybrid stabilization in unstable burst fractures at the thoracolumbar spine in patients between 60 and 70 years of age," *Archives of Orthopaedic and Trauma Surgery*, vol. 138, no. 10, pp. 1407–1414, 2018.

[4] A. S. Moon, C. A. Cignetti, J. A. Isbell, C. Weng, and S. R. R. Manoharan, "Traumatic hyperextension-distraction injuries of the thoracolumbar spine: a technical note on surgical positioning," *European Spine Journal*, vol. 28, no. 5, pp. 1113–1120, 2019.

[5] F. Z. Ai, Q. S. Yin, Z. Y. Wang et al., "Applied anatomy of transoral atlantoaxial reduction plate internal fixation," *Spine (Phila Pa 1976)*, vol. 31, no. 2, pp. 128–132, 2006.

[6] J. Jayender, B. Xavier, F. King et al., "A novel mixed reality navigation system for laparoscopy surgery," *Medical Image Computing and Computer Assisted Intervention – MICCAI 2018*, vol. 11073, pp. 72–80, 2018.

[7] Y. Xiong, H. Zhang, S. Yu et al., "Posterior vertebrectomy via the unilateral pedicle or bilateral pedicle approach in the treatment of lumber burst fracture with neurological deficits: a comparative retrospective cohort study," *Medical Science Monitor*, vol. 26, 2020.

[8] T. J. Kovanda, S. F. Ansari, R. Qaiser, and D. H. Fulkerson, "Feasibility of CT-based intraoperative 3D stereotactic image-guided navigation in the upper cervical spine of children 10 years of age or younger: initial experience," *Journal of Neurosurgery. Pediatrics*, vol. 16, pp. 590–598, 2016.

[9] D. Zou, K. F. Ye, Y. Tian et al., "Characteristics of vertebral CT Hounsfield units in elderly patients with acute vertebral fragility fractures," *European Spine Journal*, vol. 29, no. 5, pp. 1092–1097, 2020.

[10] J. Wei, L. Zeng, S. Li, F. Luo, Z. Xiang, and Q. Ding, "Relationship between comorbidities and treatment decision-making in elderly hip fracture patients," *Aging Clinical and Experimental Research*, vol. 31, no. 12, pp. 1735–1741, 2019.

[11] T. J. Ziemlewicz, A. Maciejewski, N. Binkley, A. D. Brett, J. K. Brown, and P. J. Pickhardt, "Opportunistic quantitative CT bone mineral density measurement at the proximal femur using routine contrast-enhanced scans: direct comparison with DXA in 355 adults," *Journal of Bone and Mineral Research*, vol. 31, no. 10, pp. 1835–1840, 2016.

[12] H. Yan, D. Jiang, L. Xu et al., "Does the full power-assisted technique used in pedical screw placement affect the safety and efficacy of adolescent idiopathic scoliosis surgery?," *World Neurosurgery*, vol. 116, pp. e79–e85, 2018.

[13] S. D. Hodges, J. C. Eck, and D. Newton, "Analysis of CTbased navigation system for pedicle screw placement," *Orthopedics*, vol. 35, no. 8, pp. e1221–e1224, 2012.

[14] A. Elmi-Terander, G. Burström, R. Nachabé et al., "Augmented reality navigation with intraoperative 3D imaging vs fluoroscopy- assisted free-hand surgery for spine fixation surgery: a matched-control study comparing accuracy," *Scientific Reports*, vol. 10, no. 1, p. 707, 2020.

[15] S. Peh, A. Chatterjea, J. Pfarr et al., "Accuracy of augmented reality surgical Navigation for minimally invasive pedicle screw insertion in thetThoracic and lumbar spine with a new tracking device," *The Spine Journal*, vol. 20, no. 4, 2020.

[16] E. Edström, G. Burström, A. Omar et al., "Augmented reality surgical navigation in spine surgery to minimize staff radiation exposure," *Spine*, vol. 45, no. 1, pp. E45–E53, 2020.

[17] G. Coelho, E. G. Figueiredo, N. N. Rabelo, M. J. Teixeira, and N. Zanon, "Development and evaluation of a new pediatric mixed-reality model for neurosurgical training," *Journal of Neurosurgery. Pediatrics*, vol. 45, pp. 423–432, 2019.

[18] Z. Y. Zhang, W. C. Duan, R. K. Chen et al., "Preliminary application of mxed reality in neurosurgery: development and evaluation of a new intraoperative procedure," *Journal of Clinical Neuroscience*, vol. 67, pp. 234–238, 2019.

Hindawi
BioMed Research International
Volume 2021, Article ID 6693446, 14 pages
https://doi.org/10.1155/2021/6693446

Research Article

Oblique Lateral Interbody Fusion versus Transforaminal Lumbar Interbody Fusion in Degenerative Lumbar Spondylolisthesis: A Single-Center Retrospective Comparative Study

Xing Du, Yuxiao She, Yunsheng Ou, Yong Zhu, Wei Luo, and Dianming Jiang

Department of Orthopedics, The First Affiliated Hospital of Chongqing Medical University, 400016 Chongqing, China

Correspondence should be addressed to Yunsheng Ou; ouyunsheng2001@163.com

Received 30 December 2020; Revised 18 February 2021; Accepted 15 March 2021; Published 22 March 2021

Academic Editor: Ying-Qi Zhang

Copyright © 2021 Xing Du et al. This is an open access article distributed under the Creative Commons Attribution License, which permits unrestricted use, distribution, and reproduction in any medium, provided the original work is properly cited.

Objective. To compare the efficacy of oblique lateral interbody fusion (OLIF) and transforaminal lumbar interbody fusion (TLIF) in single-level degenerative lumbar spondylolisthesis (DLS). *Methods*. A retrospective analysis of patients who underwent single-level DLS surgery in our department from 2015 to 2018 was performed. According to the surgical method, the enrolled patients were divided into two groups, namely, the OLIF group who underwent OLIF combined with percutaneous pedicle screw fixation (PPSF) and the TLIF group. Clinical outcomes included operation time, operation blood loss, postoperative drainage, hospital stay, visual analog scale (VAS) score, Oswestry disability index (ODI), and complications, and imaging outcomes included upper vertebral slip, intervertebral space height (ISH), intervertebral foramen height (IFH), intervertebral space angle (ISA), lumbar lordosis (LL), and bone fusion rate. All outcomes were recorded and analyzed. *Results*. A total of 65 patients were finally included, and there were 28 patients and 37 patients in the OLIF group and the TLIF group, respectively. The OLIF group showed shorter operation time, less blood loss, less postoperative drainage, and shorter hospital stay than the TLIF group ($P < 0.05$). The ISH, IFH, ISA, and LL were all larger in the OLIF group at postoperative and last follow-up ($P < 0.05$), but the degree of upper vertebral slip was found no difference between the two groups ($P > 0.05$). The bone graft fusion rate of OLIF group and TLIF group at 3 months, 6 months, and last follow-up was 78.57%, 92.86%, and 100% and 70.27%, 86.49%, and 97.30%, respectively, and no significant differences were found ($P > 0.05$). Compared with the TLIF group, the OLIF group showed a superior improvement in VAS and ODI at 1 month, 3 months, and 6 months postoperative ($P < 0.05$), but no differences were found at 12 months postoperative and the last follow-up ($P > 0.05$). There was no significant difference in complications between the two groups, with 4 patients and 6 patients in the OLIF group and TLIF group, respectively ($P > 0.05$). *Conclusions*. Compared with TLIF, OLIF showed the advantages of less surgical invasion, better decompression effect, and faster postoperative recovery in single-level DLS surgery.

1. Introduction

Lumbar spondylolisthesis is defined as the forward slip of the upper vertebrae relative to the lower. There are many causes of lumbar spondylolisthesis, including degeneration, trauma, dysplasia, and pathology, among which degenerative lumbar spondylolisthesis (DLS) is the most common [1]. It is reported that the incidence of DLS is about 5% to 7% and often causes low back pain, lower limb pain, or weakness, and even cauda equina syndrome in severe cases [2]. The treatment of DLS mainly includes conservative and surgical treatment. For patients with no obvious efficacy after regular conservative treatment for more than 3 months, surgery should be considered [3].

The surgical methods of DLS mainly include anterior and posterior surgery [4]. In anterior lumbar interbody fusion (ALIF), the discectomy and spondylolisthesis reduction can be performed under direct vision, and the correction and maintain of intervertebral space height and lumbar lordosis (LL) can be also achieved by implanting a large cage [5]. But ALIF has a high risk of abdominal vascular or viscera injury, as well as the rate of postoperative complications [6]. In recent years, transforaminal lumbar interbody fusion (TLIF) has been the most commonly used posterior surgery for DLS [7]. By resecting the facet joints, loosening surrounding fibrous tissue, and implanting pedicle screws and intervertebral cage, TLIF can obtain a good spondylolisthesis reduction effect and maintain satisfactory spinal stability [8]. However, patients undergoing TLIF often suffer from chronic back pain after surgery, which may be due to the resection of paravertebral muscle and facet joints [9]. In addition, surgeons need to open the spinal canal in TLIF surgery, and the intraoperative nerve stimulation may also cause numbness or weakness of the lower limbs after surgery [10]. Thus, more and more surgeons have been seeking minimally invasive surgical methods for DLS.

Oblique lateral interbody fusion (OLIF) is a minimally invasive anterior retroperitoneal approach surgery, which has been very popular in recent years. In OLIF surgery, the surgeon enters the retroperitoneal space through blunt separation, pulls the psoas muscle backward, reaches the operative segment or intervertebral space through the anatomical space between the abdominal aorta and the psoas muscle, and performs decompression and fusion procedures [11]. OLIF was reported with satisfactory efficacy in lumbar degenerative diseases in cohort studies [12, 13]; however, no study compared its efficacy with TLIF surgery in DLS. Our previous study conclude that OLIF combined with percutaneous pedicle screw fixation (PPSF) had less surgical trauma and faster pain relief and rapid lumbar function recovery in lumbar tuberculosis [14]. Thus, we really wondered whether OLIF may or may not be extrapolated to the DLS surgery.

Therefore, we conducted this retrospective study to compare the efficacy of OLIF and TLIF in single-level DLS, in order to provide evidence for the application of OLIF in DLS patients.

2. Materials and Methods

The ethical approval of this study was obtained from the Ethics Committee of the First Affiliated Hospital of Chongqing Medical University (No. 2020-049), and all the participants gave the informed consent before taking part. This study had been registered in the Chinese Clinical Trial Registry (ChiCTR2000039446). This study was reported according to the STROCSS criteria [15].

2.1. Patients. A retrospective analysis of medical records of DLS patients hospitalized in our hospital from 2015 to 2018 was conducted.

Inclusion criteria: (1) single-level DLS (L2/3-L4/5). (2) Mild symptomatic DLS (Meyerding Grade: I or II). (3) Age > 18 years. (3) Underwent OLIF combined with PPSF (OLIF group) or TLIF (TLIF group). (4) More than 12 months of follow-up time. (5) Clinical and imaging data were completed.

Exclusion criteria: (1) a previous lumbar spinal surgery history. (2) Recurrent DLS after surgical treatment. (3) DLS with severe cardiovascular disease or malignant tumor, etc.

2.2. Preoperative Management. X-rays, CT, and MRI were taken in all patients to assess the surgical window between the psoas and abdominal aorta, as well as the extent of upper vertebral slip, spinal canal stenosis, and nerve root compression. Surgery was performed when basic diseases such as diabetes, coronary heart disease, and high blood pressure were under control.

2.3. Surgical Procedure. The choice of surgical method was mainly based on the following principles: OLIF combined PPSF was mainly used for patients whose preoperative MRI or CT showed an appropriate operative window between the psoas and abdominal aorta. If preoperative MRI or CT showed no operative window between the psoas and abdominal aorta or the operative window was narrow, TLIF should be considered.

2.3.1. OLIF Group. Place the patient in a lateral supine position after general anaesthesia and use C-arm X-rays to identify the surgical level. Then cut a 4 cm incision in the outer abdominal area, separate the layers of abdominal muscles, and push away the extraperitoneal fat with fingers. Find the front edge of the psoas with a Cobb periosteal stripper, push back the psoas and place an OLIF retractor. After exposing the vertebra, insert a positioning needle and confirm the surgical level by C-arm X-rays and place different extenders to extend the channel to 22 mm. Then, remove the intervertebral disc completely and implant a cage (Medtronic, USA) filled with granular bone, which was derived from allogeneic bone (Gold Bone Way, China). Not any bone fusion promoting substance was used in bone graft materials. Then, place a drainage tube and close the incision layer by layer. Adjust the patient to a prone position and do posterior internal fixation with percutaneous pedicle screw instrumentation (IRENE, China). Finally, use a C-arm X-ray to confirm the good position of posterior fixation and close the posterior incision.

2.3.2. TLIF Group. Place the patient in a prone position after general anaesthesia. Make a posterior median incision after identification of the surgical level by C-arm X-rays. According to preoperative clinical features, the side with lower limb symptoms was defined as the decompression side. Strip the sacrospinous muscle of the decompression side, expose the lamina and facet joints of the surgical level, and then implant the pedicle screws. For the contralateral side, expose the facet joints and implant the pedicle screws via the Wiltes approach. Then, resect part of facet joints and lamina of the decompression side and remove the intervertebral disc completely and implant a cage (Guona, China) filled with granular bone through the intervertebral foramen. The used granular bone was derived from the lamina, spinous process, and facet articular process. However, in most cases, the autologous bone volume was not enough, so they were often mixed with some allogeneic granular bone (Gold Bone Way, China). Not any bone fusion promoting substance was used in bone graft materials. Then, correct the spondylolisthesis by properly pulling up and pressurizing the posterior screw system (IRENE, China) and obtain an appropriate LL by using a prebending rod. After the confirmation of correction by C-arm X-rays, the surgical wound was rinsed and hemostasis was carefully performed. The posterior screw system was then properly pulled up and pressurized in order to correct the spondylolisthesis and obtain an appropriate LL, and a C-arm X-ray was used to confirm the correction. The surgical wound was rinsed, and hemostasis was carefully performed. Finally, place a drainage tube and close the incision layer by layer.

2.4. Postoperative Management. In the first 3 days after surgery, antibiotics were used to prevent infection. When postoperative drainage was less than 40 ml/d, the drainage tube was removed. An X-ray examination of the lumbar spine was taken after extubation. After discharge, a modeled rigid lumbar brace was applied continuously for 3 months. Patients were requested to wear the lumbar braces every day when getting out of bed, moving, or sitting. Their family members were asked to supervise the brace wearing, and the medical team conducted telephone follow-up once a week to timely evaluate the patient's compliance. Follow-up of X-rays, CT, and MRI (if necessary) was conducted for 1, 3, 6, and 12 months after surgery.

2.5. Outcomes. Clinical outcomes: (1) operation time, operation blood loss, postoperative drainage, and hospital stay. (2) Visual analog scale (VAS) score and Oswestry disability index (ODI) at 1, 3, 6, and 12 months postoperative and the last follow-up. (3) Complications.

Imaging outcomes: (1) the degree of upper vertebral slip: the ratio of the slip distance of the upper vertebrae to the length of the upper endplate of the lower vertebrae. (2) Intervertebral space height (ISH): the mean of anterior and posterior ISH. (3) Intervertebral space foramen (IFH): the distance between the lower margin of the superior pedicle and vertebral body connection and the upper margin of the inferior pedicle and vertebral body connection. (4) Intervertebral space angle (ISA): the angle between the upper and lower endplate of the intervertebral space. (5) Lumbar lordosis (LL): the angle between the upper endplate of the L1 vertebral body and the upper endplate of the S1 vertebral body. The measurement methods of ISH, IFH, ISA, and LL were shown in Figure 1. (6) Bone graft fusion: according to Bridwell et al.'s study [16], bone graft fusion was divided into four levels. Grade I: fused with remodeling and trabeculae. Grade II: graft intact, not fully remodeled and incorporated though; no lucencies. Grade III: graft intact, but a definite lucency at the top or bottom of the graft. Grade IV: definitely not fused with resorption of bone graft and with collapse. Grade I and II were defined as bone graft fusion in this study.

2.6. Statistical Analysis. Quantitative data was represented in mean ± standard deviation (SD). Intergroup and intragroup comparison of quantitative data were performed by student t-test and paired t-test, respectively. The X^2 test and the Mann–Whitney rank-sum test were used for comparison of disordered and ordered qualitative data, respectively. Statistical analysis was conducted by SPSS 19.0 software, and $P < 0.05$ was regarded as a significant difference.

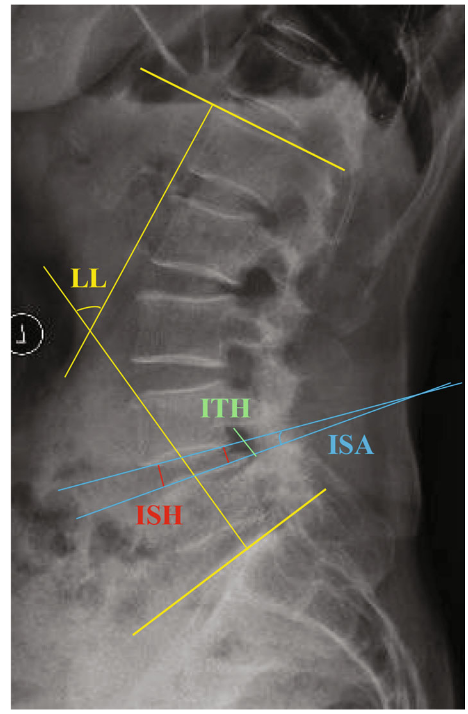

Figure 1: Diagram of the measurement of ISH (red line), ITH (green line), ISA (blue line), and LL (yellow line).

3. Results

According to the inclusion and exclusion criteria, our study finally included 65 patients, and there were 28 patients and 37 patients in the OLIF group and the TLIF group, respectively. There were no significant differences in age ($P = 0.641$), gender ($P = 0.683$), body mass index (BMI) ($P = 0.591$), ASA grade ($P = 0.779$), operative level ($P = 0.890$), bone mineral density (BMD) ($P = 0.101$), and follow-up time ($P = 0.282$) between the two groups. (Table 1).

The OLIF group showed shorter operation time ($P < 0.001$), less operation blood loss ($P < 0.001$), less postoperative drainage ($P < 0.001$), and shorter hospital stay ($P < 0.001$) than the PLIF group. (Figure 2).

No significant differences were found in preoperative ISH, IFH, ISA, and LL between the two groups ($P = 0.508$, 0.649, 0.231, and 0.522, respectively). However, the ISH, IFH, ISA, and LL at postoperative and the last follow-up were significantly larger in the OLIF group than those in the TLIF group (postoperative: $P < 0.001$, 0.002, <0.001, and<0.001, respectively; last follow-up: $P = 0.032$, 0.015, 0.014, and 0.002, respectively). The upper vertebral slip in the two groups was significantly corrected ($P < 0.001$ for both groups) and lost during the follow-up ($P < 0.001$ for both groups). But no significant differences were found in upper vertebral slip between the two groups at preoperative, postoperative, and last follow-up ($P = 0.728$, 0.453, and 0.531, respectively). The bone graft fusion rate of OLIF group and TLIF group for 3 months, 6 months, and last follow-up was 78.57%, 92.86%, and 100% and 70.27%, 86.49%, and 97.30%, respectively, and no differences were found between

Table 1: Comparison of preoperative clinical features between the two groups.

Clinical features	TLIF group ($N = 37$)	OLIF group ($N = 28$)	P value
Age (year), mean ± SD	52.8 ± 7.1	53.6 ± 6.4	0.641
Gender (n), Male/Female	23/14	16/12	0.683
BMI (kg/m^2), mean ± SD	22.5 ± 2.3	22.8 ± 2.1	0.591
ASA grade (n)			0.779
I	24	17	
II	10	9	
III	3	2	
Operation level (n)			0.890
L3/4	10	8	
L4/5	27	21	
BMD (T score), mean ± SD	−2.3 ± 1.0	−1.9 ± 0.9	0.101
Follow-up time (month), mean ± SD	22.1 ± 7.0	20.3 ± 6.1	0.282

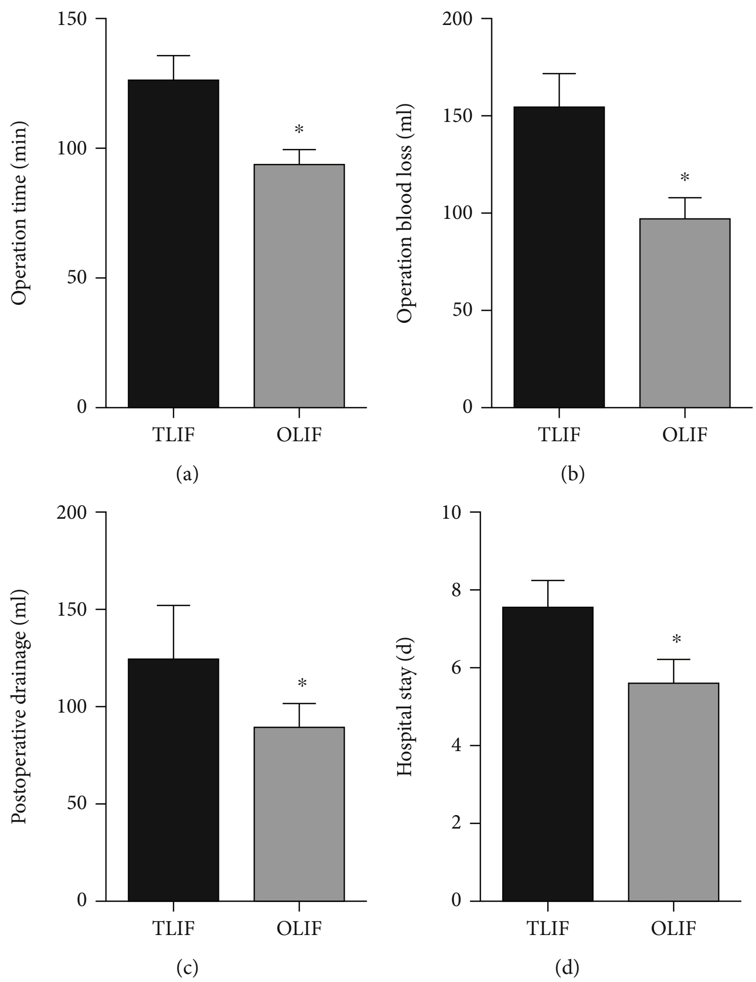

Figure 2: Comparison of operation time (a), operation blood loss (b), postoperative drainage (c), and hospital stay (d) between the two groups. (*Compared with TLIF group, $P < 0.05$).

the two groups ($P = 0.451$, 0.412, and 0.389, respectively) (Figure 3).

No significant differences were found in VAS score and ODI between the two groups at preoperative, 12 months postoperative, and last follow-up (VAS score: $P = 0.760$, 0.064, and 0.408, respectively; ODI: $P = 0.604$, 0.088, and 0.216, respectively). However, the OLIF group showed a better improvement in VAS score and ODI at 1 month, 3

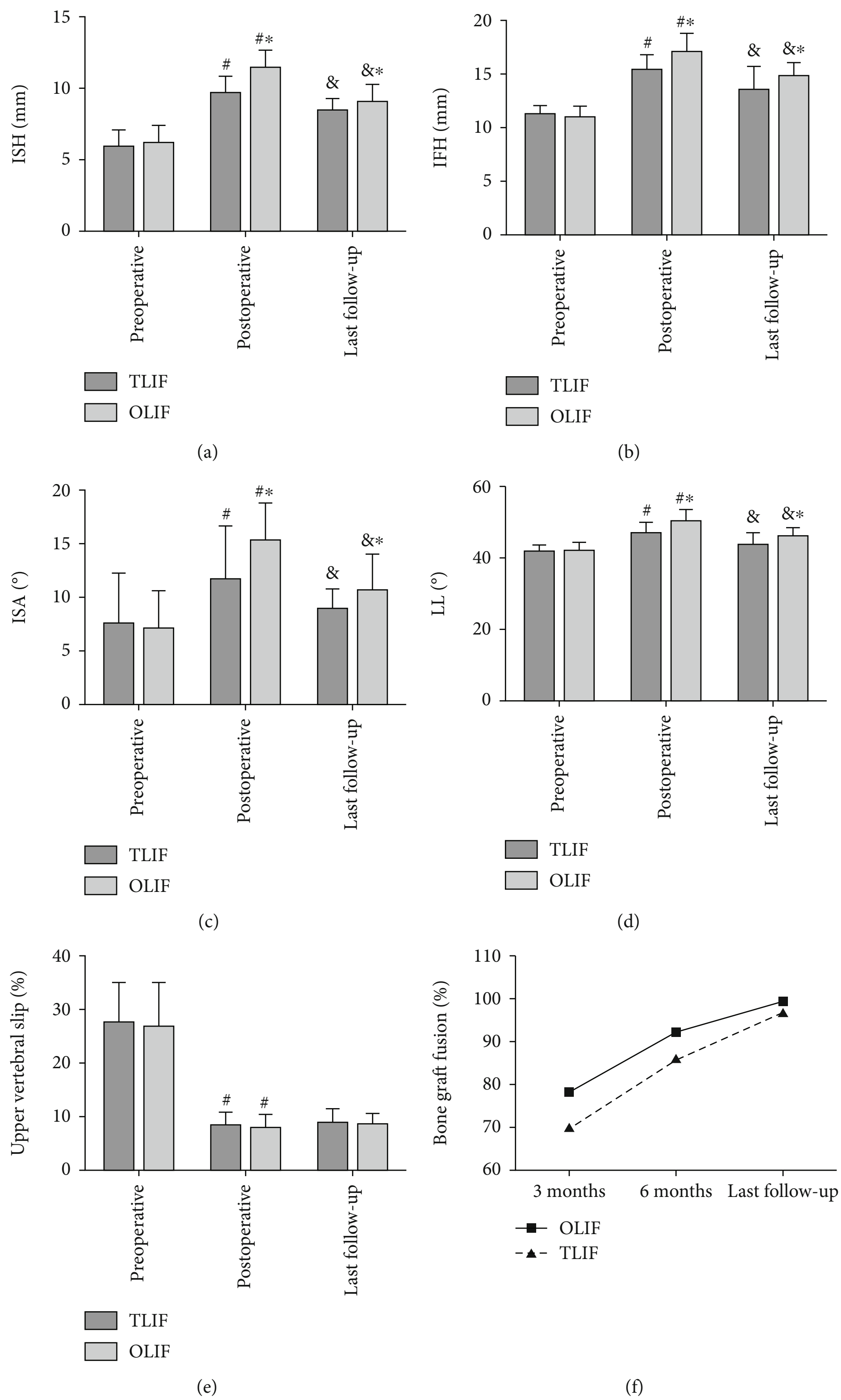

Figure 3: Comparison of ISH (a), ITH (b), ISA (c), LL (d), degree of upper vertebral slip (e), and bone graft fusion rate (f) between the two groups at different follow-up time. (*Compared with TLIF group, $P < 0.05$; [&]compared with preoperative, $P < 0.05$; [#]compared with postoperative, $P < 0.05$).

months, and 6 months postoperative than the TLIF group (VAS score: $P < 0.001$, <0.001, and 0.002, respectively; ODI: $P < 0.001$ for all the three, respectively) (Figure 4).

Four patients with complications were found in the OLIF group, including 2 patients of transient thigh flexion weakness, 1 patient of segmental artery injury, and 1 patient of

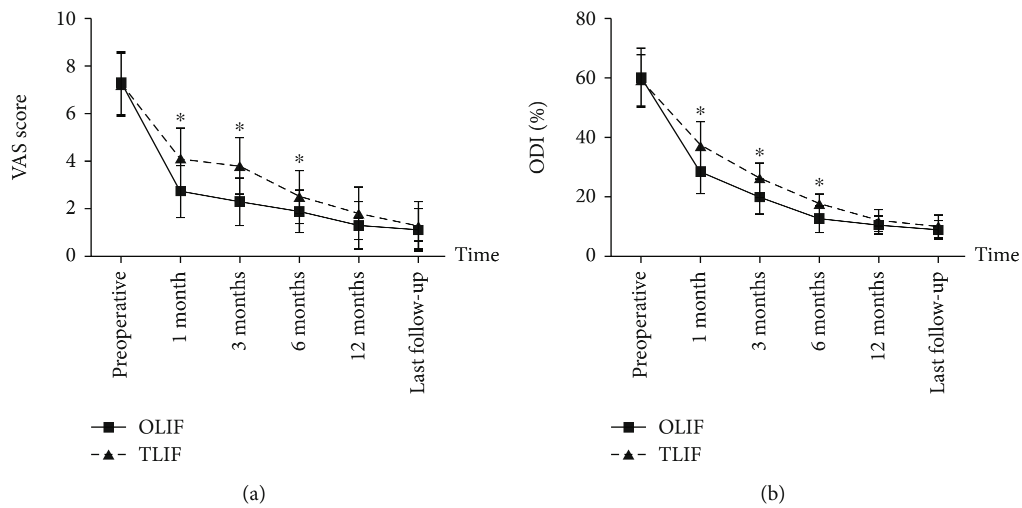

Figure 4: Comparison of VAS score (a) and ODI (b) between the two groups at different follow-up time. (*Compared with TLIF group, $P < 0.05$).

transient sympathetic injury. While 6 patients with complications were found in the TLIF group, including 3 patients of dural tear, 1 patient of transient thigh pain and/or numbness, 1 patient of transient ankle dorsiflexion weakness, and 1 patient of postoperative incision infection. There was no significant difference in the complications rate (14.3% vs. 16.2%) between the two groups ($P = 0.446$). Finally, all complications were cured after treatment.

3.1. Typical Cases. Typical cases were shown in Figures 5 and 6.

4. Discussion

In this study, TLIF showed longer operation time and more operation blood loss than OLIF. This result was similar to a previous study. The possible reasons were as follows: (1) in TLIF surgery, one side of paravertebral muscle was peeled off, and part of facet joints and lamina was also resected [17], while neither was done in OLIF surgery. (2) In OLIF surgery, surgeons could directly reach the operative intervertebral space and did the discectomy under direct vision [18], while in TLIF surgery, discectomy could not be performed under direct vision, especially for the contralateral side of the decompression side [19]. (3) In OLIF surgery, the spinal canal was not opened, so the risk of nerve injury was low, while TLIF surgery required opening the intervertebral foramina, which had a risk of nerve injury, so surgeons paid more attention to the separation and the protection of the nerve roots [20]. The less postoperative drainage and shorter hospital stay of the OLIF group may also be related to the larger surgical damage of TLIF surgery. In addition, the prolonged postoperative bedtime caused by the risk of spinal instability due to the intraoperative dissection of paravertebral muscle and facet joints may also be the reasons for the longer hospital stay of the TLIF group.

OLIF is an indirect decompression surgery, and many studies are aimed at evaluating the decompression effect of OLIF by comparing the changes of imaging parameters before and after surgery [21–23]. In our study, it was found that the ISH, IFH, and ISA for postoperative and last follow-up were significantly larger in the OLIF group than the TLIF group. The reasons may be as follows: (1) in OLIF surgery, a large cage with a degree of inclination angle was implanted into the intervertebral space, while in TLIF surgery, because of the narrow operating space, only a small cage, almost without an inclination angle, could be implanted through the intervertebral foramen [24]. (2) In TILF surgery, only one side of the paravertebral muscle and the facet joints was removed while the contralateral side was usually preserved, so the intervertebral space may not be effectively extended, especially for patients with severe facet joints degeneration or even facet joints fusion [25]. LL is an important imaging index to evaluate the efficacy of DLS surgery. It was confirmed that LL was closely related to postoperative lumbar back pain, and effective correction and maintenance of LL were of great significance to relieve lumbar back pain and improve lumbar function [26]. In this study, both the postoperative and last follow-up LL were found significantly larger in the OLIF group than the TLIF group. This was closely related to the effective correction and maintenance of ISH, IFH, and ISA in the OLIF group [27]. However, no differences in upper vertebral slip at preoperative, postoperative, and last follow-up were found between the two groups. This may be owing to the following reasons: (1) in TLIF surgery, the posterior pedicle system could effectively correct spondylolisthesis by its strong pulling force [28]. (2) Both of the two groups achieved a higher rate of bone graft fusion during the follow-up, and vertebral spondylolisthesis would not deteriorate once bone graft fusion was achieved. Although OLIF showed a better decompression efficacy than TLIF in this study, it is still necessary to extend the follow-up time to confirm this conclusion in future research, as spinal canal remodeling during long-term follow-up after surgery had been proved [29].

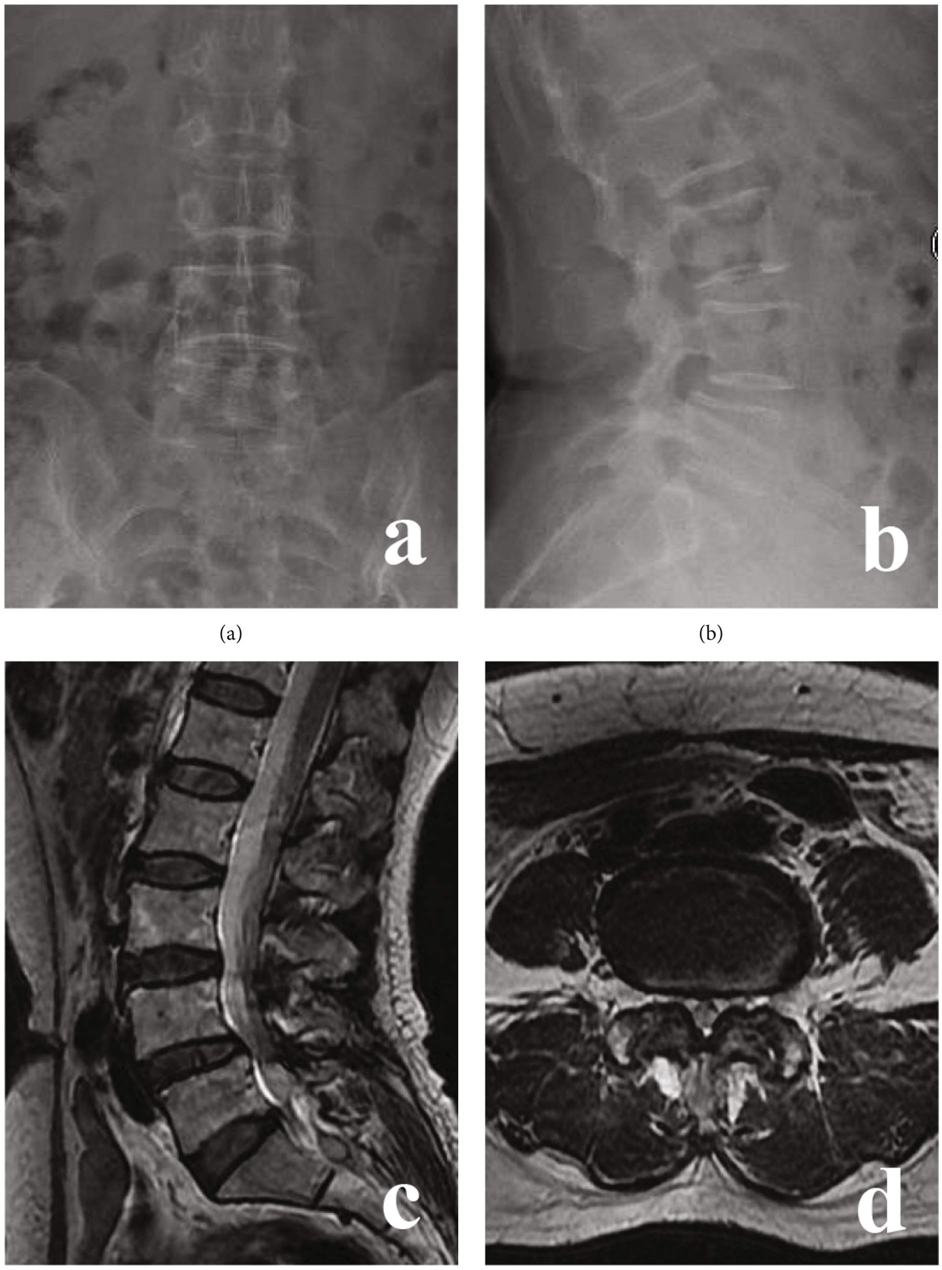

(a) (b) (c) (d)

Figure 5: Continued.

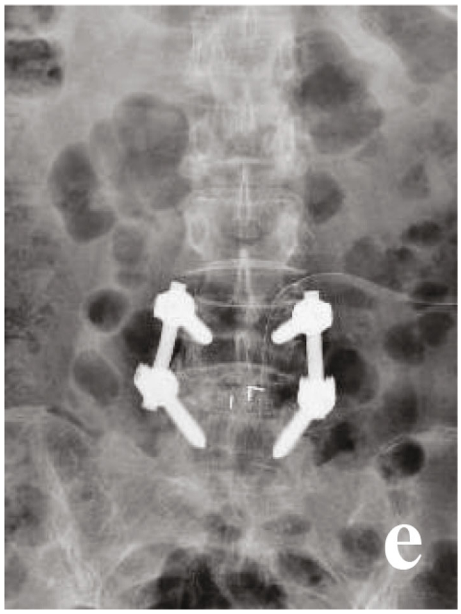

(e)

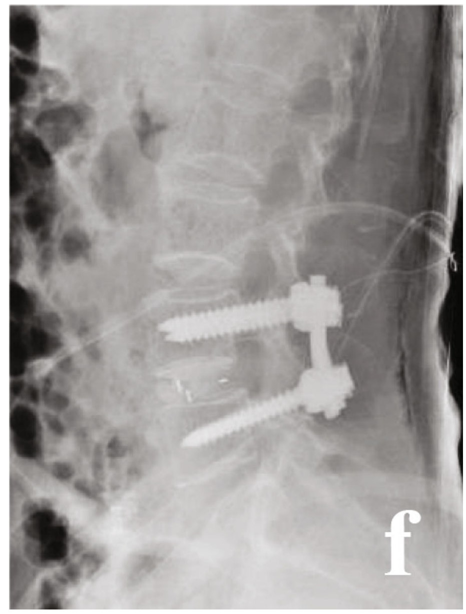

(f)

(g)

(h)

Figure 5: Continued.

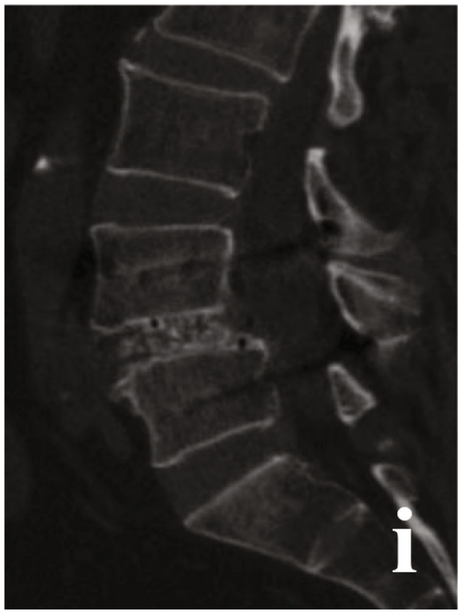

(i)

(j)

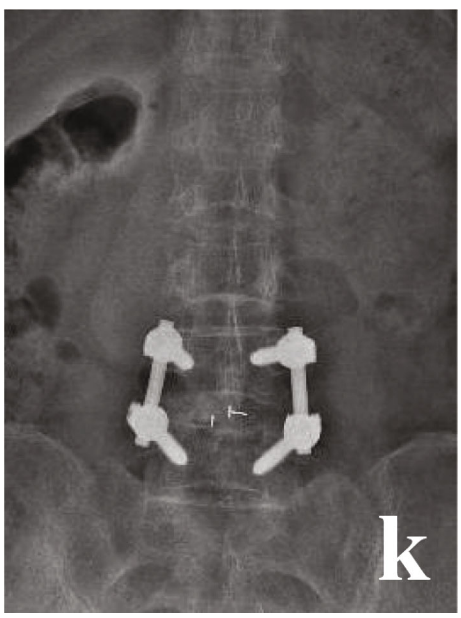

(k)

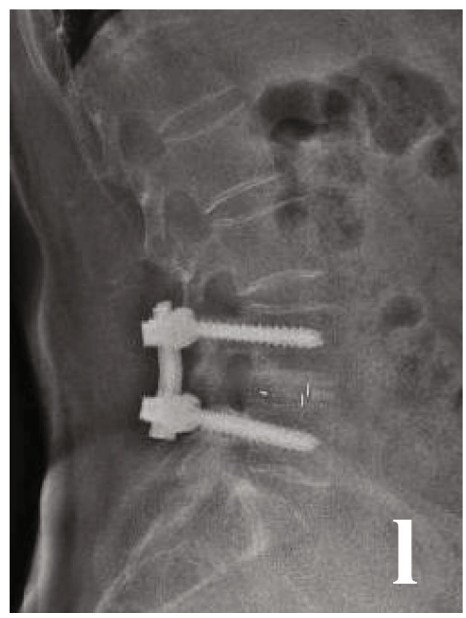

(l)

Figure 5: A 49-year-old male with L4/5 DLS in TLIF group. (a)–(d) Preoperative X-ray and MRI. (e) and (f) Postoperative X-ray. (g)–(j) CT at 6 months postoperative. (k) and (l) X-ray at 18 months postoperative.

In the present study, the OLIF group and TLIF group showed similar bone graft fusion rate. We thought the reasons may be as follows: (1) in both groups, the intervertebral discs were completely removed, and the cartilage endplate was also completely scraped. This would create a suitable good graft bed for fusion [30]. (2) Granular bone graft was used in both groups, and our previous study had showed that granular bone graft had a high fusion rate [31]. (3) Both groups used a posterior pedicle screw system to create a stable local mechanical environment, which was also beneficial for bone graft fusion [32].

Postoperative pain relief and lumbar function recovery were the main focus of both the surgeons and patients. In this study, it was found that the short-term (in 12 months) postoperative pain and lumbar functional in the OLIF group were superior to the TLIF group, but there were no significant differences in long-term follow-up. The reasons may be as follows: (1) less damage to paraspinal muscles and facet joints was found in the OLIF group [33], so low back pain and lumbar function were better than the TLIF group in the short-term follow-up. (2) OLIF surgery did not open the spinal canal and had little stimulation to nerve roots [34]. (3) For

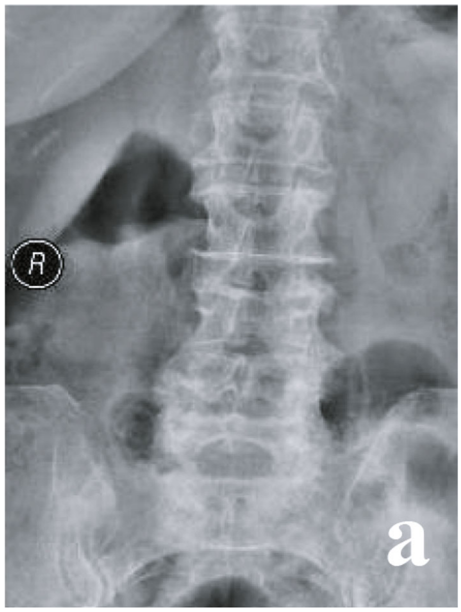

(a)

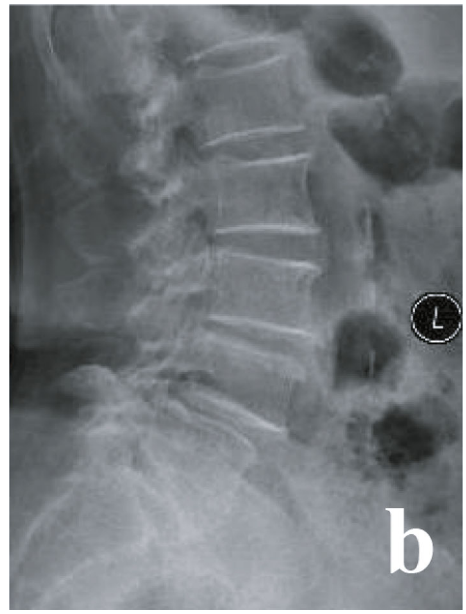

(b)

(c)

(d)

Figure 6: Continued.

(e)

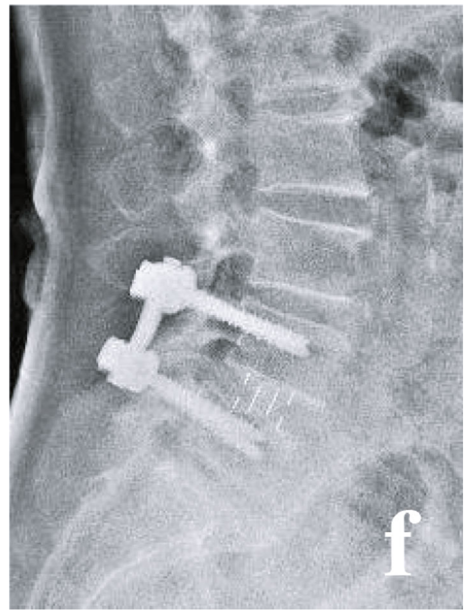

(f)

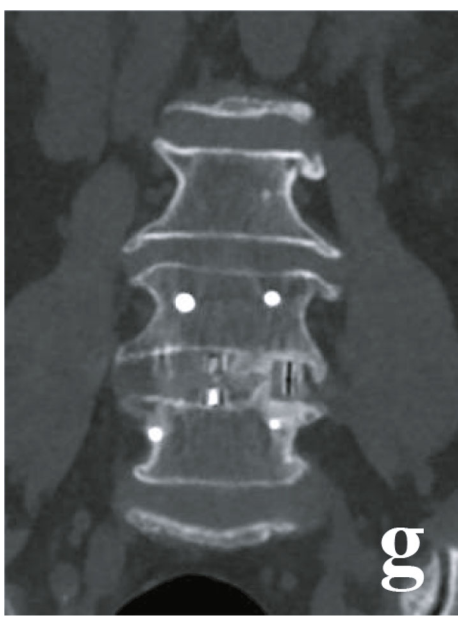

(g)

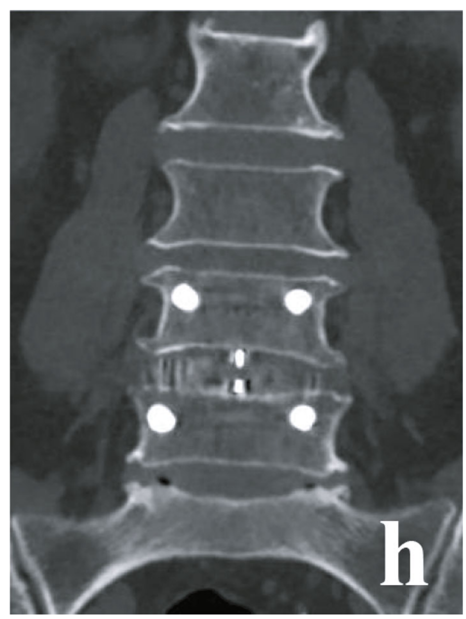

(h)

Figure 6: Continued.

(i)

(j)

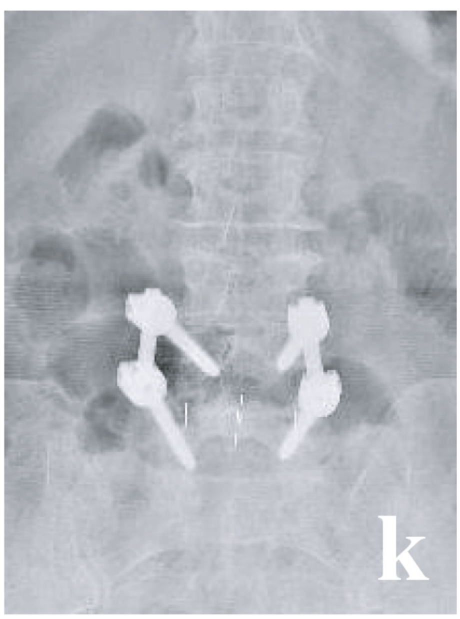

(k)

(l)

Figure 6: A 50-year-old female with L4/5 DLS in the OLIF group. (a)–(d) Preoperative X-ray and MRI. (e) and (f) Postoperative X-ray. (g)–(j) CT at 5 months postoperative. (k) and (l) X-ray at 20 months postoperative.

most patients in both groups, bone graft fusion had achieved, and the paravertebral muscles had also been recovered at 1 year postoperative. The above results were also the reasons for shorter hospital stays in the OLIF group. Although stand-alone OLIF was reported with less injury to paravertebral muscles [33], PPSF was used in the OLIF group in our study, because preoperative BMD revealed that most patients had osteopenia or even osteoporosis.

Segmental artery injury, transient thigh numbness were the common complications in the OLIF group [35], because the lumbar plexus, lumbar sympathetic trunk, and segmental artery are all located laterally in front of the lumbar vertebrae and susceptible to being irritated or injured [36, 37]. The main complications of TLIF were nerve root stimulation or injury and dural tear [38]. However, we found no significant difference in complication rate between the two groups. This result also indicated the safety of the two surgical methods for DLS.

In our opinion, the indications of OLIF combined PPSF for DLS were as follows: (1) severe back pain and/or leg pain with poor response to regular conservative treatment of 3 months. (2) Progressive exacerbation of instability or spondylolisthesis. (3) Single-segmental DLS (L2/3-L4/5) with mild degree of spondylolisthesis (Grade I or II). (5) An appropriate operative window was shown between the psoas and abdominal aorta on preoperative MRI or CT [39].

This study also has some limitations. First, it is a retrospective study with a small sample size and short follow-up period. Second, different experiences in OLIF/TLIF surgery may also cause bias.

5. Conclusion

Compared with TLIF, OLIF showed the advantages of less surgical invasion, better decompression effect, and faster postoperative recovery in single-level DLS surgery.

Abbreviations

DLS: Degenerative lumbar spondylolisthesis
ALIF: Anterior lumbar interbody fusion
TLIF: Transforaminal lumbar interbody fusion
OLIF: Oblique lateral interbody fusion
PPSF: Percutaneous pedicle screw fixation
VAS: Visual analog scale
ODI: Oswestry disability index
ISH: Intervertebral space height
IFH: Intervertebral foramen height
ISA: Intervertebral space angle
LL: Lumbar lordosis
SD: Standard deviation
BMI: Body mass index
BMD: Bone mineral density.

Data Availability

The clinical data in this study is available from the corresponding author on reasonable request.

Additional Points

Research Registration. This study had been registered in Chinese Clinical Trial Registry (Number: ChiCTR2000039446, http://www.chictr.org.cn/showproj.aspx?proj=63238).

Conflicts of Interest

The authors have no conflicts of interest to disclose in relation to this article.

Authors' Contributions

Conception and design were done by Xing Du and Yunsheng Ou; data analysis and interpretation were done by Xing Du, Yuxiao She, and Yong Zhu; data collection and management were done by Xing Du, Yuxiao She, Wei Luo, and Dianming Jiang; manuscript writing and critical revisions were done by all authors; overall responsibility was done by Xing Du and Yunsheng Ou.

Acknowledgments

This work was supported by the Natural Science Foundation of Chongqing (cstc2019jcyj-msxmX0358) and the Technology Innovation and Application Development Project of Chongqing (cstc2020jscx-msxmX0219).

References

[1] M. Bydon, M. A. Alvi, and A. Goyal, "Degenerative lumbar spondylolisthesis: definition, natural history, conservative management, and surgical treatment," *Neurosurgery Clinics of North America*, vol. 30, no. 3, pp. 299–304, 2019.

[2] Y. X. J. Wang, Z. Káplár, M. Deng, and J. C. S. Leung, "Lumbar degenerative spondylolisthesis epidemiology: a systematic review with a focus on gender-specific and age-specific prevalence," *Journal of Orthopaedic Translation*, vol. 11, pp. 39–52, 2017.

[3] M. Karsy and E. F. Bisson, "Surgical versus nonsurgical treatment of lumbar spondylolisthesis," *Neurosurgery Clinics of North America*, vol. 30, no. 3, pp. 333–340, 2019.

[4] W. R. Spiker, V. Goz, and D. S. Brodke, "Lumbar interbody fusions for degenerative spondylolisthesis: review of techniques, indications, and outcomes," *Global Spine Journal*, vol. 9, no. 1, pp. 77–84, 2018.

[5] J. Y. Cho, T. S. Goh, S. M. Son, D. S. Kim, and J. S. Lee, "Comparison of anterior approach and posterior approach to instrumented interbody fusion for spondylolisthesis: a meta-analysis," *World Neurosurgery*, vol. 129, pp. e286–e293, 2019.

[6] B. Kapustka, G. Kiwic, P. Chodakowski et al., "Anterior lumbar interbody fusion (ALIF): biometrical results and own experiences," *Neurosurgical Review*, vol. 43, no. 2, pp. 687–693, 2020.

[7] A. K. Chan, V. Sharma, L. C. Robinson, and P. V. Mummaneni, "Summary of guidelines for the treatment of lumbar spondylolisthesis," *Neurosurgery Clinics of North America*, vol. 30, no. 3, pp. 353–364, 2019.

[8] C. Wipplinger, C. Melcher, R. N. Hernandez et al., ""One and a half" minimally invasive transforaminal lumbar interbody fusion: single level transforaminal lumbar interbody fusion with adjacent segment unilateral laminotomy for bilateral decompression for spondylolisthesis with bisegmental stenosis," *J Spine Surg*, vol. 4, no. 4, pp. 780–786, 2018.

[9] S. H. Min, M. H. Kim, J. B. Seo, J. Y. Lee, and D. H. Lee, "The quantitative analysis of back muscle degeneration after posterior lumbar fusion: comparison of minimally invasive and conventional open surgery," *Asian Spine J*, vol. 3, no. 2, pp. 89–95, 2009.

[10] V. A. Mehta, M. J. McGirt, G. L. Garcés Ambrossi et al., "Trans-foraminal versus posterior lumbar interbody fusion: comparison of surgical morbidity," *Neurological Research*, vol. 33, no. 1, pp. 38–42, 2013.

[11] J. X. J. Li, K. Phan, and R. Mobbs, "Oblique lumbar interbody fusion: technical aspects, operative outcomes, and complications," *World Neurosurgery*, vol. 98, pp. 113–123, 2017.

[12] J. Li, D. Zhang, Y. Shen, and X. Qi, "Lumbar degenerative disease after oblique lateral interbody fusion: sagittal spinopelvic alignment and its impact on low back pain," *Journal of Orthopaedic Surgery and Research*, vol. 15, no. 1, p. 326, 2020.

[13] S. Y. Chang, Y. Nam, J. Lee, B. S. Chang, C. K. Lee, and H. Kim, "Impact of preoperative diagnosis on clinical outcomes of oblique lateral interbody fusion for lumbar degenerative disease in a single-institution prospective cohort," *Orthopaedic Surgery*, vol. 11, no. 1, pp. 66–74, 2019.

[14] X. Du, Y. S. Ou, Y. Zhu, W. Luo, G. Y. Jiang, and D. M. Jiang, "Oblique lateral interbody fusion combined percutaneous pedicle screw fixation in the surgical treatment of single-segment lumbar tuberculosis: a single- center retrospective comparative study," *International Journal of Surgery*, vol. 83, pp. 39–46, 2020.

[15] R. Agha, A. Abdall-Razak, E. Crossley et al., "STROCSS 2019 guideline: strengthening the reporting of cohort studies in surgery," *International Journal of Surgery*, vol. 72, pp. 156–165, 2019.

[16] K. H. Bridwell, L. G. Lenke, K. W. McEnery, C. Baldus, and K. Blanke, "Anterior fresh frozen structural allografts in the thoracic and lumbar spine," *Spine*, vol. 20, no. 12, pp. 1410–1418, 1995.

[17] C. J. Fu, W. C. Chen, M. L. Lu, C. H. Cheng, and C. C. Niu, "Comparison of paraspinal muscle degeneration and decompression effect between conventional open and minimal invasive approaches for posterior lumbar spine surgery," *Scientific Reports*, vol. 10, no. 1, p. 14635, 2020.

[18] S. Ohtori, S. Orita, K. Yamauchi et al., "Mini-open anterior retroperitoneal lumbar interbody fusion: oblique lateral Interbody fusion for lumbar spinal degeneration disease," *Yonsei Medical Journal*, vol. 56, no. 4, pp. 1051–1059, 2015.

[19] X. Cheng, K. Zhang, X. Sun et al., "Clinical and radiographic outcomes of bilateral decompression via a unilateral approach with transforaminal lumbar interbody fusion for degenerative lumbar spondylolisthesis with stenosis," *The Spine Journal*, vol. 17, no. 8, pp. 1127–1133, 2017.

[20] N. E. Epstein, "More nerve root injuries occur with minimally invasive lumbar surgery: let's tell someone," *Surgical Neurology International*, vol. 7, Suppl 3, pp. S96–S101, 2016.

[21] W. Limthongkul, T. Tanasansomboon, W. Yingsakmongkol, T. Tanaviriyachai, K. Radcliff, and W. Singhatanadgige, "Indirect decompression effect to central canal and ligamentum flavum after extreme lateral lumbar interbody fusion and oblique lumbar interbody fusion," *Spine (Phila Pa 1976)*, vol. 45, no. 17, pp. E1077–E1084, 2020.

[22] M. Wu, J. Li, M. Zhang et al., "Efficacy and radiographic analysis of oblique lumbar interbody fusion for degenerative lumbar spondylolisthesis," *Journal of Orthopaedic Surgery and Research*, vol. 14, no. 1, p. 399, 2019.

[23] J. Sato, S. Ohtori, S. Orita et al., "Radiographic evaluation of indirect decompression of mini-open anterior retroperitoneal lumbar interbody fusion: oblique lateral interbody fusion for degenerated lumbar spondylolisthesis," *European Spine Journal*, vol. 26, no. 3, pp. 671–678, 2017.

[24] C. Sun, H. Wang, J. Jiang, F. Lu, X. Ma, and X. Xia, "Length of lumbar interbody cage using radiological measurements of Chinese endplates and the apophyseal ring," *World Neurosurgery*, vol. 116, pp. e1204–e1213, 2018.

[25] P. A. Robertson, W. A. Armstrong, D. L. Woods, and J. J. Rawlinson, "Lordosis recreation in transforaminal and posterior lumbar interbody fusion: a cadaveric study of the influence of surgical bone resection and cage angle," *Spine (Phila Pa 1976)*, vol. 43, no. 22, pp. E1350–E1357, 2018.

[26] C. Y. Chuang, M. Y. Liaw, L. Y. Wang et al., "Spino-pelvic alignment, balance, and functional disability in patients with low-grade degenerative lumbar spondylolisthesis," *Journal of Rehabilitation Medicine*, vol. 50, no. 10, pp. 898–907, 2018.

[27] L. Xiao, Q. Zhao, X. Sun, C. Liu, Y. Zhang, and H. Xu, "Relationship between alterations of spinal/pelvic sagittal parameters and clinical outcomes after oblique lumbar interbody fusion," *World Neurosurgery*, vol. 133, pp. e156–e164, 2020.

[28] Z. X. Wu, C. Zhan, G. Cui et al., "Stress distribution on the screws in posterior lumbar fusion of isthmic spondylolisthesis with 2- or 3-vertebra fixation techniques: a biomechanical cadaveric study," *The Journal of Surgical Research*, vol. 176, no. 1, pp. 95–101, 2012.

[29] S. Ohtori, S. Orita, K. Yamauchi et al., "Change of lumbar ligamentum flavum after indirect decompression using anterior lumbar interbody fusion," *Asian Spine J*, vol. 11, no. 1, pp. 105–112, 2017.

[30] T. Steffen, A. Tsantrizos, and M. Aebi, "Effect of implant design and endplate preparation on the compressive strength of interbody fusion constructs," *Spine (Phila Pa 1976)*, vol. 25, no. 9, pp. 1077–1084, 2000.

[31] X. Du, Y. S. Ou, S. Xu, B. He, W. Luo, and D. M. Jiang, "Comparison of three different bone graft methods for single segment lumbar tuberculosis: a retrospective single-center cohort study," *International Journal of Surgery*, vol. 79, pp. 95–102, 2020.

[32] Y. Y. Hsieh, F. Y. Tsuang, Y. J. Kuo, C. H. Chen, C. J. Chiang, and C. L. Lin, "Biomechanical analysis of single-level interbody fusion with different internal fixation rod materials: a finite element analysis," *BMC Musculoskeletal Disorders*, vol. 21, no. 1, p. 100, 2020.

[33] W. He, Y. S. Da He, Y. Xing et al., "Quantitative analysis of paraspinal muscle atrophy after oblique lateral interbody fusion alone vs. combined with percutaneous pedicle screw fixation in patients with spondylolisthesis," *BMC Musculoskeletal Disorders*, vol. 21, no. 1, p. 30, 2020.

[34] R. J. Mobbs, K. Phan, G. Malham, K. Seex, and P. J. Rao, "Lumbar interbody fusion: techniques, indications and comparison of interbody fusion options including PLIF, TLIF, MI-TLIF, OLIF/ATP, LLIF and ALIF," *Journal Spine Surgery*, vol. 1, no. 1, pp. 2–18, 2015.

[35] Z. Y. Zeng, Z. W. Xu, D. W. He et al., "Complications and prevention strategies of oblique lateral interbody fusion technique," *Orthopaedic Surgery*, vol. 10, no. 2, pp. 98–106, 2018.

[36] H. Wang, Y. Zhang, X. Ma, X. Xia, F. Lu, and J. Jiang, "Radiographic study of lumbar sympathetic trunk in oblique lateral interbody fusion surgery," *World Neurosurgery*, vol. 116, pp. e380–e385, 2018.

[37] S. Orita, K. Inage, T. Sainoh et al., "Lower lumbar segmental arteries can intersect over the intervertebral disc in the oblique lateral interbody fusion approach with a risk for arterial injury: radiological analysis of lumbar segmental arteries by using magnetic resonance imaging," *Spine (Phila Pa 1976)*, vol. 42, no. 3, pp. 135–142, 2017.

[38] B. Garg and N. Mehta, "Minimally invasive transforaminal lumbar interbody fusion (MI-TLIF): a review of indications, technique, results and complications," *J Clin Orthop Trauma*, vol. 10, Suppl 1, pp. S156–S162, 2019.

[39] L. Liu, Y. Liang, H. Zhang et al., "Imaging anatomical research on the operative windows of oblique lumbar interbody fusion," *PLoS One*, vol. 11, no. 9, article e0163452, 2016.

Hindawi
BioMed Research International
Volume 2021, Article ID 5575524, 8 pages
https://doi.org/10.1155/2021/5575524

Research Article

The Location of the Fibular Tunnel for Anatomically Accurate Reconstruction of the Lateral Ankle Ligament: A Cadaveric Study

Jeong-Hyun Park,[1] Hyung-Wook Kwon,[1] Digud Kim,[1] Kwang-Rak Park,[1] Mijeong Lee,[1] Yu-Jin Choi,[1] and Jaeho Cho[2]

[1]*Department of Anatomy & Cell Biology, Graduate School of Medicine, Kangwon National University, Kangwon, Republic of Korea*
[2]*Department of Orthopaedic Surgery, Chuncheon Sacred Heart Hospital, Hallym University, Chuncheon, Republic of Korea*

Correspondence should be addressed to Jaeho Cho; hohotoy@nate.com

Received 11 January 2021; Revised 8 February 2021; Accepted 9 March 2021; Published 19 March 2021

Academic Editor: Ying-Qi Zhang

Copyright © 2021 Jeong-Hyun Park et al. This is an open access article distributed under the Creative Commons Attribution License, which permits unrestricted use, distribution, and reproduction in any medium, provided the original work is properly cited.

We aimed to describe the location of fibular footprint of each anterior talofibular ligament (ATFL) and calcaneofibular ligament (CFL), as well as their common origin in relation to bony landmarks of the fibula in order to determine the location of the fibular tunnel. In 105 ankle specimens, the center of the footprints of the ATFL and CFL (cATFL and cCFL, respectively) and the intersection point of their origin (intATFL-CFL) were investigated, and the distances from selected bony landmarks (the articular tip (AT) and the inferior tip (IT) of the fibula) were measured. Forty-two (40%) specimens had single-bundle ATFL, and 63 (60%) had double-bundle patterns. The distance between intATFL-CFL and IT was 12.0 ± 2.5 mm, and a significant difference was observed between the two groups ($p = 0.001$). Moreover, the ratio of the intATFL-CFL location based on the anterior fibular border for all cadavers was 0.386. The present study suggests a reference ratio that can help surgeons locate the fibular tunnel for a more anatomically accurate reconstruction of the lateral ankle ligament. Also, it may be necessary to make a difference in the location of the fibular tunnel according to the number of ATFL bundles during surgery.

1. Introduction

Ankle sprain is the most common sports-related injury that usually involves the lateral ligament complex (LLC) of the ankle [1, 2]. Among the three ligaments of the LLC, anterior talofibular ligament (ATFL) rupture occurs in 80% of patients, the rest showing rupture of the calcaneofibular ligament (CFL) combined with ATFL. The latter condition causes instability of the ankle or subtalar joint, although the posterior talofibular ligament (PTFL) is rarely involved [3–6]. Nonoperative treatment is generally performed for acute ankle sprain, but failed conservative treatment causes chronic ankle instability (CAI) that may require surgical treatment; it has an incidence of ~10-30% of patients [3, 7–9].

To achieve a good clinical result for CAI treatment, many surgical techniques with anatomical repair or reconstruction of the ATFL and/or CFL have been proposed [10–14]. Early techniques for repair or reconstruction of the ATFL and/or CFL were invasive and nonanatomic. Common complications of this procedure include delayed recovery, wound infection, and nerve damage [15, 16]. The minimally invasive surgical (MIS) technique recently emerged and reduces the incidence of postoperative complications. Also, these procedures using percutaneous or arthroscopic techniques are focused on the anatomic repair or reconstruction of the ATFL and/or CFL [17].

The fibular origins of ATFL and CFL are concentrated in the lower part of the lateral malleolus and connected with connective fiber [18]. Also, ligament injury is likely to occur at the fibular side or substantial part of the ligament [4, 6]. Most MIS procedures for CAI require a single fibular tunnel with a common origin site of ATFL and CFL in both percutaneous and arthroscopic techniques [7, 9, 17, 19, 20]. Therefore, the identification of the common origin site of the ATFL and CFL for precise construction of the fibular tunnel is essential to reconstruct the lateral ankle ligament more anatomically.

Therefore, we aimed to describe the location of the fibular footprint of each ATFL and CFL, as well as the location of their common origin in relation to the easily identifiable bony landmarks of the fibula. Furthermore, we intend to suggest a reference ratio that can easily detect the location of the fibular tunnel as the common origin site of the ATFL and CFL by considering the anatomical variation of the ligaments.

2. Materials and Methods

This study was approved by the Institutional Ethics Committee.

105 specimens were included for this study. Of the 105 ankle specimens dissected from adult formalin-fixed cadavers, 40 (38.1%) were from females and 65 (61.9%) from males. The mean age of the donors at death was 76.4 (range, 44-99) years. Subjects with traces or scars from trauma or surgery on the skin and those with bony morphologic deformation due to bone union after fracture in the lateral aspect of the ankle were excluded. In addition, in order to discriminate the history of ligament injury, subjects in whom the shape of the ligament itself was damaged by previous injury after exposing the ligament through dissection were excluded. Even if the shape of the ligament itself was preserved, subjects in whom the tension of the ligament was not maintained and the fiber of ligament was abnormal when the ankle joint was placed in a neutral position were also excluded.

2.1. Dissection. The ankle specimens were stabilized in a lateral position with the ankle in neutral position. The lateral side of the ankle was completely exposed using detailed dissection to remove skin and soft tissue overlying the lateral hind foot. Care was taken to avoid injury or disruption to the native anatomy.

After careful dissection, the number of ATFL bundles was noted to detect anatomical variability. Next, the anterior border of distal fibula (lateral malleolus) was confirmed using combined visual inspection and direct palpation of bone with all soft tissues removed. The following two reference points were marked: the articular tip of the lateral malleolus (AT) and the inferior tip of the lateral malleolus (IT). Further dissection to identify the center of the fibular footprint of the ATFL and CFL was performed (cATFL and cCFL, respectively). Finally, the intersection point of the fibular origin of the ATFL and CFL (intATFL-CFL) was identified by minimal dissection of the most inferior and posterior fibers of the ATFL and the most anterior fiber of the CFL (Figure 1). The points identified for this study were defined as follows.

(1) The articular tip of the lateral malleolus (AT) was defined as the anterior fibular tubercle located most superior to the anterior border of the lateral malleolus

(2) The inferior tip of the lateral malleolus (IT) was defined as the tip located most inferior to the anterior border of the lateral malleolus

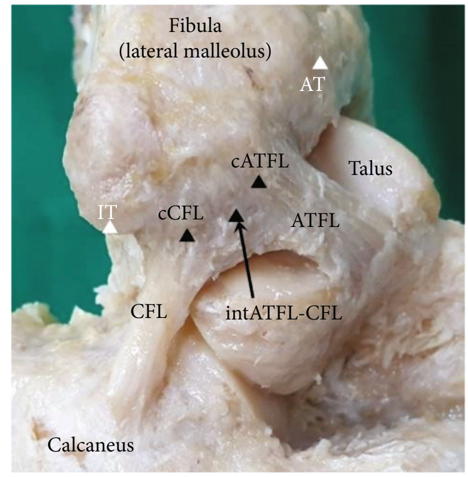

Figure 1: Lateral view of a right ankle in neutral plantar flexion and dorsiflexion, demonstrating the anatomic footprint sites of the lateral ankle ligaments and bony landmarks. AT: the articular tip of the lateral malleolus; ATFL: anterior talofibular ligament; cATFL: the center of the fibular footprint of the ATFL; cCFL: the center of the fibular footprint of the CFL; CFL: calcaneofibular ligament; intATFL-CFL: the intersection point of the fibular origin of the ATFL and CFL; IT: the inferior tip of the lateral malleolus.

(3) The center of the fibular footprint of the ATFL (cATFL) was defined as the midcentral point bisecting the superior and inferior margins of the ATFL band at the fibular attachment

(4) The center of the fibular footprint of the CFL (cCFL) was defined as the midcentral point bisecting the superior and inferior margins of the CFL band at the fibular attachment

(5) The intersection point of the fibular origin of the ATFL and CFL (intATFL-CFL) was defined as the point where the most inferior and posterior fiber of the ATFL band and the most superior and anterior fiber of the CFL band intersect each other

2.2. Measurements. If the ATFL had multiple bundles, the center of the footprint including all bundles was used for measurements. The distances from the center of the fibular footprint of the ATFL and CFL to the inferior tip of the lateral malleolus were measured using a flexible surgical ruler. Also, the distance from the intersection point of the fibular origin of the ATFL and CFL to the inferior tip of the lateral malleolus and the distance from the articular and inferior tips of the lateral malleolus were measured. The identification of landmarks and measurements of the distances were performed independently by two researchers. Each independent researcher repeatedly measured the distance twice after identifying the landmarks. The averages of the two researchers' measurements were adopted as data for each specimen.

2.3. Statistical Analysis. Inter- and intraobserver reliabilities for all measurements were calculated by the intraclass correlation coefficient (ICC). According to the definition of Landis and Koch [21], ICCs of 0.81 to 1.00, 0.61 to 0.80, 0.41 to 0.60, 0.21 to 0.40, and 0.00 to 0.20 were interpreted as excellent, good, moderate, fair, and poor, respectively. Each measurement was presented using the mean, standard deviation, and range; since the number of specimens was more than 30, it was applicable to the normality assumption. For comparison between the single-bundle ATFL and double-bundle ATFL groups, a two-sample t-test was used. All statistical analyses were performed using SPSS 25.0 software (SPSS, Chicago, IL), and a p value less than 0.05 was considered statistically significant.

3. Results

Intraclass correlation coefficients were generated for all measurements. All measurements were higher than 0.8 (indicating acceptable reliability) and were employed in the study.

The distance (mean ± standard deviation) between the center of the fibular footprint of the ATFL and inferior tip of the lateral malleolus was 15.9 ± 3.2 mm. The distance between the center of the fibular footprint of the CFL and inferior tip of the lateral malleolus was 8.6 ± 2.9 mm. The distance between the intersection point of the fibular origin of the ATFL and CFL and inferior tip of the lateral malleolus was 12.0 ± 2.5 mm (Table 1). The distance between the AT and IT and the distance between cATFL and IT were significantly greater in males than in females (Table 2).

Of the 105 specimens, 42 (40%) specimens had single-bundle ATFL (type 1) and 63 (60%) specimens had a double-bundle pattern (type 2). There were no triple-bundle pattern specimens (Figure 2). With regard to the type of the bundle pattern of ATFL, there were statistically significant differences in the distance from cATFL to IT between the two groups ($p < 0.001$). The average distance from cATFL to IT was 17.5 ± 3.2 mm in type 1 and 14.8 ± 2.7 mm in type 2. However, there was no significant difference between the two groups in the distance from cCFL to IT (type 1: 8.9 ± 3.2, type 2: 8.3 ± 2.7, $p = 0.266$). In terms of the distance from the intersection point of the fibular origin of the ATFL and CFL to IT, significant differences were observed between the two groups (type 1: 13.2 ± 2.6, type 2: 11.5 ± 2.2, $p = 0.001$).

In addition, the three distances from the inferior tip of the lateral malleolus to anatomic footprint sites of the lateral ankle ligaments were calculated as a ratio of the length between the articular tip and inferior tip of the lateral malleolus. All ratio values are listed in Table 3. With regard to the type of the bundle pattern of ATFL, there were statistically significant differences in the ratio of cATFL and intATFL-CFL between the two groups. Further, all ratio values between the males and females showed no statistically significant differences (Table 4).

4. Discussion

A clear understanding of the anatomical location of the ligaments in relation to the bony landmark is important for surgeons performing anatomic reconstruction of the lateral ankle ligaments. The first contribution of the present study is to propose that surgeons can use a reference ratio to locate the fibular tunnel for anatomic reconstruction of the lateral ankle ligament, particularly in a patient who is much smaller or larger than average. The second is that there is a difference in the location of the fibular tunnel for anatomic reconstruction of the lateral ankle ligament between the single and double fascicular ATFL.

Table 1: The distances between the fibular footprint of the lateral ankle ligaments and the selected bony landmarks ($n = 105$ specimens).

Measurement point	Distance (mm)			
	Mean	SD	Minimum	Maximum
cATFL~IT	15.9	3.2	10	25
cCFL~IT	8.6	2.9	0	16
intATFL-CFL~IT	12.0	2.5	5.5	19.5
AT~IT	31.8	2.6	25.5	40

AT: the articular tip of the lateral malleolus; ATFL: anterior talofibular ligament; cATFL: the center of the fibular footprint of the ATFL; cCFL: the center of the fibular footprint of the CFL; CFL: calcaneofibular ligament; intATFL-CFL: the intersection point of the fibular origin of the ATFL and CFL; IT: the inferior tip of the lateral malleolus; SD: standard deviation.

Most ankle stabilization surgeries involve repairing or reconstructing the ATFL and/or CFL. Numerous surgical procedures for chronic ankle instability have reported good clinical results [10]; but in order to overcome shortcomings such as wound complications in the open technique, minimally invasive surgery techniques have been used recently [17]. Minimally invasive surgery (MIS) for CAI includes anatomical repairs and reconstruction using arthroscopic [15, 19] and percutaneous techniques [7]. These MIS techniques commonly use bone anchors or construct bone tunnels at the anatomical origin and insert ATFL and CFL without open exposure. In particular, when both ATFL and CFL are reconstructed, a single fibular tunnel is required to insert the fibular stem by converting the ATFL and CFL into an anatomical Y graft [7, 8, 19, 20]. Therefore, for a more anatomically correct reconstruction, it is necessary to understand the anatomy of the common origin of ATFL and CFL in more detail.

The previous cadaveric study by Matsui et al. [8] suggested the fibular obscure tubercle (FOT) as a bony landmark for identifying the fibular footprint of the lateral ankle ligament. Some authors described the articular and inferior tips of the fibula (lateral malleolus) as a reference point [22–24]. However, it is somewhat insufficient to determine the location of the fibular tunnel as a common origin site of the ATFL and CFL with only one or two reference points in MIS procedures for CAI. This is because the distance between the bony landmark of the fibula and fibular footprint of the ATFL and CFL can be measured differently depending on the size and race of the cadaver. In previous cadaveric studies using 60 and 152 cadavers [23, 25], the ATFL and CFL were found to connect to each other at the anterior border of the lateral malleolus. The results of this study also showed connective fibers between ATFL and CFL covering the surface layer of the inferior part of ATFL and the anterior part of CFL in all 105 specimens. Moreover, topographically, both ATFL and CFL origins have a single confluent footprint on the anterior border of the distal fibula [26]. Therefore, the location of the

Table 2: The distances between the fibular footprint of the lateral ankle ligaments and the selected bony landmarks by sex.

Measured distance (mm)	Males ($n = 65$)	Females ($n = 40$)	p value
cATFL~IT	16.5 ± 3.3	14.7 ± 2.5	0.003
cCFL~IT	8.5 ± 3.1	8.6 ± 2.5	0.810
intATFL-CFL~IT	12.5 ± 2.7	11.6 ± 2.1	0.093
AT~IT	32.6 ± 2.3	30.1 ± 2.3	<0.001

Data are mean ± standard deviation. AT: the articular tip of the lateral malleolus; ATFL: anterior talofibular ligament; cATFL: the center of the fibular footprint of the ATFL; cCFL: the center of the fibular footprint of the CFL; CFL: calcaneofibular ligament; intATFL-CFL: the intersection point of the fibular origin of the ATFL and CFL; IT: the inferior tip of the lateral malleolus; SD: standard deviation.

single fibular tunnel for the common origin of ATFL and CFL is considered to be most anatomically reasonable to be the intersection point of the fibular origin of the ATFL and CFL (intATFL-CFL).

The intATFL-CFL was previously identified at the fibular obscure tubercle (FOT) by Buzzi et al. [27]. Based on this reference, it is recommended as an anatomical landmark for the location of the fibular tunnel when reconstructing the lateral ankle ligament [7]. However, a recent cadaveric study [8] has shown that the FOT is located proximally close to the intATFL-CFL and not at the same location. It was also found that FOT could not be manually detected in all patients. According to research on MIS techniques, if the FOT is not detectable with fluoroscopic view imaging or palpation, the inferior one-third point between the articular tip (AT) and the inferior tip (IT) of the lateral malleolus on its anterior border is suggested as an alternative, but no evidence for such an alternative was found.

A systematic review showed that the origins of the ATFL and CFL were located around 10-14 and 5-8 mm from the IT, respectively [17]. On the other hand, the fibular footprint of the ATFL and CFL was located 15.9 ± 3.2 and 8.6 ± 2.9 mm in our study. These differences in values were not significant and may be accounted for by the size and race of the cadavers and the anatomic variability. Further, the results of our study show that there is a difference in the absolute distance due to the difference in body size between males and females; however, the ratio did not differ by sex. We, therefore, determined that it would be more reliable and clinically useful to describe these values in the ratio rather than the absolute distance. In the present study, the ratio of the intATFL-CFL location based on the distance along the anterior fibular border for all cadavers was nearly 0.4. Using this reference ratio, dividing the distance from AT to IT into 5 equal parts and making the fibular tunnel along the extension of the just inferior 40% point are believed to be a more anatomically correct reconstruction of the lateral ankle ligament compared to using the current surgical techniques (Figure 3).

Although ligament injury combined with bony avulsion fracture may interfere with the reference using the bony landmarks, the importance of the applicability of this ratio using surgically relevant bony landmarks for reference during the anatomical reconstruction procedure cannot be underestimated. The indication for performing an anatomical reconstruction procedure is instability from chronic rupture rather than acute rupture of the lateral ligament. A sufficient incision may be made to expose the ligament attachment, or an arthroscopy may be used to navigate the ligament attachment. However, in chronic ankle lateral instability (CALI), the surgeon is more likely to face a complex situation in which the native ligament centers are not visible due to severe ligament damage. Use of this ratio using bony landmarks facilitates consistent and anatomical placement. Additionally, it may clinically enable minimally invasive anatomical reconstruction of the lateral ligament. A previous study has mentioned that sufficient incision is the key to anatomic reconstruction of the ligaments, but it is emphasized that attention to wound complications and nerve damage is essential [28]. Positioning the tunnel location before surgery helps to minimize the incision and reduce the risk of wound complications and nerve damage through reduction of the surgical incision. Furthermore, additional establishing unnecessary portals for tunnels can be avoided during minimally invasive surgery using arthroscopy.

The ultimate purpose of ligament reconstruction is to recreate the course of the injured ligaments [29]. Thus, ligament reconstruction has been mainly used for failure of the previous ligament surgery, athletes who want to perform high-intensity activities, generalized laxity, and insufficient ligament tissue for direct repair [28, 30]. Unfortunately, non-anatomical ligament reconstruction has been reported to show restricted ankle joint motion and early arthritic changes compared to anatomical reconstruction. In contrast, anatomical ligament reconstruction has been reported to have good clinical outcomes after the surgical procedure [28, 29, 31–33]. It can be assumed that anatomical ligament reconstruction may better mimic native joint mechanics. For more anatomical reconstruction of ligament, various factors such as the type and strength of ligament to be reconstructed (autograft vs. allograft) and the method of drilling the tunnel and fixation method for reconstructed ligaments should be considered. Only positioning the accurate anatomical location of the tunnel cannot guarantee the best biomechanics, but we believe that the results of our study could lead to more accurate anatomical reconstruction of ligament and may contribute to improving both basic and clinical outcomes after surgery.

Previous studies reported anatomical variations of the ATFL with regard to the number of bundles [18, 22, 23, 25]. Thus, there is a possibility that the location of the fibular tunnel may differ depending on the type of the bundle pattern of the ATFL. ATFL could be classified into 3 bundle types (single, double, or multiple). The single-band type consists of an isolated band. The double-band type is divided by superior and inferior fibers. The multiple-band type is divided by triple bands or more. In a systemic review [17], the frequency of the bundle pattern was reviewed in a total of 263 specimens from 10 previous studies. This review showed that the incidences of single-, double-, and triple-bundle ATFL were 162 (61.6%), 94 (35.7%), and 7 (2.7%), respectively. However, our study showed different results.

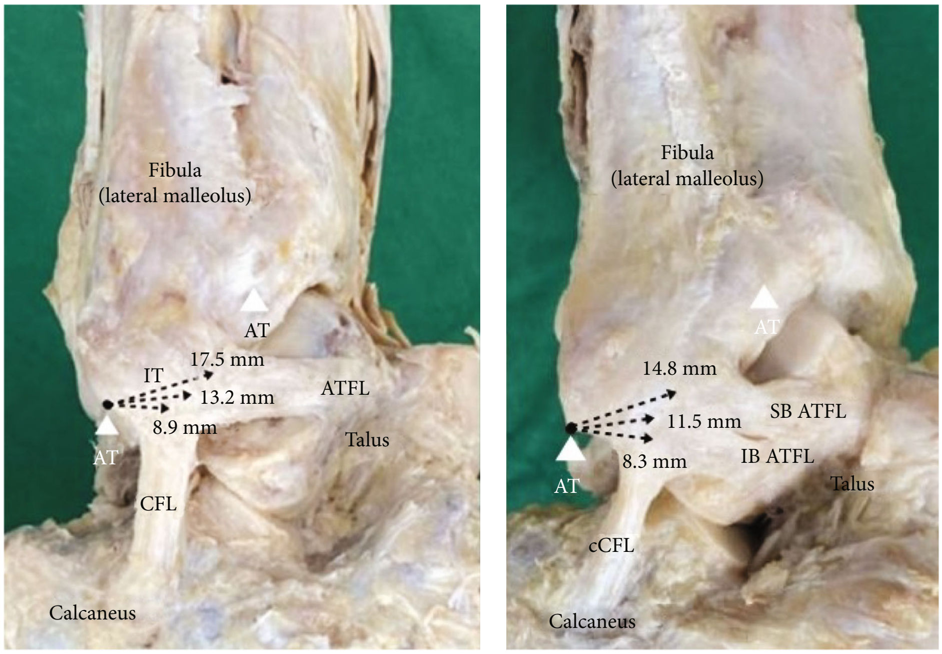

(a) (b)

Figure 2: Lateral view of a right ankle depicting distances from the inferior tip of the lateral malleolus to the anatomic footprint sites of the lateral ankle ligaments. The bundle type of the anterior talofibular ligament was classified into a single type with an isolated band (a) and a double type with a divided superior band and inferior band (b). AT: the articular tip of the lateral malleolus; ATFL: anterior talofibular ligament; CFL: calcaneofibular ligament; IB ATFL: inferior band ATFL; IT: the inferior tip of the lateral malleolus; SB ATFL: superior band ATFL.

Table 3: The ratio of three distances from the inferior tip of the lateral malleolus to the anatomic footprint of the lateral ankle ligaments to the length between the articular tip of the lateral malleolus and inferior tip of the lateral malleolus by the type of the bundle pattern of ATFL ($n = 105$ specimens).

Measurements	Ratio			
	Total	Type 1 ($n = 42$)	Type 2 ($n = 63$)	p value
(cATFL-IT)/(AT-IT)	0.500 ± 0.091	0.544 ± 0.096	0.472 ± 0.076	<0.001
(cCFL-IT)/(AT-IT)	0.267 ± 0.084	0.276 ± 0.089	0.265 ± 0.081	0.504
(intATFL-CFL)/(AT-IT)	0.386 ± 0.070	0.410 ± 0.074	0.368 ± 0.063	0.003

Data are mean ± standard deviation. AT: the articular tip of the lateral malleolus; ATFL: anterior talofibular ligament; cATFL: the center of the fibular footprint of the ATFL; cCFL: the center of the fibular footprint of the CFL; CFL: calcaneofibular ligament; intATFL-CFL: the intersection point of the fibular origin of the ATFL and CFL; IT: the inferior tip of the lateral malleolus.

Of the 105 specimens, 42 (40%) had single-bundle ATFL (type 1) and 63 (60%) had a double-bundle pattern (type 2). There were no specimens of the triple-bundle pattern. Moreover, recent studies with larger sample sizes in Japanese ankles showed that the frequency of the ATFL bundle patterns was similar to our results. Edama et al. [34] studied 81 ankles and found that type 2 occurred most frequently (57%). Kobayashi et al. [25] studied 152 ankles and found that type 2 was the most frequent (54.6%) as well. This uncertainty may be attributable to differences in human races or bias based on the small number of specimens.

Although no conclusions were reached regarding frequencies of ATFL bundle patterns, there may be a possibility that the location of the fibular tunnel may differ depending on the type of ATFL bundle patterns. To date, there is no description of a comparative analysis of intATFL-CFL according to the number of ATFL bundles in the literature. Although the measured value was the difference in small units such as mm, our findings have shown that both the absolute value and the ratio of the location of intATFL-CFL differ significantly according to the number of ATFL bundles. In the double fascicular ATFL, the fibular tunnel for more anatomically correct ligament reconstruction would have to be located more distal than that in single fascicular ATFL, although achieving this small difference may not be surgically feasible.

This study was limited by the use of fixed cadavers to evaluate the morphological characteristics of the lateral ankle ligament. With regard to postmortem changes, there may be differences in the measurements taken for a live person and those from a cadaver. Further, the cadavers were limited to

Table 4: The ratio of three distances from the inferior tip of the lateral malleolus to the anatomic footprint of the lateral ankle ligaments to the length between the articular tip of the lateral malleolus and inferior tip of the lateral malleolus by sex.

Measurements	Ratio Males ($n = 65$)	Ratio Females ($n = 40$)	p value
(cATFL-IT)/(AT-IT)	0.509 ± 0.099	0.488 ± 0.077	0.264
(cCFL-IT)/(AT-IT)	0.260 ± 0.092	0.284 ± 0.070	0.177
(intATFL-CFL)/(AT-IT)	0.385 ± 0.078	0.386 ± 0.056	0.933

Data are mean ± standard deviation. AT: the articular tip of the lateral malleolus; ATFL: anterior talofibular ligament; cATFL: the center of the fibular footprint of the ATFL; cCFL: the center of the fibular footprint of the CFL; CFL: calcaneofibular ligament; intATFL-CFL: the intersection point of the fibular origin of the ATFL and CFL; IT: the inferior tip of the lateral malleolus.

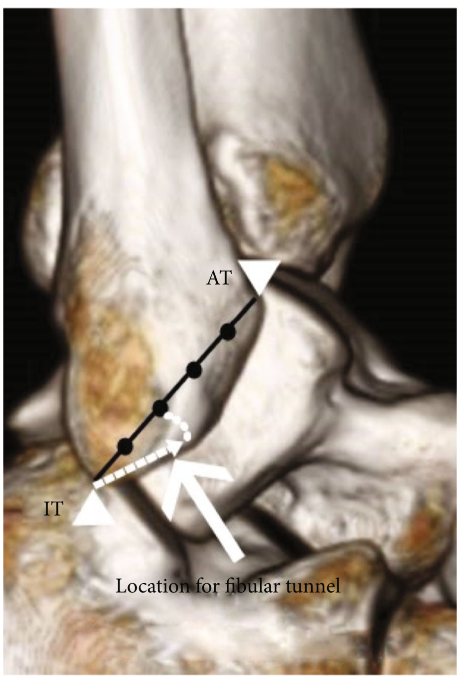

Figure 3: Schematic diagram with three-dimensional CT reconstruction of the lateral side of a normal hind foot. The black circles represent points that divide the distance from AT to IT into 5 equal parts. The white dotted line shows the extension area of the inferior 40% of the distance from AT to IT. The white arrow indicates the location of the fibular tunnel for clinical application. AT: articular tip of the lateral malleolus; IT: inferior tip of the lateral malleolus.

those of elderly individuals (mean age, 76.4 years) and the trauma history of the ankle may not be fully certain because the corpse specimens donated for research do not provide the past medical history.

5. Conclusions

The present study suggests a reference ratio that can help surgeons to locate the fibular tunnel for more anatomically correct reconstruction of the lateral ankle ligament. Also, it may be necessary to make a difference in the location of the fibular tunnel according to the number of ATFL bundles during surgery. Further clinical trials on this will be needed in the future.

Data Availability

The data used to support the findings of this study are available from the corresponding author upon request.

Ethical Approval

The study was conducted according to the guidelines of the Declaration of Helsinki. The cadavers used in the present study were donated to the University of Medicine with consent for education and research. In addition, this study was approved by the Ethics Committee of Chuncheon Sacred Heart Hospital, Hallym University (Institutional Review Board number: NON2020-005).

Disclosure

The funders had no role in the design of the study; in the collection, analyses, or interpretation of data; in the writing of the manuscript; or in the decision to publish the results.

Conflicts of Interest

The authors declare that there are no conflicts of interest.

Authors' Contributions

J.H.P. and J.C. conceptualized the study. H.W.K. and J.C. contributed to the methodology. H.W.K. and J.C. performed the formal analysis. H.W.K., D.K., K.R.P., and J.C. contributed to the investigation. D.K., H.W.K., M.L., Y.J.C., and J.C. performed data curation. H.W.K. and J.C. prepared the original draft. J.H.P., H.W.K., and J.C. reviewed and edited the manuscript. H.W.K. and J.C. performed visualization. J.H.P. and H.W.K. contributed equally to this work.

Acknowledgments

We thank Prof. Seung-Ho Han, Prof. Ki-Hwan Han, Prof. Jong-Tae Park, and Prof. Tae-Cheon Kang for contributing to the collection of the cadavers. This study was supported by the Hallym University Research Fund 2020 (HURF-2020-52).

References

[1] F. C. Balduini and J. Tetzlaff, "Historical perspectives on injuries of the ligaments of the ankle," *Clinics in Sports Medicine*, vol. 1, no. 1, pp. 3–11, 1982.

[2] D. T.-P. Fong, Y. Hong, L.-K. Chan, P. S.-H. Yung, and K.-M. Chan, "A systematic review on ankle injury and ankle sprain in sports," *Sports Medicine*, vol. 37, no. 1, pp. 73–94, 2007.

[3] M. A. Freeman, "Instability of the foot after injuries to the lateral ligament of the ankle," *Journal of Bone and Joint Surgery. British Volume (London)*, vol. 47, no. 4, pp. 669–677, 1965.

[4] T. Kumai, Y. Takakura, A. Rufai, S. Milz, and M. Benjamin, “The functional anatomy of the human anterior talofibular ligament in relation to ankle sprains,” *Journal of Anatomy*, vol. 200, no. 5, pp. 457–465, 2002.

[5] K. Sugimoto, N. Samoto, T. Takaoka, Y. Takakura, and S. Tamai, “Subtalar arthrography in acute injuries of the calcaneofibular ligament,” *Journal of Bone and Joint Surgery. British Volume (London)*, vol. 80-B, no. 5, pp. 785–790, 1998.

[6] M. P. J. van den Bekerom, R. J. Oostra, P. G. Alvarez, and C. N. van Dijk, “The anatomy in relation to injury of the lateral collateral ligaments of the ankle: a current concepts review,” *Clinical Anatomy*, vol. 21, no. 7, pp. 619–626, 2008.

[7] M. Glazebrook, M. Eid, M. Alhadhoud, J. Stone, K. Matsui, and M. Takao, “Percutaneous ankle reconstruction of lateral ligaments,” *Foot and Ankle Clinics*, vol. 23, no. 4, pp. 581–592, 2018.

[8] K. Matsui, ESSKA AFAS Ankle Instability Group, X. M. Oliva et al., “Bony landmarks available for minimally invasive lateral ankle stabilization surgery: a cadaveric anatomical study,” *Knee Surgery, Sports Traumatology, Arthroscopy*, vol. 25, no. 6, pp. 1916–1924, 2017.

[9] M. Takao, W. Miyamoto, K. Matsui, J. Sasahara, and T. Matsushita, “Functional treatment after surgical repair for acute lateral ligament disruption of the ankle in athletes,” *The American Journal of Sports Medicine*, vol. 40, no. 2, pp. 447–451, 2012.

[10] S. Guillo, T. Bauer, J. W. Lee et al., “Consensus in chronic ankle instability: aetiology, assessment, surgical indications and place for arthroscopy,” *Orthopaedics & Traumatology, Surgery & Research*, vol. 99, no. 8, pp. S411–S419, 2013.

[11] S. A. Lynch and P. A. F. H. Renström, “Treatment of acute lateral ankle ligament rupture in the athlete. Conservative versus surgical treatment,” *Sports Medicine*, vol. 27, no. 1, pp. 61–71, 1999.

[12] W. Petersen, I. V. Rembitzki, A. G. Koppenburg et al., “Treatment of acute ankle ligament injuries: a systematic review,” *Archives of Orthopaedic and Trauma Surgery*, vol. 133, no. 8, pp. 1129–1141, 2013.

[13] J. E. Strauss, J. A. Forsberg, and F. G. Lippert 3rd, “Chronic lateral ankle instability and associated conditions: a rationale for treatment,” *Foot & Ankle International*, vol. 28, no. 10, pp. 1041–1044, 2007.

[14] W. J. White, G. A. McCollum, and J. D. Calder, “Return to sport following acute lateral ligament repair of the ankle in professional athletes,” *Knee Surgery, Sports Traumatology, Arthroscopy*, vol. 24, no. 4, pp. 1124–1129, 2016.

[15] A. J. Brown, Y. Shimozono, E. T. Hurley, and J. G. Kennedy, “Arthroscopic versus open repair of lateral ankle ligament for chronic lateral ankle instability: a meta-analysis,” *Knee Surgery, Sports Traumatology, Arthroscopy*, vol. 28, no. 5, pp. 1611–1618, 2020.

[16] D. A. Porter and K. A. Kamman, “Chronic lateral ankle instability: open surgical management,” *Foot and Ankle Clinics*, vol. 23, no. 4, pp. 539–554, 2018.

[17] K. Matsui, ESSKA AFAS Ankle Instability Group, B. Burgesson et al., “Minimally invasive surgical treatment for chronic ankle instability: a systematic review,” *Knee Surgery, Sports Traumatology, Arthroscopy*, vol. 24, no. 4, pp. 1040–1048, 2016.

[18] P. Szaro, K. Ghali Gataa, M. Polaczek, and B. Ciszek, “The double fascicular variations of the anterior talofibular ligament and the calcaneofibular ligament correlate with interconnections between lateral ankle structures revealed on magnetic resonance imaging,” *Scientific Reports*, vol. 10, no. 1, article 20801, 2020.

[19] S. Guillo, P. Archbold, A. Perera, T. Bauer, and B. Sonnery-Cottet, “Arthroscopic anatomic reconstruction of the lateral ligaments of the ankle with gracilis autograft,” *Arthroscopy Techniques*, vol. 3, no. 5, pp. e593–e598, 2014.

[20] S. Guillo, G. Cordier, B. Sonnery-Cottet, and T. Bauer, “Anatomical reconstruction of the anterior talofibular and calcaneofibular ligaments with an all-arthroscopic surgical technique,” *Orthopaedics & Traumatology, Surgery & Research*, vol. 100, no. 8, pp. S413–S417, 2014.

[21] J. R. Landis and G. G. Koch, “The measurement of observer agreement for categorical data,” *Biometrics*, vol. 33, no. 1, pp. 159–174, 1977.

[22] T. O. Clanton, K. J. Campbell, K. J. Wilson et al., “Qualitative and quantitative anatomic investigation of the lateral ankle ligaments for surgical reconstruction procedures,” *Journal of Bone and Joint Surgery*, vol. 96, no. 12, p. e98, 2014.

[23] A. Kakegawa, Y. Mori, A. Tsuchiya, N. Sumitomo, N. Fukushima, and T. Moriizumi, “Independent attachment of lateral ankle ligaments: anterior talofibular and calcaneofibular ligaments - a cadaveric study,” *The Journal of Foot and Ankle Surgery*, vol. 58, no. 4, pp. 717–722, 2019.

[24] F. Taser, Q. Shafiq, and N. A. Ebraheim, “Anatomy of lateral ankle ligaments and their relationship to bony landmarks,” *Surgical and Radiologic Anatomy*, vol. 28, no. 4, pp. 391–397, 2006.

[25] T. Kobayashi, D. Suzuki, Y. Kondo et al., “Morphological characteristics of the lateral ankle ligament complex,” *Surgical and Radiologic Anatomy*, vol. 42, no. 10, pp. 1153–1159, 2020.

[26] T. B. Neuschwander, A. A. Indresano, T. H. Hughes, and B. W. Smith, “Footprint of the lateral ligament complex of the ankle,” *Foot & Ankle International*, vol. 34, no. 4, pp. 582–586, 2013.

[27] R. Buzzi, E. Brenner, F. Segoni, A. Inderster, and P. Aglietti, “Reconstruction of the lateral ligaments of the ankle: an anatomic study with evaluation of isometry,” *Journal of Sports Traumatology and Related Research*, vol. 15, pp. 55–74, 1993.

[28] D. W. Lee, I. K. Park, M. J. Kim et al., “Three-dimensional computed tomography tunnel assessment of allograft anatomic reconstruction in chronic ankle instability: 33 cases,” *Orthopaedics & Traumatology, Surgery & Research*, vol. 105, no. 1, pp. 145–152, 2019.

[29] Y. Tourne and C. Mabit, “Lateral ligament reconstruction procedures for the ankle,” *Orthopaedics & Traumatology, Surgery & Research*, vol. 103, no. 1, pp. S171–S181, 2017.

[30] B. D. Dierckman and R. D. Ferkel, “Anatomic reconstruction with a semitendinosus allograft for chronic lateral ankle instability,” *The American Journal of Sports Medicine*, vol. 43, no. 8, pp. 1941–1950, 2015.

[31] H. G. Jung, T. H. Kim, J. Y. Park, and E. J. Bae, “Anatomic reconstruction of the anterior talofibular and calcaneofibular ligaments using a semitendinosus tendon allograft and interference screws,” *Knee Surgery, Sports Traumatology, Arthroscopy*, vol. 20, no. 8, pp. 1432–1437, 2012.

[32] R. Krips, C. N. van Dijk, T. Halasi et al., “Long-term outcome of anatomical reconstruction versus tenodesis for the treatment of chronic anterolateral instability of the ankle joint: a multicenter study,” *Foot & Ankle International*, vol. 22, no. 5, pp. 415–421, 2001.

[33] R. Schmidt, E. Cordier, C. Bertsch et al., "Reconstruction of the lateral ligaments: do the anatomical procedures restore physiologic ankle kinematics?," *Foot & Ankle International*, vol. 25, no. 1, pp. 31–36, 2004.

[34] M. Edama, I. Kageyama, T. Kikumoto et al., "Morphological features of the anterior talofibular ligament by the number of fiber bundles," *Annals of Anatomy*, vol. 216, pp. 69–74, 2018.